Norwegian University of Science and Technology

Department of Marine Technology

Hybrid Control of Autonomous Ferries

Author:
Tobias Valentin Rye Torben

Main supervisor:
Asgeir Sørensen
Co-supervisor:
Astrid Brodtkorb

December 21, 2018

NTNU Trondheim
Norwegian University of Science and Technology
Department of Marine Technology

PROJECT THESIS IN MARINE CYBERNETICS

AUTUMN 2018

FOR

STUD. TECHN. TOBIAS VALENTIN RYE TORBEN

Hybrid control of autonomous ferries

Work description (short description)
The framework of hybrid control provides a promising approach for the design of highly autonomous systems. This project thesis investigates how this can be applied to autonomous fjord crossing ferries. The work will consist of the design of controllers and models for the continuous dynamics of the different modes of operation, as well as a supervisory switching controller to switch between them. Previous work has shown that switching between different modes, such as crossing to docking, has been challenging with respect to controller performance. The thesis will also investigate how a hybrid control approach might improve on this.

Scope of work

1. Perform a literature survey within the fields of hybrid systems, supervisory control and observer and controller design for marine surface vessels.
2. Setup a realistic simulation environment for fjord crossing ferries. This includes a high-fidelity model of the hull and thrusters and models of environmental loads.
3. Investigate control allocation methods for ferries with symmetrical thruster configuration.
4. Investigate the possibility of using extended sensor solutions, such as Inertial Measurement Units for improved transient performance and disturbance rejection.
5. Establish the appropriate modes of operation and design controllers, observers and guidance laws for the continuous dynamics of the different modes.
6. Design a supervisory switching controller to switch between the discrete modes.
7. Formulate a model of the combined hybrid system using an appropriate framework.
8. Evaluate the system performance through high-fidelity simulation.

The report shall be written in English and edited as a research report including literature survey, description of mathematical models, description of control algorithms, simulation results, model test results, discussion and a conclusion including a proposal for further work. Source code should be provided. It is supposed that Department of Marine Technology, NTNU, can use the results freely in its research work, unless otherwise agreed upon, by referring to the student's work.

The thesis should be submitted within 21. December.

Co-supervisor: Astrid H. Brodtkorb

Professor Asgeir J. Sørensen
Supervisor

Summary

In the recent years, there has been high activity related to autonomy in ferry operations. Due to the relatively low mission complexity, ferry operations make a good candidate for piloting the transition towards autonomous ships.

There are several challenges in automating crossing operations from the perspective of motion control. A crossing consists of several distinct modes of operation, with vastly different speed regimes and control objectives. In particular, the transition from high speed waypoint tracking to low speed docking is challenging, as there is a rapid change in the hydrodynamic forces on the hull, and there is a switch from underactuated to overactuated control. The topic of this thesis is the development of a hybrid control system to support the different modes of operation and to switch between them.

Five modes of operation are defined:

1. Takeoff
2. Transit
3. Transition
4. Docking
5. Dockside

This thesis considers guidance, observer design, motion control and control allocation for the transit, transition and docking modes.

A review of the history and literature of hybrid systems is given first. Applications to marine control systems are presented. A mathematical framework for modelling hybrid dynamical systems is introduced next.

Then, a method for disturbance estimation and rejection using acceleration measurements is proposed. A Kalman based wave filter is developed to filter out the first order wave frequency acceleration components. The performance is evaluated in a case study.

Next, a novel control allocation algorithm for double ended ferries with symmetrical thruster configuration is presented. The algorithm formulates the allocation problem as a bounded scalar optimization problem, for which there exists fast nonlinear solvers. The algorithm also supports a way of controlling the thruster inspired by how manual thruster control is done by ferry captains. A case study evaluates its performance, and compares it with the commonly used Pseudo Inverse method.

The development of a hybrid control system is presented next. It features a GNSS aided Inertial Navigation System (INS) to perform state estimation and filtering for all modes of operation, a switched control allocation system building on the novel allocation algorithm, and guidance and controllers for the three modes of operation. The methodology of disturbance estimation and rejection using acceleration measurements is applied to speed control during the transition mode of operation. In addition to the system as a whole. this chapter introduces two novelties:

- A modified attitude estimator in the GNSS Aided INS for improved estimation of the roll and pitch angles.
- An adaptive Line-of-sight guidance law to provide good performance in high speed path following and good disturbance rejection at low speed.

Finally, a case study is performed for the double ended car ferry MF Gloppefjord at the Anda-Lote site. A high-fidelity simulator for testing of control is developed. The hybrid control systems is tested through several scenarios in the simulator.

The results show promising performance for the developed methods, and the system as a whole. The disturbance estimation and rejection method using acceleration measurements gave improved performance compared to conventional integral action. The thrust allocation algorithm showed superior performance to the Pseudo Inverse method, and reduced computational complexity compared to the Quadratic Programming method. In the switched allocation system, a small transient response was observed when switching from transit to transition. The results also indicates that the modified attitude estimator gives better estimation of the pitch angles compared to the original estimator. The adaptive Line-of-sight algorithm showed improved rejection of cross-currents at low speed while conserving good path following performance at high speed. Wave filtering in the observer is not treated in this thesis. Simulations in waves show that this introduces unacceptable oscillations in the control action.

Suggestions for further work include investigation of disturbance rejection of lateral disturbances, wave filtering in the observer, extensions to support the Takeoff and Dockside modes of operation and formal analysis of the developed methods.

Acknowledgements

Several people have contributed to the completion of this thesis. In particular, I would like to thank my supervisors, Asgeir Sørensen and Astrid Brodtkorb, for invaluable guidance and inspiration throughout the semester. In addition, I would like to thank Bjørnar Vik from Rolls-Royce Marine for important contributions to the topic of this thesis, for providing the vessel model for the simulator and for help and guidance with setting up the simulator. I would also like to thank Martin Rindarøy and Dariusz Fathi from SINTEF Ocean for support and help with getting the simulator up and running.

Several other people have contributed by sharing valuable insight. This includes Øyvind Kjerstad, Torleiv Bryne, Tor Arne Johansen, Roger Skjetne and Thor Inge Fossen.

Finally, I would like to thank Robert Rogne for providing real-life data used for testing wave filtering methods and my office mate, Thomas Johansen, for sharing his simulation model of the azimuth thrusters.

Contents

List of Figures

List of Tables

1 Introduction

This thesis presents a hybrid control approach for autonomous ferries. In this section the background and motivation for increased autonomy in ferry operations is presented, together with how a hybrid control approach might fit in to this.

1.1 Background and motivation

In the recent years, there has been a significant increase in the activity related to autonomy in ships, both in academia and in the industry. The motivating factors for increased autonomy are multiple. Operational costs may be cut by reduced manning and optimized operation. Safety may be improved by limiting human errors and reducing the number of humans involved in the operation. Also, it may enable operations that are impossible or impractical with a human operator. To realize this, a lot of new work needs to be done both in the technology, regulations and integration with existing solutions.

To build confidence and social acceptance in the technology, the first uses of autonomous ships needs to be simple. Due to its relatively low mission complexity, ferries are proposed as a good candidate for piloting the transition towards increased autonomy in ships.

Several research and industry projects related to autonomous ferry operations exist already, most within double-ended car ferries. Rolls-Royce has a contract with Fjord 1 AS to deliver auto-crossing capabilities at 18 ferry sites in Norway [33]. Kongsberg Maritime has a contract with Torghatten AS to deliver an automated crossing and docking system for the Bastø-Fosen strech [37]. Wartsila has developed an autocrossing and autodocking system for NORLED AS with succesful full-scale tests [43]. Also, the Autoferry project at NTNU is developing a small, unmanned ferry to carry passangers and bikes across the Trondheim channel [42].

(a) The Autoferry prototype milliAmpere docking at Ravnkloa in Trondheim. Photo: Kai Dragland

(b) The sister ships MF Gloppefjord and MF Eidsfjord crossing the Anda-Lote strech with autocrossing system from Rolls-Royce. Source: Fjord1

Figure 1: Examples of activity related to autonomy in ferry operations.

1.1.1 Operation and construction of double ended ferries

This thesis will focus on double ended car ferries, and so an introduction to their construction and the way they operate is given next.

The objective of double ended car ferries is to connect a road separated by a short distance of water. These are particularly common in Norway, with its many narrow fjords interrupting normal traffic flow along the western coast. As of 2017, there was about 150 connections in Norway, carrying 43 million people and 21

million vehicles [31].

Double ended car ferries have fore-aft symmetry and have gates opening at both sides to allow cars to roll on and off without having to back their way out. Normally, they also have fore-aft symmetry in the thruster configuration, having one centered azimuth thruster in each end. See Figure 2.

Figure 2: Typical construction and thruster configuration of a double ended car ferry. Source: Skipsrevyen

A crossing operation may be divided into several phases, or modes of operation. In this thesis, the following modes are defined for a crossing from A to B:

1. **Takeoff from A**: The ferry leaves the dock at A and accelerates to service speed.
2. **Transit A to B**: The ferry travels at a constant service speed for the majority of the crossing.
3. **Transition A to B**: As the ferry approaches the dock at B, it decelerates from service speed to low speed and positions itself for docking.
4. **Docking at B**: The ferry maneuvers at low speed until it enables contact with the dock at B.
5. **Dockside at B**: The ferry thrusts against the dock at B to keep the ferry in place while unloading and loading cars and passengers.

After finishing the on-loading at B, the same process repeats itself from B to A. A typical speed profile and route is shown in Figure 3, with corresponding modes of operation.

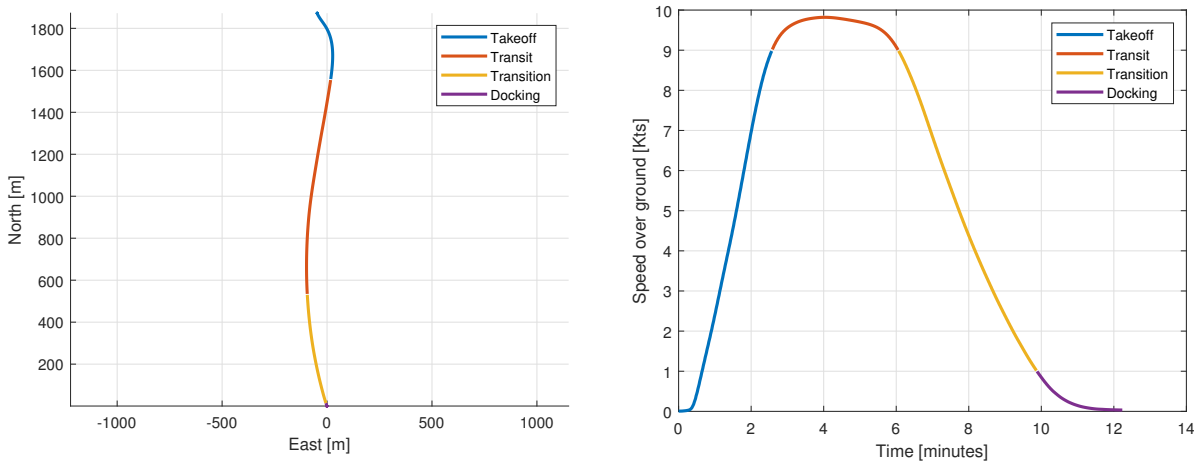

(a) Sample route

(b) Sample speed profile

Figure 3: A typical route and speed profile for a crossing operation.

1.1.2 Hybrid systems

As described in Section 1.1, a ferry operation is naturally divided into several distinct modes of operation. These modes exhibit vastly different physical behaviour, and have different control objectives. Designing one unified controller for this is not feasible, and thus a switched system is called for. Designing a hybrid control system for autonomous ferry operations therefore seems appropriate [20].

Hybrid dynamical systems are systems with both discrete and continuous dynamics. Their solutions may flow continuously and jump discontinuously. This behaviour can model a wide range of systems, for example the impulsive behaviour of a bouncing ball or the interaction of a digital computer with the physical world.

Hybrid systems also have applications to control synthesis and analysis, and opens up possibilities not possible by classical control theory of purely discrete or continuous systems. A prime example of this is the switching between controllers, enabling adaptive behaviour with structurally different controllers.

The mathematical framework of hybrid systems is maturing, and there exists many powerful results for analyzing and verifying hybrid systems. This, together with their strong expressive power, make hybrid system a promising platform for designing and verifying control systems with a high level of autonomy.

1.2 Research questions and scope

The title of this thesis is *Hybrid control of autonomous ferries*. The objectives are summarized in the following.

1. Do a review of the history and literature of hybrid systems theory.
2. Set up a high-fidelity simulation environment for ferry operations.
3. Investigate control allocation algorithms for double ended ferries.
4. Investigate control design using extended sensor solutions to handle the rapidly changing loads experienced during the transition mode.

5. Design the continuous components for the different modes, and design a supervisor to switch between them. Formulate the resulting system as a hybrid dynamical system.

6. Evaluate the system in simulation.

This thesis only considers three modes of operation: Transit, Transition and Docking. Special attention will be given to the Transition mode, as this represents the greatest challenge from a control perspective.

The authors idea of the control architecture for the automatic sailing system in an autonomous ferry is illustrated in Figure 4. In this thesis, only the blocks indicated by green color is considered. In particular, it is assumed that the guidance system is provided with a path in the form of fixed waypoints. Hence, path planning, situational awareness and collision avoidance is not treated here.

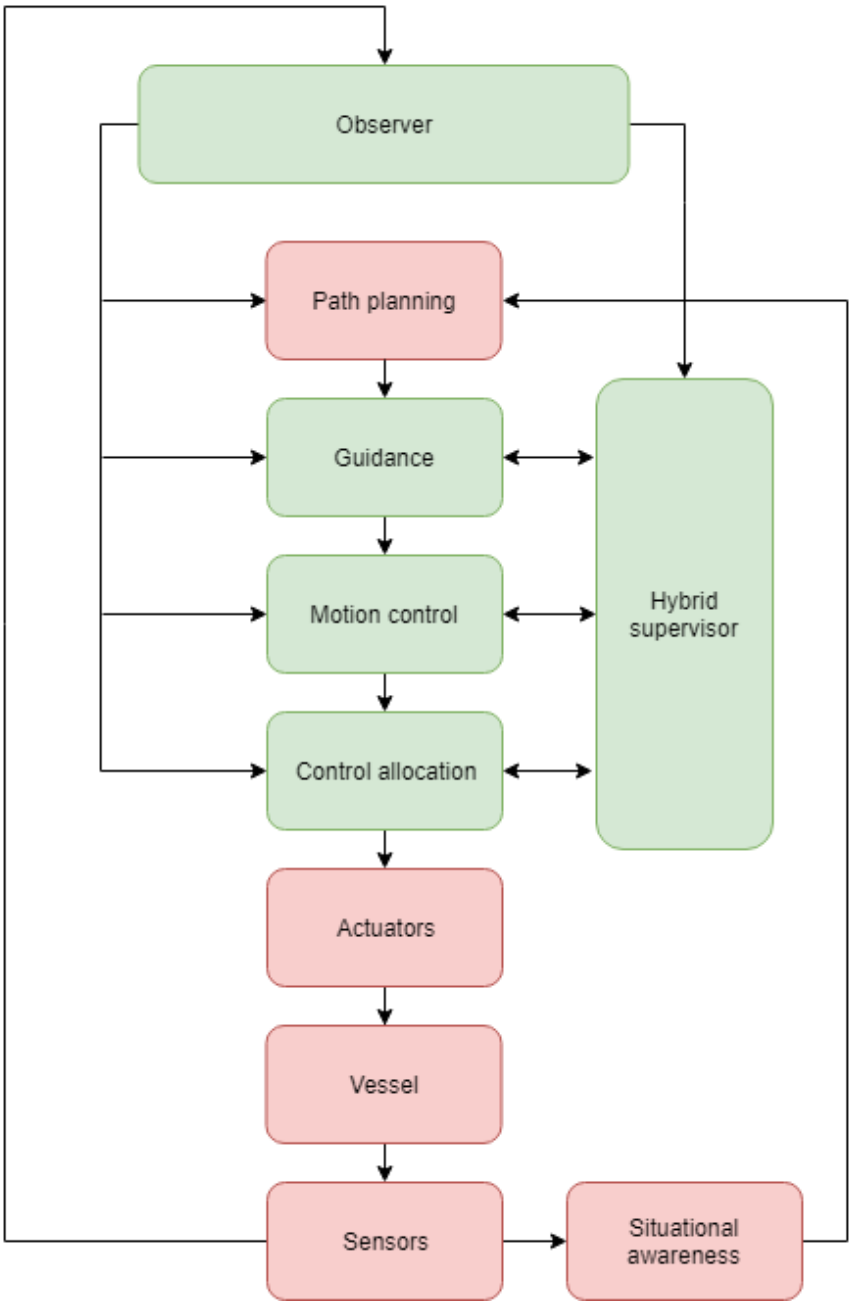

Figure 4: Control architecture for an autonomous ferry

1.3 Main contributions

The main contributions of this thesis are summarized below.

1. A high-fidelity simulation environment for ferry operations is set up.
2. A novel control allocation algorithm is presented for solving the allocation problem for ferries with symmetric thruster configuration.

3. A disturbance estimator utilizing accelerometer measurements is presented and integrated into a motion controller for rapid disturbance rejection.

4. An adaptive Line-of-sight guidance law is proposed for improved disturbance rejection at low speeds.

5. A modified attitude estimator based on [27] is proposed.

6. A hybrid control system for a ferry undergoing the Transit, Transition and Docking phases is designed. In addition to the developed components of this thesis, the system includes:

   - An observer based on GNSS aided inertial navigation
   - Integral Line-of-sight guidance
   - Low speed docking controller
   - Control allocation algorithms for Transition and Docking

1.4 Outline

The thesis is structured as follows:
In Chapter 2, preliminaries in modelling and control of marine vessels is briefly presented, with references for further reading.
In Chapter 3, a historic review of hybrid systems theory is given, and the mathematical framework for hybrid systems used in this thesis is presented.
In Chapter 4, a method for disturbance estimation and rejection using acceleration measurements is presented, and a case study is conducted.
In Chapter 5 a novel control allocation algorithm is presented, with specific implementations for Transition and Docking. It finishes off with a case study.
In Chapter 6, a hybrid control system for integrating all components developed in this thesis is presented. Also, the adaptive Line-of-sight guidance law and the modified attitude estimator is presented here.
In Chapter 7, a case study for the ferry MF Gloppefjord is conducted. The ferry site and the vessel is presented. Then, a high-fidelity simulator for the ferry is developed. The hybrid control system developed in this thesis is then tested in this simulator. Presentation and discussion of results follow next.
Finally, concluding remarks are given in Chapter 8, with suggestions for further work.

2 Mathematical modelling and control of marine vessels

This chapter presents the preliminaries in modelling and control of marine vessels for the thesis. The objective is not to give a complete description, but rather to introduce the most important aspects and refer to other sources for further reading.

2.1 Modelling of marine surface vessels

2.1.1 Notation and frames of reference

This thesis adopts the notation used in [21], building on the SNAME 1950 standard notation. The reader is referred there for details on the notation and symbols.

Two important frames of reference are used in this thesis: The inertial **NED frame**, with origin at a fixed point relative to the earth surface, and axis pointing North, East and Down, and the **BODY frame**, with origin at a point fixed to the vessel and axis pointing in surge, sway and heave.

The definition of the BODY frame axis for a ship is shown in Figure 5.

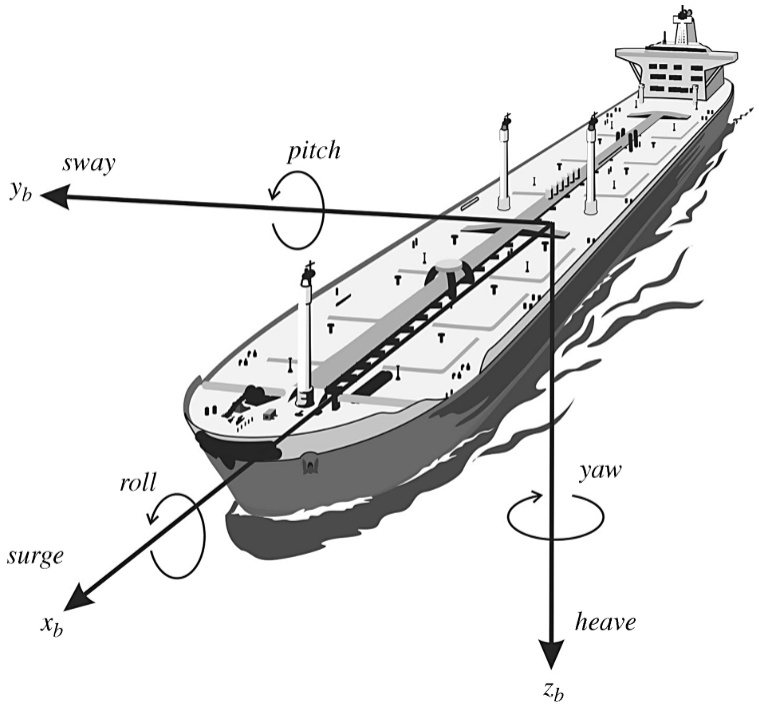

Figure 5: Definition of ship coordinate axis. Source: [21].

Variables in BODY frame are denoted by superscript b, and variables in NED frame are denoted by superscript n. In cases where it is not obvious, variable expressing motion of frame b relative to frame a are denoted by subscript ab.

Element i of a vector v is denoted $v_{(i)}$. The entry in row i column j of a matrix M is denoted $M_{(i,j)}$.

2.1.2 Vessel kinematics and kinetics

The kinematic and kinetic equations of motion for a general six degree of freedom marine vessel is derived in [21], using vectorial mechanics:

$$\dot{\eta} = J_k(\eta)\nu \tag{1}$$

$$M\dot{\nu} + C(\nu)\nu + D(\nu)\nu + g(\eta) + g_0 = \tau + \tau_{wind} + \tau_{wave} + \tau_{curr} \tag{2}$$

where $\eta \in \mathbb{R}^{6\times1}$ is the position and orientation in NED frame, $\nu \in \mathbb{R}^{6\times1}$ is the linear and angular velocities in BODY frame. $J_k(\eta) \in \mathbb{R}^{6\times6}$ is a transformation matrix mapping the BODY velocities to NED velocities. $M \in \mathbb{R}^{6\times6}$ is the rigid body and added mass matrix, $C(\nu)\nu$ contains centripital and coriolis forces and moments due to (2) being expressed in the non-inertial BODY frame. $D(\nu)\nu$ is a damping term, and $g(\eta) + g_0$ are gravitational and hydrostatic forces and moments. The right hand side (RHS) of (2) represents the exiting forces, and may include thruster forces, $\tau \in \mathbb{R}^{6\times1}$, wind loads, $\tau_{wind} \in \mathbb{R}^{6\times1}$, wave loads, $\tau_{wave} \in \mathbb{R}^{6\times1}$ and current forces, $\tau_{curr} \in \mathbb{R}^{6\times1}$ Current forces may also be added by using the relative velocity through the water, ν_r in place of ν. This requires the assumption of constant, irrotational currents and a special parametrization of $C(\nu)\nu$. See [21] for details. This model does not include lift forces, and is therefore not applicable for very high speeds [10].

2.1.3 Low speed vessel model

The general six degree of freedom model of (1)-(2) may be reduced to a three degree of freedom control plant model describing the horizontal motion (surge, sway and yaw):

$$\dot{\eta} = R(\psi)\nu \tag{3}$$

$$M\dot{\nu} + D\nu = R^T(\psi)b + \tau + \tau_{wind} + \tau_{wave}. \tag{4}$$

$$\dot{b} = 0 \tag{5}$$

This is a valid model reduction under the assumption of low speed. Then, the coriolis and centripetal forces are negligible and linear viscous damping dominates. The current forces and unmodelled dynamics from (2) are modelled as a slowly varying bias term $b \in \mathbb{R}^{3\times1}$. $R(\psi) \in \mathbb{R}^{3\times3}$ contains the surge, sway and yaw terms of $J_k(\eta)$ with the assumption of zero roll and pitch.

This model is used in DP observer and control design.

2.1.4 Autopilot model

By again considering the horizontal degrees of freedom in (1)-(2), linearizing the kinetics about a service speed and supressing the second order dynamics, the first order autopilot model of Nomoto is obtained:

$$T\ddot{\psi} + \psi = K\delta \tag{6}$$

where ψ is the heading, T is a time constant determined by the inertial and damping properties of the ship, δ is the rudder angle and K is the rudder constant.

This model is used in transit observer and control design.

2.2 Motion control

2.2.1 Dynamic positioning

The control objective in dynamic positioning is station keeping or low speed maneuvering. Normally, only the horizontal degrees of freedom are controlled, but in vessels with small waterplane area, roll and pitch damping may also be included [36].

A horizontal plane control law may be synthesized from the control plant model of (3)-(4). For station keeping applications with small deviations about a fixed desired heading, ψ_d, a linear PID control law may be used [36]:

$$\tilde{\eta}_p = R^T(\psi_d)(\eta - \eta_d) \tag{7}$$

$$\tilde{\nu} = \nu - \nu_d \tag{8}$$

$$\dot{\xi} = \tilde{\eta}_p \tag{9}$$

$$\tau = -K_p\tilde{\eta}_p - K_d\tilde{\nu} - K_i\xi \tag{10}$$

where subscript d denotes reference signals, and K_p, K_d, $K_i \in \mathbb{R}^{3\times3}$ are the proportinal, derivative and integral gain matrices, respectively. For (7)-(10), linear control synthesis methods such as LQR or pole-placement can be used. Note that this control law is based on a linearization of (3)-(4) about the desired heading.

For low speed maneuvering applications, the nonlinear PID control law of [21], with reference feedforward, is be more appropriate:

$$\tau = -R^T(\psi)K_p(\eta - \eta_d) - K_d(\nu - \nu_d) - R^T(\psi)K_i\int(\eta - \eta_d)dt + Ma_d + D\nu_d \tag{11}$$

$a_d \in \mathbb{R}^{3\times1}$ is the acceleration reference in the BODY frame. Note that the actual heading angle, ψ is used in the rotation matrices, instead of the constant desired heading as seen in the linear PID control law. Note also that the integrator is expressed in NED coordinates. This is rationalized by the fact that the integral term counteracts slowly varying loads such as current and wind, which are usually changes less in the NED frame than the BODY frame.

2.2.2 Autopilot

The control objective of an autopilot system is to track a desired heading at constant forward speed, u_d. Autopilot systems differ in complexity, from simple constant course keeping controllers to path following systems tracking heading references from a guidance system.

A simple PID autopilot control law based on the control plant model of (6) can be used:

$$\tau_N = -K_p(\psi - \psi_d) - K_d(r - \dot{\psi}_d) - K_i\int(\psi - \psi_d)dt \tag{12}$$

Knowing the Nomoto time constant in (6) and the rigid body and added mass in yaw, pole placement may be used in the control design. Note that under presence of current, the heading and course will differ. Methods to handle this include sideslip estimation and adding integral action to the guidance law. See [21] for details.

In an autonomous autopilot system, a speed controller is also necessary to maintain a constant forward speed. Since there is only one integrator between thruster force and speed, a PI controller is appropriate:

$$\tau_X = -K_p(u - u_d) - K_i \int (u - u_d)dt \tag{13}$$

Here, u_d is the speed reference.

2.3 Observer

The observer is a vital part of an autonomous navigation system. Its purpose is to do filtering of measurements to remove noise and wave frequency components, and also to estimate unmeasured states. For marine surface vessels, velocity is usually not measured, and thus needs to be estimated. Measurements from a Global Navigation Satellite System (GNSS) of speed over ground and course over ground are available, but the measurement quality is often poor at low speeds.

2.3.1 Model based observers

Model based observers have been used successfully in DP systems for decades. Examples include the Kalman filter approach [2], Extended kalman filter approach [36] and Passive Nonlinear approach [11]. They all have in common that disturbances and modelling errors are handled by a slowly varying bias term. Often, this renders them too slow to capture transient behaviour.

When designing a model based observer a specific model must be chosen. If the assumptions of this model is not met, the performance may be poor. Finding a unified control plant model for low-speed and high-speed regimes is very difficult. Using a single model based observer for all operational modes in a ferry operation is thus not feasible. An option is to use hybrid switching approach, as in [17] and [20].

2.3.2 Inertial navigation

By extending the sensor suite to include an *Inertial Measurement Unit* (IMU), it is possible to design observers that address the issues raised by model based observers in Section 2.3.1. Inertial Measurement Units include accelerometers and rate gyros. These signals can be used in place of a kinetic model in an observer, and thus yield a model free approach. Observers based on inertial navigation typically also have better transient behaviour [34].

An IMU measures *specific force*, $f_{ib}^b \in \mathbb{R}^{3\times1}$ and angular rates $\omega_{ib}^b \in \mathbb{R}^{3\times1}$. f_{ib}^b is the acceleration of the IMU casing relative to an inertial frame, i, plus the gravitational acceleration. It is decomposed in body frame coordinates. Both sensor measurements, $f_{imu}^b \in \mathbb{R}^{3\times1}$ and $\omega_{imu}^b \in \mathbb{R}^{3\times1}$, are usually corrupted by sensor noise and sensor bias. The following sensor model is therefore used [28]:

$$\omega_{imu}^b = \omega_{ib}^b + b_{ars}^b + w_{ars}^b \tag{14}$$

$$f_{imu}^b = f_{ib}^b + b_{acc}^b + w_{acc}^b \tag{15}$$

where $\omega_{ib}^b \in \mathbb{R}^{3\times1}$ and $f_{ib}^b \in \mathbb{R}^{3\times1}$ are the true values, $b_{ars}^b \in \mathbb{R}^{3\times1}$ and $b_{acc}^b \in \mathbb{R}^{3\times1}$ are bias terms and $w_{ars}^b \in \mathbb{R}^{3\times1}$ and $w_{acc}^b \in \mathbb{R}^{3\times1}$ are noise terms.

The bias term in the rate gyros may be substantial, and have poor in-run stability. That is, it can change while operating, and can therefore not be counteracted by pre-run calibration. Hence, it must be estimated and compensated for online. The bias term in the accelerometers typically have better in-run stability, and they are difficult to estimate online. In fact, for a combined attitude and position observer, observability is lost when including an unknown accelerometer bias. The standard practice is therefore to do pre-run

calibration to compensate for this [21].

The kinematics on an inertial navigation system are governed by the *Strapdown Inertial Equations*. Under the assumption of NED being inertial, these are given by [28]:

$$\dot{p}^n_{nb} = v^n_{nb} \tag{16}$$

$$\dot{v}^n_{nb} = R^n_b f^b_{ib} + g^n_b \tag{17}$$

$$\dot{R}^n_b = R^n_b S(\omega^b_{nb}) \tag{18}$$

Here, $p \in \mathbb{R}^{3\times1}$ is linear position, $v \in \mathbb{R}^{3\times1}$ is linear velocity and $g \in \mathbb{R}^{3\times1}$ is the gravitational acceleration. $S \in \mathbb{R}^{3\times3}$ is a skew symmetric matrix, such that $S(a)b = a \times b$. See [21] for details.

When using INS based observers for marine vessels, it is required by class that they are backed by model based observers for redundancy in case of a sensor failure. Model based observers also have the advantage of not being linked to a physical device. In an operational setting, this is appreciated since the user does not need to worry about hardware specific challenges, such as alignment errors, calibration, sensor integrity etc. Because of this, model based observers are still the industry standard.

2.3.3 GNSS aided inertial navigation

The linear position and velocity and the attitude may be estimated by integrating the strapdown inertial equations. This gives very high accuracy at short time horizons. However, due to sensor bias, misalignment errors etc. the estimates will drift over time. To resolve this, the observer needs to be corrected by an external position and attitude reference.

Several observers based on variations of Extended Kalman Filters (EKF) have be suggested over the years, with good results [28]. However, a caveat with the EKF is the lack of global stability results. Because of this, researchers have investigated nonlinear observers for GNSS/INS integration, including Salcudean (1991) [5], Vik et al. (2001) [13] and Mahony et al. (2008) [19].

Building on this, Grip et al. proposed a nonlinear observer for GNSS aided inertial navigation in 2015 [27]. Instead of estimating the attitude vector, the rotation matrix is estimated directly:

$$\dot{\hat{R}} = \hat{R}S(\omega^b_{imu} - \hat{b}^b_{ars}) + \sigma K_P \hat{J} \tag{19}$$

$$\dot{\hat{b}}^b_{ars} = Proj(\hat{b}^b_{ars}, -k_I vex(\mathbb{P}_a(\hat{R}^T_s K_P \hat{J}))) \tag{20}$$

Again, S is a skew symmetric matrix representing the cross product operator in matrix form. The operator $\mathbb{P}_a(X)$ denotes the skew symmetric part of a matrix X: $\mathbb{P}_a(X) = \frac{1}{2}(X - X^T)$. The function $vex(X)$ is defined such that $S(vex(X)) = X$ and $vex(S(x)) = x$ for all skew-symmetric matrix arguments. $Proj(\cdot,\cdot)$ is a special case of the Parameter Projection function, which makes sure that the gyro bias estimate stays bounded. $\hat{J} \in \mathbb{R}^{3\times3}$ is a stabilizing injection term for attitude measurements, which may take several forms. σ, K_P and k_I are tunable constants. See [27] for details.

The translational motion observer (TMO) uses the estimated rotation matrix from (19) and (20), integrates acceleration measurements and corrects by injection of position and velocity measurements:

$$\dot{\hat{p}}^n = \hat{v}^n + K_{pp}(p^n - \hat{p}^n) + K_{pv}(v^n - C_v \hat{v}^n) \tag{21}$$

$$\dot{\hat{v}}^n = \hat{f}^n + g^n + K_{vp}(p^n - \hat{p}^n) + K_{vv}(v^n - C_v\hat{v}^n) \tag{22}$$

$$\dot{\xi} = -\sigma K_P \hat{J} f_{imu} + K_{\xi p}(p^n - \hat{p}^n) + K_{\xi v}(v^n - C_v\hat{v}^n) \tag{23}$$

$$\hat{f}^n = \hat{R} f_{imu} + \xi \tag{24}$$

Where K_{pp}, K_{pv}, K_{vp}, K_{vv}, $K_{\xi p}$ and $K_{\xi v}$ are observer gains, and C_v is a selection matrix extracting the degrees of freedom for which we have measurements from v^n. In [27] it is shown that the origin of the error dynamics for the combined GNSS/INS observer is Globally Exponentially Stable (GES), under reasonable assumptions.

Bryne et al. introduced the Virtual Vertical Reference for GNSS aided INS in vessels operating at the ocean surface [25]. This work was motivated by the poor vertical measurements provided by GNSS systems. The main idea is to use the fact that the vessel oscillates about zero vertical position, and the average vertical position is thus zero. This is equivalent to saying that the integral of vertical position over time approaches zero as time goes to infinity. By augmenting the observer with a state for the integral of the vertical position estimate, this can be injected into the position observer and keep the vertical position estimate from drifting. Bryne et al. went on to prove that the origin of the error dynamics of a translational motion observer for surface vessels with VVR and the attitude observer of Grip et al. (2013) [23] is Uniformly Semi-globally Exponentially Stable (USGES). The attitude observer of Grip et. at (2013) is closely related to that of (19)-(20), but uses quaternion estimation instead of the Euler angel rotation matrix. See [25] for details.

In 2018, Brodtkorb et al. used the attitude observer of (19)-(20) together with the translational motion observer of Bryne et al. (2015) and states that the combined system is Uniformly Globally Exponentially Stable (UGES). See [34] for details.

2.4 Guidance

The purpose of a guidance system is to provide the motion controllers with smooth references. In this section, two common guidance laws are presented.

2.4.1 Line-of-sight

In *path following*, the control objective is to follow a predefined path without any temporal restrictions along the path [21]. In the case of a path defined by line-segments between waypoints, this may be solved by the *Line-of-sight* (LOS) guidance law, as shown in Figure 6

The idea in line-of-sight guidance is to steer towards a point which is a fixed distance, Δ, along the path in front of the ship. This is called the *lookahead* distance. Given a linear path, $\mathcal{P}$ from point P_0 to P_1, a coordinate frame is defined with the x-axis running along the path, and the y-axis perpendicular to the path. The origin of this frame is at P_0.

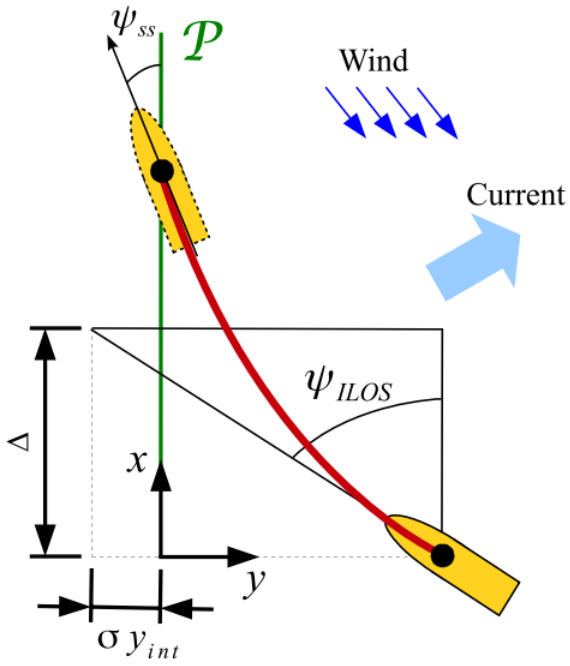

Figure 6: ILOS guidance for surface vessels. Source: [29]

y is called the *cross-track error*, and the control objective in path following of linear paths may thus be expressed as:

$$\lim_{t\to\infty} y(t) = 0 \tag{25}$$

In presence of disturbances such as currents and wind, the vessel may need to crab at a steady state heading angle, ψ_{ss} to track the path with zero steady state offset. To accommodate this, integral effect is introduced. The resulting guidance law is known as *Integral Line-of-sight* (ILOS).

The ILOS guidance law is given by [29]:

$$\psi_{ILOS} = -\arctan(\frac{y + \sigma y_{int}}{\Delta}) \tag{26}$$

$$\dot{y}_{int} = \frac{\Delta y}{(y + \sigma y_{int})^2 + \Delta^2} \tag{27}$$

where σ is an integral gain.

Caharija et al. shows that the equillibrium point for a simplified vessel model with the ILOS guidance law is Uniformly Globally Asymptotically Stable (UGAS) ans Uniformly Locally Exponentially Stable (ULES) under certain assumptions. See [29] for details.

2.4.2 Reference filter

For DP applications, a guidance law is often introduced to provide smooth trajectories during setpoint changes. A common approach is to use a third order transfer function from setpoint to reference [21]:

$$\eta_d^{(3)} + (2\Gamma + I_{3\times3})\Omega\ddot{\eta}_d + (2\Gamma + I_{3\times3})\Omega^2\dot{\eta}_d + \Omega^3\eta_d = \Omega^3 r^n \tag{28}$$

where $\eta_d \in \mathbb{R}^{3\times1}$ is the position reference, $r^n \in \mathbb{R}^{3\times1}$ is the setpoint, $\Gamma \in \mathbb{R}^{3\times3}$ is a diagonal matrix of filter damping rations and $\Omega \in \mathbb{R}^{3\times3}$ is a diagonal matrix of filter natural frequencies.

To ensure feasible references to follow for all ranges of setpoints, saturation elements should be added for velocity and acceleration. A block diagram of the reference filter in (28) with saturation elements is shown in Figure 7.

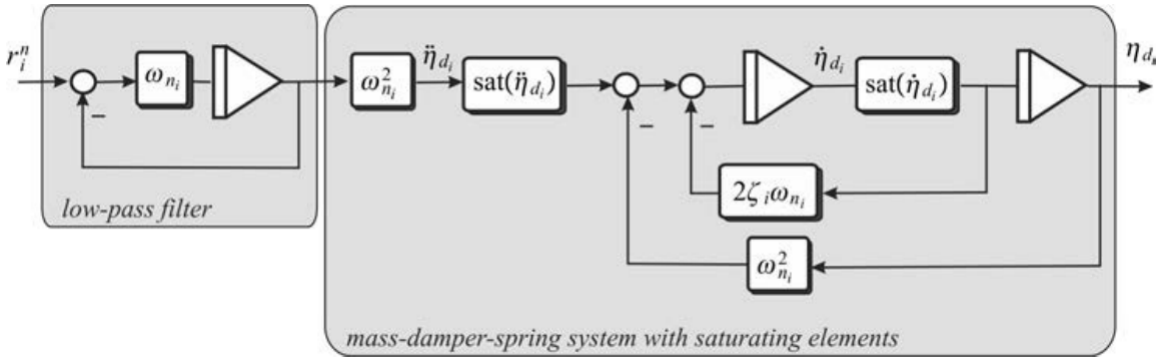

Figure 7: Third order reference filter with saturation on velocity and acceleration. Source: [21]

Note that this is an *open-loop guidance law*. This is, its output does not depend on the position of the ship. Also, having the reference be the solution of a differential equation, as in (28), may not always yield the desired behaviour. Fernandez proposes an alternative solution in [26], by dividing a setpoint change into 4 phases, and stitching together smooth trajectory.

2.5 Control allocation

2.5.1 The control allocation problem

Control allocation is the problem of allocating the desired control action for a vehicle to its actuators. For marine vessels this is often referred to as *thrust allocation*.

For a marine vessels with the horizontal plane as its working space, the input to the thrust allocation module is the desired body frame control action $\tau = [X, Y, N]^T$. The output from the thrust allocation is the setpoints to the propulsors. This can be in form of e.g. propeller speed, propeller pitch, azimuth angle or rudder angle, depending on the type of the propulsor.

The mapping from actuator setpoints to body frame control action is often formulated as

$$\tau = B(\alpha)u \tag{29}$$

where α is a vector of unknown actuator angles and u is an unknown vector of thrust setpoints. The matrix B is called the *thrust configuration matrix*. The system of (29) is in many cases under-determined, that is, there are infinitely many solution. This gives the thrust allocation algorithm freedom to choose one that is optimal in some sense.

2.5.2 Pseudo inverse solution

In the case where the thrust configuration matrix, B, does not depend on α, a widely used method is the pseudo inverse (Moore-Penrose inverse). The pseudo inverse is a generalisation of an inverse matrix for non-square matrices. In relation to solving linear systems of equations, it has the property that is provides the minimum 2-norm solution. That is, it minimises the squared sum of thrusts. The pseudo inverse, $B^\dagger$, of a matrix, B can be calculated explicitly from

$$B^\dagger = (B^T B)^{-1} B^T \tag{30}$$

The thrust setpoints can then be calculated as

$$u = B^\dagger \tau \tag{31}$$

The advantages of the pseudo inverse method is simplicity and low computational cost. The pseudo inverse of the thrust configuration matrix can be pre-computed once, and solving the thrust allocation problem is then reduced to a matrix-vector multiplication. One weakness of the method is that is only optimizes for thrust norm, whereas other objectives may be more important in some cases. Also, it can not be applied when the thrust configuration matrix depends on the thruster angles, and constraints can not be added.

2.5.3 Quadratic programming solution

In the case of azimuthing thrusters, a widely used approach is to formulate the thrust allocation problem as a quadratic programming problem. Different objective functions are possible, but it is common to minimize power consumption and azimuth angle change. A quadratic programming problem must have a convex, quadratic function objective function, and linear constraints. Both the power consumption and the thrust configuration constraint are, in general, nonlinear and must thus be linearized.

A quadratic programming problem which minimizes power consumption and angle change, and constrains the change of angle, maximum and maximum thrust can be formulated as [18]:

$$\min_{\Delta f, \Delta\alpha, s} J = (f_0 + \Delta f)^T P (f_0 + \Delta f) + s^T Q s + \Delta\alpha^T \Omega \Delta\alpha \tag{32}$$

subject to

$$s + B(\alpha_0)\Delta f + \frac{\partial}{\partial \alpha}(B(\alpha) f)|_{\alpha_0, f_0} \Delta\alpha = \tau - B(\alpha_0) f_0 \tag{33a}$$

$$f_{min} - f_0 \leq \ \leq f_{max} - f_0 \tag{33b}$$

$$\alpha_{min} - \alpha_0 \leq \Delta\alpha \leq \alpha_{max} - \alpha_0 \tag{33c}$$

$$\Delta\alpha_{min} \leq \Delta\alpha \leq \Delta\alpha_{max} \tag{33d}$$

Here, f_0 and α_0 are the thrusts and angles from the last time step, and Δf and $\Delta\alpha$ are the change from last to current time step. Furthermore, s is a vector of slack variables, and P, Q, Ω are weight matrices.
This method has the advantage over the Pseudo inverse method in that is can optimize for a more general objective, and constraints can be added. The challanges with this method is increased computational cost, and the fact that it is a linearization of the actual problem. Since the optimization problem is linearized about the last solution, the solver can only optimize locally about this point and thus lacks a global perspective.

For an in-depth review of control allocation methods, the reader is referred to [18]. A more recent approach by Skjong and Pedersen (2017) formulates the thrust allocation problem as an MPC problem, and thus finds an optimal sequence of allocations within a time horizon [32].

3 Hybrid systems and control

Hybrid dynamical systems are systems with both continuous and discrete dynamics. Many phenomena may be modelled naturally as hybrid dynamical systems, and hybrid approaches opens up for many new possibilities to control of dynamical systems. Because of this, a lot of work has been done in the field of hybrid systems and control over the past couple of decades. This chapter reviews the literature and history of hybrid systems and control and then gives a short presentation of a mathematical framework for modelling and analysis of hybrid dynamical systems.

3.1 Overview

One can argue that hybrid control systems have been in use for a long time, for example with the introduction of relay switch circuits, introduced in the 1830's [39]. The earliest work related explicitly to hybrid systems dates back to the work of Witsenhausen at MIT in 1966 [1]. Since then, many quite different approaches has been taken to the modelling and analysis of hybrid systems. These may be coarsly divided into four paradigms [9]:

- **Aggregation**: The continuous dynamics are suppressed so that the hybrid system is approximated by a finite automaton or a discrete-event dynamical system.
- **Continuation**: Complmentary to aggreation, the discrete dynamics are supressed to yield a system of differential equations.
- **Automata approach**: View the hybrid system as a network of interacting automata based on an input-output language behaviour.
- **Systems approach**: View the hybrid system as interacting dynamical systems, usually described by differential and difference equations.

The different approaches highlight different aspects of hybrid systems, and are suitable for analyzing different phenomena. There is also a trade-off between the expressiveness of a model and the properties you can prove for the model. The automata approach has been most used by the computer science community, whereas the systems approach has been most used by the control engineering community.

The discrete phenomena related to hybrid systems may be classified into four cases [9], and different approaches to the modelling are only suited for analyzing a subset set of these:

- **Autonomous switching**: The vector field describing the continuous dynamics undergoes discontinuous changes based on the conditions on the continuous states.
- **Autonomous jumps**: The continuous state undergoes discontinuous jumps based on the conditions on the continuous states.
- **Controlled switching**: The vector field describing the continuous dynamics changes discontinuously in response to a control input.
- **Controlled jumps**: The continuous state changes discontinuously in response to a control input.

The main contributions to the theory of hybrid systems originate from two research communities. Foremost, the control theory community, for which the use of hybrid systems are many. In particular, switched control systems are studied extensively. The computer science community has also made significant contributions, often with applications to verification methodologies.

3.2 Hybrid system models

Several models have been proposed for hybrid systems. In the following, the most important ones are presented briefly in order of publication date. For a more in-depth review, the reader is referred to [9].

As mentioned, the first work related directly to hybrid systems was due to **Witsenhausen** in 1966 [1]. He proposed a model for describing autonomous switching. The dynamics of this system is described by the differential equation

$$\dot{x} = f(q(t), x(t), u(t)) \tag{34}$$

where $x \in \mathbb{R}^n$ is the continuous state, $q \in \mathbb{Z}$ is the discrete state and $u \in \mathbb{R}^m$ is the continuous input.
The coupling discrete dynamics are governed by the continuous state. If the discrete state $q = i$ and the continuous state enters the set $M_{i,j}$, the discrete state transitions from i to j. Under reasonable topological assumptions on $M_{i,j}$ and certain smoothness assumptions on $f(q, \cdot, \cdot)$ Witsenhausen defined the solution for this type of system, and proved the existance and uniqueness of these. He continued to give some optimal control results.

Building on the results of Witsenhausen, **Tavernini** introduced the *differential automata* in 1987 [4]. For this he proved that the initial value problem has a unique solution with finitely many switching points. The focus of his work was the analysis of numerical simulations of the solutions to differential automata.

In 1993 **Back, Guckenheimer and Myers** introduced a generalization of the Tavernini model [7]. Most notably, the model allows jumps in continuous states. The model also has a number of sets X_q for the continuous state, associated with the vector field f_q. The sets X_q are not assumed disjoint, and uniqueness can thus not be guaranteed for the solutions.

Also in 1993, **Nerode and Kohn** introduced a quite different hybrid systems model building on automata theory [8]. As illustrated in Figure 8, the model consists of three components:

1. A continuous time plant
2. A digital automaton
3. An interface

The interface consists of an analog-to-digital map, mapping the continuous plant state to symbols input to the digital automaton, and digital-to-analog map converting symbols from the digital automaton to continuous time inputs to the plant.

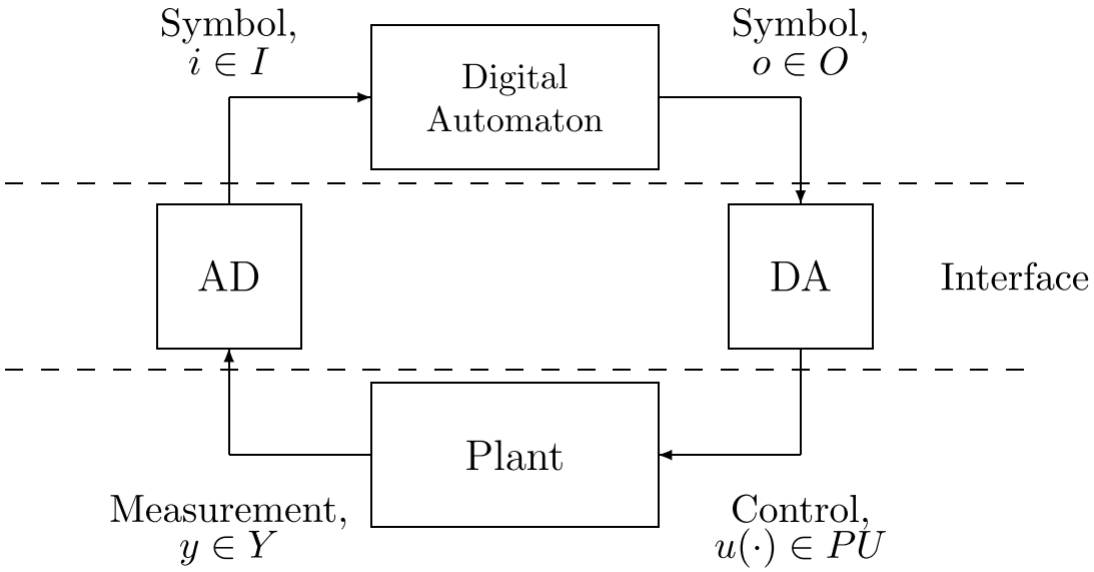

Figure 8: Hybrid system model of Nerode and Kohn. Figure from [9].

The same year, **Antsaklis, Stiver and Lemmon** considered discrete-event dynamical systems, which are closely related to the model of Narode and Kohn [6]. The interface between the discrete controller and the continuous plant is given particular attention. The digital-to-analog mapping, here called *actuating function*, is implemented as a piecewise constant plant input. The analog-to-digital mapping (here called *generating function*) is implemented by partitioning the statespace by hypersurfaces, and issuing symbols to the discrete controller when the continuous state crosses these.

More recently (2004) **Goebel, Hespanha, Teel, Chaohong and Sanfelice** introduced a model based on a *constrained differential inclusion* and a *constrained difference inclusion*. The notion of a generalized solution was introduced, and in the following years many of the stability results from continuous-time nonlinear systems (from e.g [15]) were proved for their hybrid system model. Because of the expressive power of this model, and the fact that it builds on concepts that are familiar to most control engineers, this model will used in this thesis. The model is presented in detail in Section 3.4.
This model was recently extended to consider *stochastic hybrid dynamical systems*, which is still an active area of research.

3.3 Marine hybrid control systems

The predominant application of hybrid control in motion control systems is to switch between stabilizing controllers. An example is switching between a high-performance/low-robustness controller when close to the reference and a low-performance/high-robustness controller when further away. This is called *supervisory switching control*, and is treated in detail by Hespanha et al. in [12], [14] and [16]. This is not a trivial problem, because interestingly, switching between stabilizing controllers may yield an unstable hybrid system. Using the results of Hespanha et al., supervisory switching control has been successfully applied to control of aircraft and land-based vehicles.

The results of Hespanha et al. have also been used by Nguyen, Sørensen and Quek to design supervisory switching controllers for marine surface vessels. The architecture of this control system is shown in Figure 9. A bank of candidate controllers and candidate observers are run in parallel. A switching signal is calculated

based on which observer is closest to the measured output. This was applied to switch from calm to extreme seas in 2007 [17], and from station keeping to transit in 2008 [20].

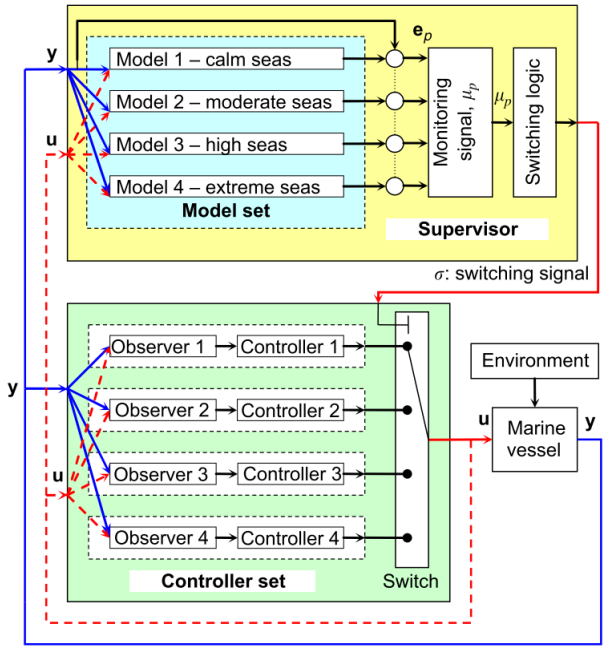

Figure 9: Hybrid control system architecture used by Nguyen et al. Figure from [17]

In 2016, Tutturen and Skjetne used the hybrid framework of Teel et al. [22] to design a hybrid controller to switch between agressive/non-agressive integral action for dynamically positioned vessels.

In 2018, Brodtkorb et al. designed a hybrid observer for marine vessels in DP, also using the framework of Teel et al. [34]. Here, the a passive nonlinear observer of Fossen and Stand [11] was used in steady state, and the signal based observer of Grip et al. [27], utilizing acceleration measurements, was used during transient behaviour.

3.4 Mathematical framework for hybrid dynamical systems

In Section 3.2, several mathematical frameworks for hybrid systems were presented. In this section, the framework of Goebel et al. is presented in greater detail. This framework is very general, and thus has great expressive power. Also, it extends well known concepts from nonlinear systems theory to hybrid dynamical systems. This makes is familiar for people with a control engineering background, and also simplifies the development of stability proofs, as existing stability results for continuous components may be adopted. The reader is referred to [22] for details.

In this framework, a hybrid dynamical system, $\mathcal{H} = (C, F, D, G)$, is modelled as a *constrained differential inclusion* and a *constrained difference inclusion*:

$$x \in C \quad \dot{x} \in F(x) \tag{35a}$$

$$x \in D \quad x^+ \in G(x) \tag{35b}$$

When x is in the set C, it *flows* according to the *set-valued mapping* $\dot{x} = f(x)$ for some $f \in F$. When x is in the set D, it *jumps* according to set-valued mapping $x^+ = g(x)$ for some $g \in G$. x^+ denotes the value of

x after the jump.

Goebel et al. continues to give a precise definition of the solutions to $\mathcal{H} = (C, F, D, G)$. To arrive at this, two other definitions are needed first. The first is the notion of a *hybrid time domain*.

Definition 3.1. *Hybrid time domain ([22] Def. 2.3)*
A subset $E \subset \mathbb{R}_{\geq 0} \times \mathbb{N}$ is a compact hybrid time domain if

$$E = \bigcup_{j=0}^{J-1} ([t_j, tj + 1], j)$$

for some finite sequence of times $0 = t_0 \leq t_1 \leq t_2 ... \leq t_J$. It is a hybrid time domain if for all $(T, J) \in E$, $E \cap ([0, T] \times \{0, 1, ..., J\})$ is a compact hybrid time domain.

where $\cup$ is the set union, $\cap$ is the set intersection and $\times$ is the cartesian product.

Next, the notion of *hybrid arcs* is defined.

Definition 3.2. *Hybrid arc ([22] Def. 2.4)*
A hybrid arc $\phi : E \mapsto \mathbb{R}^n$ is a hybrid arc if E is a hybrid time domain and if for each $j \in \mathbb{N}$, the function $t \mapsto \phi(t, j)$ is locally absolutely continuous on the interval $I^j := \{t : (t, j) \in E\}$.

A function is *locally absolutely continuou* if the derivative is continuous for almost all times, and the function can be recovered by integrating the derivative.

Finally, the notion of a solution to $\mathcal{H} = (C, F, D, G)$ can be defined.

Definition 3.3. *Solution to a hybrid system ([22] Def 2.6)*
A hybrid arc ϕ is a solution to a hybrid system $\mathcal{H} = (C, F, D, G)$ if $\phi(0, 0) \in \bar{C} \cup D$, and

(i) for all $j \in \mathbb{N}$ such that $I^j := \{t : (t, j) \in dom(\phi)\}$ has a nonempty interior

$$\phi(t, j) \in C \quad \text{for all} \quad t \in int(I^j)$$

$$\dot{\phi}(t, j) \in F(\phi(t, j)) \quad \text{for almost all} \quad t \in I^j$$

(ii) for all $t, j \in dom(\phi)$ such that $(t, j + 1) \in dom(\phi)$

$$\phi(t, j) \in D$$

$$\phi(t, j + 1) \in G(\phi(t, j))$$

where $\bar{C}$ is the closure of the set C, $dom(\phi)$ is the domain of ϕ and $int(I^j)$ is the interior of the set I^j.

Goebel et al. continues to define the notion of *well-posed hybrid systems*, and give conditions $\mathcal{H} = (C, F, D, G)$ must satisfy for well-posedness. Concepts such as Lyapunov functions, Lyapunov stability, Asymptotic stability and Uniform stability are defined next, with several results with conditions for which stability can be proved. See [22] for details.

4 Disturbance estimation and rejection using acceleration measurements

External disturbances and modelling errors degrade controller performance, and methods for counteracting this are called *disturbance rejection*. The classical approach to disturbance rejection is integral action. This is a good approach for slowly varying disturbances, but rapidly changing disturbances are challenging. Integral action has a destabilizing effect on the feedback loop, and there is thus a limit to how fast an integrator can be.

For motion control systems, an alternative approach is to extend the sensor suite with an accelerometer. Knowledge of the acceleration is very interesting, as it is possible to calculate sum of forces acting on the body from it, if the inertia of the system is known. By subtracting the known control input and model based terms, it is possible to get an estimate of the disturbances. In the extreme case, it is possible to design a model free controller, where all forces acting on the body are considered as disturbances. Then, these can be estimated and counteracted, and the feedback loop may be shaped as desired.

This approach to control is not commonly used. There are several reasons for this. As described in 2.3.2, accelerometers are often corrupted by sensor noise and sensor bias, and also their measurements include the gravitational acceleration. To remove gravity from the measurement, accurate knowledge of the three axis attitude is required, which is not always trivial to find. If the sensor is not placed in the center of gravity, the measurements will include accelerations due to angular accelerations and centripetal accelerations. Centripital accelerations can be removed with the knowledge of the angular velocities of the body. Angular rate sensors are usually packaged together with acceleromenters in IMUs, as mentioned in Section 2.3.2. Angular accelerations are, however, seldom measured, and accelerations induced by these can thus not be removed in the case of a single IMU. Also, the accelerations of interest in control applications are often small in magnitude compared to other accelerations, such as vibrations and impulsive loads. Careful filtering is thus often necessary. A final, important reason is historic: IMUs have previously been very expensive. However, this is changing fast with the advent of Micro Electrical-Mechanical Sensor technology (MEMS). Compact, high quality sensors are now available at a fraction of the price of legacy technologies [21].

The topic of disturbance rejection by acceleration feedforward has been treated by Kjerstad and Skjetne in 2016, with applications to dynamic positioning in ice [30]. The authors also propose a solution for removing the acceleration terms due to the sensor being offset from CG, by using 4 spatially distributed IMUs.

In this section, disturbance estimation and rejection using acceleration measurements is investigated. This may be an important component in a hybrid control system for ferries, because as previously mentioned, there are rapidly changing hydrodynamic forces the hull during the transition mode, which are not easily modelled. Also, ferries often operate across narrow fjords with strong cross currents. When the ferry approaches the dock, this current will abruptly change as the ferry comes in shelter behind the pier. Classical integral action may not be fast enough to handle this well, and alternative solutions are thus called for.

4.1 Rigid body modelling for motion control

This section presents a rigid body model suitable for control purposes, and shows how a disturbance force can be expressed in terms of accelerometer measurements.

Consider a rigid body in three dimensional space with mass m_{RB}. Assuming NED to be inertial, Newtons second law of motion gives

$$m_{RB}\dot{v}^n = F^n \tag{36}$$

where $F^n \in \mathbb{R}^{3\times 1}$ is the sum of forces acting on the body.

For control purposes, the motion is most conveniently expressed in the BODY frame. Velocities in the BODY frame are related to the NED frame by

$$v^n = Rv^b \tag{37}$$

where $R \in \mathbb{R}^{3\times3}$ a rotation matrix, given in [21].
Time differentiation of (37) yields

$$\dot{v}^n = \dot{R}v^b + R\dot{v}^b = RS(\omega^b)v^b + R\dot{v}^b \tag{38}$$

where $\omega \in \mathbb{R}^{3\times1}$ is the angular velocity of the BODY frame relative to the NED frame.

Furthermore, let F be split into an actuating term, τ, a known model based term, ρ, and an unknown disturbance term, d. Inserting this and (38) into (36) yields

$$m_{RB}R(S(\omega^b)v^b + \dot{v}^b) = R(\rho^b + \tau^b + d^b) \tag{39}$$

Multiplying both sides by R^T and using the orthonormal property, $R^T = R^{-1}$ yields

$$m_{RB}\dot{v}^b = -m_{RB}S(\omega^b)v^b + \rho^b + \tau^b + d^b \tag{40}$$

Next, consider an ideal model for an IMU placed in the center of gravity, simplified from (15):

$$f_{imu} = R^T\dot{v}^n - R^Tg^n \tag{41}$$

where $g \in \mathbb{R}^{3\times1}$ is the gravitational acceleration.

Again using (38) yields

$$f_{imu} = S(\omega^b)v^b + \dot{v}^b - R^Tg^n \tag{42}$$

Inserting the body frame acceleration, $\dot{v}^b$ from (42) into (40) gives

$$m_{RB}(f_{imu} - S(\omega^b)v^b + R^Tg^n) = -m_{RB}S(\omega^b)v^b + \rho^b + \tau^b + d^b \tag{43}$$

where it can be observed that the coriolis terms cancel. Solving for the disturbance, d^b, yields finally an expression of the disturbance in terms of an accelerometer measurement:

$$d^b = m_{RB}(f_{imu} + R^Tg^n) - \rho^b - \tau^b \tag{44}$$

4.2 Disturbance estimation and rejection

Using the results from the previous section, a controller setup combining classical feedback control with disturbance estimation and rejection is proposed in this section.

Let the actuating term, τ^b be split into a nominal term τ^b_{nom} and a feedforward term τ^b_{ff}:

$$\tau^b = \tau^b_{nom} + \tau^b_{ff} \tag{45}$$

τ_{nom} can be chosen to yield the desired behaviour for the *nominal control plant model*

$$m_{RB}\dot{v}^b = -m_{RB}S(\omega^b)v^b + \rho^b + \tau^b \tag{46}$$

Next, let the tracking law for the disturbance estimator be:

$$\dot{\hat{d}}^b = \gamma(d^b - \hat{d}^b) \tag{47}$$

where $\hat{d}^b$ is the disturbance estimate and γ is an estimator gain. Note that d^b in this expression is of course not known, so this law can not be used in its current form.

The feedforward actuation force is chosen to cancel the disturbance, such that $t_{ff}^b = -\hat{d}^b$.

Inserting $\tau^b = \tau_{nom}^b - \hat{d}^b$ into (44) gives the sought after corrective term from (47) in terms of the accelerometer measurements:

$$d^b - \hat{d}^b = m_{RB}(f_{imu} + R^T g^n) - \rho^b - \tau_{nom} \tag{48}$$

The final equations for the combined controller and estimator stated next:

$$\tau^b = \tau_{nom}^b - \hat{d}^b \tag{49a}$$

$$\dot{\hat{d}}^b = \gamma(m_{RB}(f_{imu} + R^T g^n) - \rho^b - \tau_{nom}) \tag{49b}$$

4.3 Wave filtering of acceleration measurements

A challenge for using acceleration measurements in motion control of marine surface vessels, is that the measurements can be strongly influenced by the wave motion of the ship. Normally, it is not desirable to control the first order wave frequency motion, as it is too fast and large for the ships actuators to counteract and will therefore only contribute to increased wear and tear.

For marine surface vessel, only the surge and sway components of the acceleration measurements are of interest, since the heave motion is rarely controlled. Wave frequency components in the surge and sway measurements may enter in several ways:

1. Due to actual acceleration in surge and sway from the wave motion
2. Due to angular acceleration if the sensor is not placed at the center of rotation.
3. Due to errors in the gravity compensation caused by inaccurate roll and pitch estimates.

The latter may be significant because the gravitational acceleration is usually very large compared to the low-frequency horizontal acceleration. Small errors in the roll and pitch estimates may thus give significant horizontal accelerations.

Wave filtering by applying a notch filter on the signal will give a phase lag in the output. Wave filtering based on Kalman filters has been used succesfully for model based position and velocity observers for many years, with low phase lag [36]. A challenge with wave filtering of acceleration measurements is that a model for how the acceleration changes is usually not available. Neither are jerk measurements. Wave filtering without phase lag is therefore challenging.

A Kalman filter for wave and noise filtering of acceleration measurements is proposed next. The stochastic control plant model used in the Kalman filter design is:

$$\dot{\xi} = a_w \tag{50a}$$

$$\dot{a}_w = -\Omega^2 \xi - 2\Gamma\Omega a_w + w_1 \tag{50b}$$

$$\dot{a} = w_2 \tag{50c}$$

$$y = a + a_w + v \tag{50d}$$

(50a)-(50b) is a two degree of freedom damped harmonic oscillator driven by Gaussian white noise, $w_1 \in \mathbb{R}^{2\times 1}$. This is modelling the wave frequency component of the acceleration. It is defined by a diagonal matrix

of filter frequencies, $\Omega \in \mathbb{R}^{2\times 2}$, and a diagonal matrix of filter damping ratios, $\Omega \in \mathbb{R}^{2\times 2}$.

In (50c), the dynamics of the low-frequency acceleration, $a \in \mathbb{R}^{2\times 1}$, is given by a Wiener model (see [36]) driven by Gaussian white noise, $w_2 \in \mathbb{R}^{2\times 1}$.

The measurement model states that the measured acceleration, $y \in \mathbb{R}^{2\times 1}$, is the sum of the low-frequency acceleration and the wave frequency acceleration. The measurement is subject to additive Gaussian white noise, $v \in \mathbb{R}^{2\times 1}$.

This model can be written in state-space form as

$$\dot{x} = Ax + Ew \tag{51}$$

$$y = Cx \tag{52}$$

$$x = [\xi^T, a_w^T, a^T]^T, \quad w = [w_1^T, w_2^T]^T \tag{53}$$

$$A = \begin{pmatrix} 0_{2\times 2} & I_{2\times 2} & 0_{2\times 2} \\ -\Omega^2 & -2\Gamma\Omega & 0_{2\times 2} \\ 0_{2\times 2} & 0_{2\times 2} & 0_{2\times 2} \end{pmatrix} \tag{54}$$

$$E = \begin{pmatrix} 0_{2\times 2} & 0_{2\times 2} \\ I_{2\times 2} & 0_{2\times 2} \\ 0_{2\times 2} & I_{2\times 2} \end{pmatrix} \tag{55}$$

$$C = \begin{pmatrix} 0_{2\times 2} & I_{2\times 2} & I_{2\times 2} \end{pmatrix} \tag{56}$$

With a stochastic state space model in place, a Discrete Time Kalman filter may be designed, see e.g. [21]. Using the output of the Kalman filter in place of f_{imu} in (49) should give a reduction of the wave frequency component entering the control loop. However, care must be taken when tuning the Kalman filter, since there will be a trade-off between the level wave filtering and phase lag.

4.4 Case study: Decoupled surge model

In this section, a case study is performed to evaluate the performance of methodology presented in this chapter, and illustrate its use.

The plant used in the case study is the *decoupled surge model* of [21]. This is a nonlinear, first order model to describe the surge dynamics of a ship:

$$(m_{RB} - X_{\dot{u}})\dot{u} - X_u u - X_{|u|u}|u|u = \tau_X \tag{57}$$

where $X_{\dot{u}}$ is the surge added mass, X_u is the linear surge drag coefficient and $X_{|u|u}$ is the quadratic surge drag coefficient. The control objective is to regulate the surge speed to a constant reference. All parameters used in this case study can be found in Appendix A.1.

First, perfect measurement of the surge acceleration is assumed. A model-free approach is used, where both the added mass force, $X_{\dot{u}}\dot{u}$, and the hydrodynamic drag, $X_u u + X_{|u|u}|u|u$, are considered to be unknown disturbances to be estimated. The nominal control law is chosen to be a proportional controller. The performance of this controller is compared to a PI controller with equal proportional gain to evaluate its disturbance rejection capabilities. The ship travels at a constant speed of 5 m/s. After 50 seconds, it is attacked by a disturbance in form of a square pulse with amplitude 50 kN and a duration of 100 seconds.

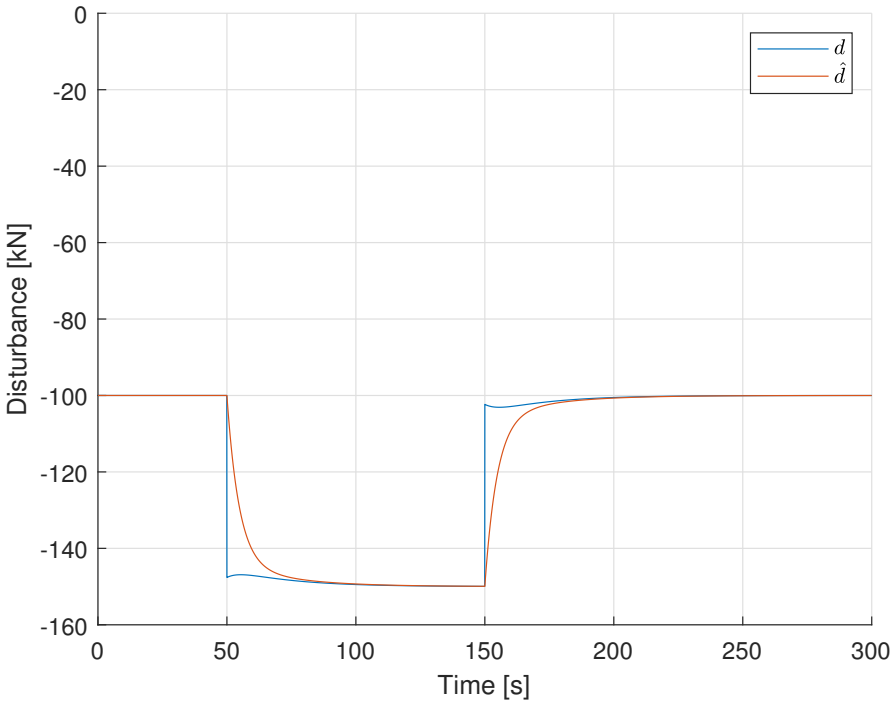

Figure 10: Disturbance tracking of a square pulse

Figure 10 shows the estimated disturbance compared to the true disturbance (pulse + drag + added mass force). It indicates that the disturbance tracking law tracks the true disturbance very well with no steady-state offset and no overshoot. In the case of perfect acceleration measurements, the estimator can track the disturbances arbitrarily fast with no overshoot by increasing the value of γ in (49).

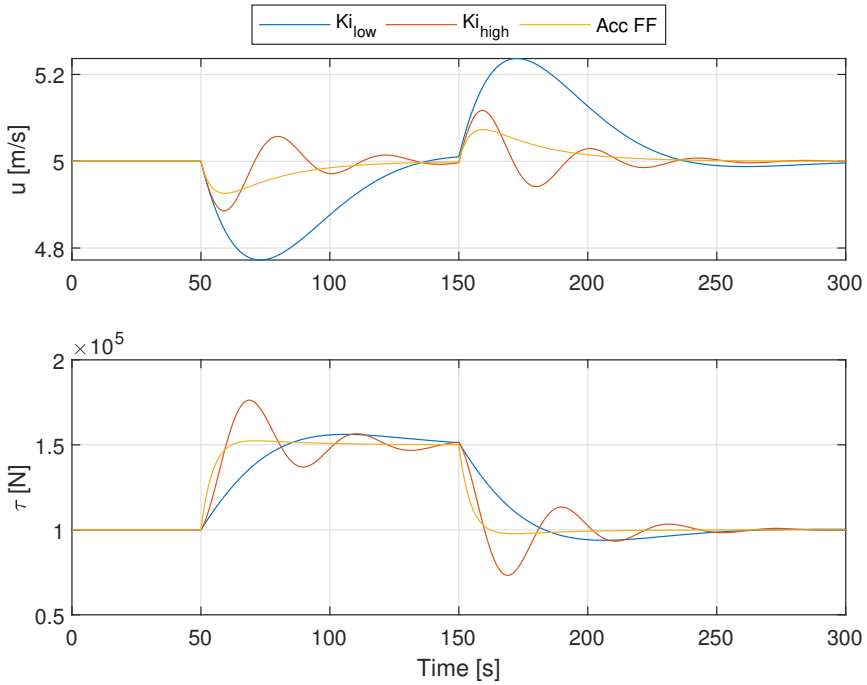

Figure 11: Control performance of the acceleration based controller compared to fast/slow integral action for a square pulse disturbance

Figure 11 shows the control performance of the speed controller compared with a PI controller with fast and slow integration. Compared to the slow integrator, acceleration based controller offers significantly lower tracking error. This can be improved by using a faster integral term, however, this inevitably introduces oscillations. This indicates that the disturbance rejection capabilities of the acceleration based controller can not be matched by traditional feedback integral action.

As discussed in Section 4.3, wave motion may corrupt the acceleration measurements in several ways. The effect of this on the disturbance estimation and rejection is investigated next.

To evaluate this, a sinusoidal wave is superimposed on true acceleration. In addition, zero-mean Gaussian white noise is added to model sensor noise. For simplicity, the waves are assumed to only affect the measurements, not the actual acceleration.

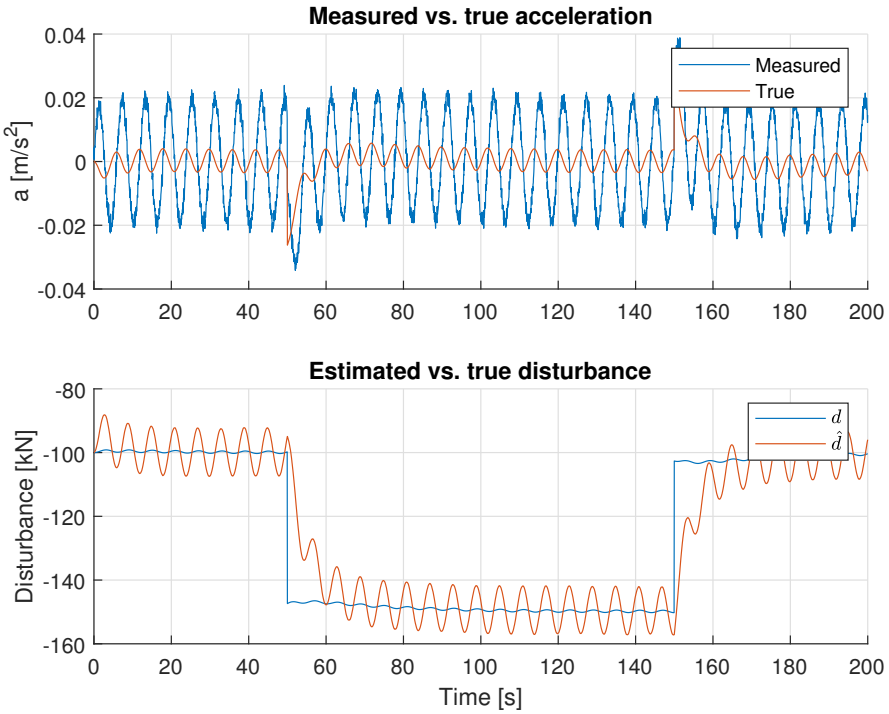

Figure 12: Measured and true acceleration and disturbance tracking for decoupled surge model attacked by a square pulse disturbance in waves.

Figure 12 shows the measured and true accelerations and the disturbance tracking. It shows that the disturbance estimate has a large wave frequency component. Figure 13 shows that this induces unacceptable wave frequency oscillations in the control action which in turn yields an oscillatory surge velocity.

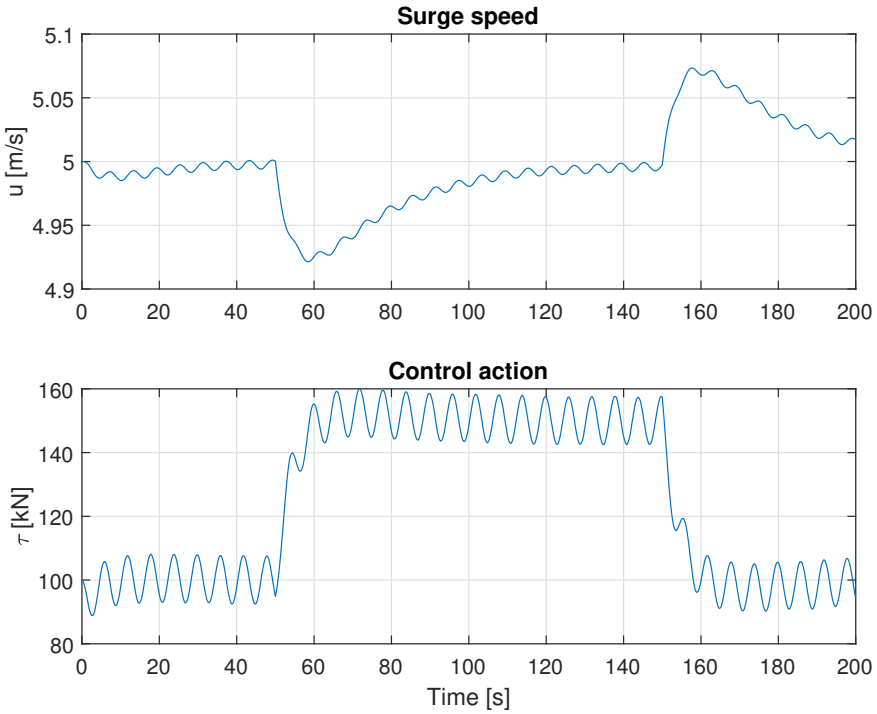

Figure 13: Control performance for decoupled surge model attacked by a square pulse disturbance in waves.

To address the problems due to wave motion and sensor noise, the Kalman filter of Section 4.3 is introduced, and the wave filtered acceleration is used in place of the measured acceleration in the disturbance estimator.

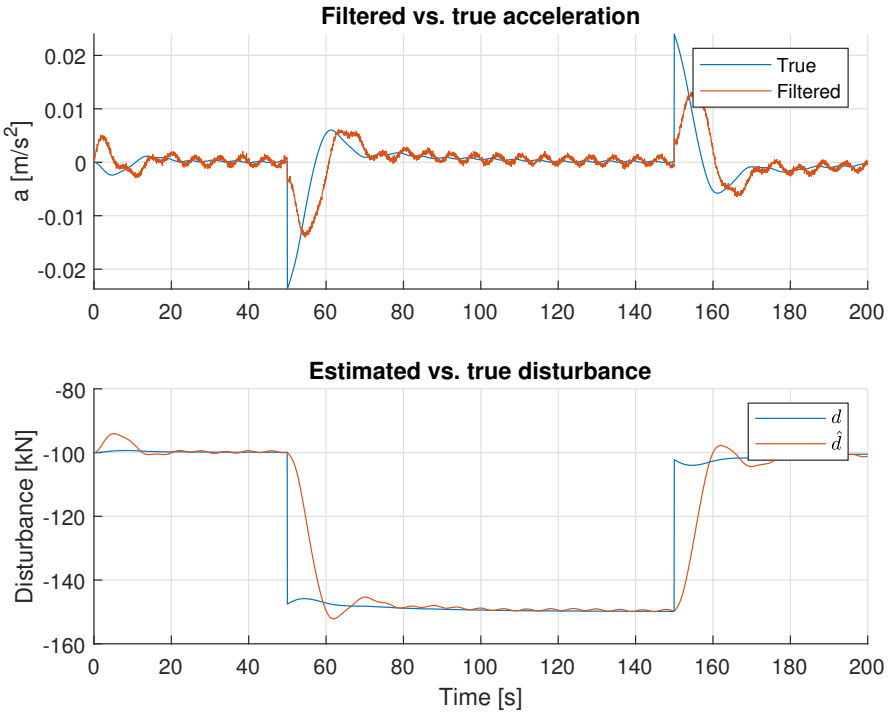

Figure 14: Measured and Kalman filtered acceleration and disturbance tracking for decoupled surge model attacked by a square pulse disturbance in waves.

Figure 14 shows that the filtered acceleration successfully suppresses most of the wave frequency signal component of Figure 12. However, the filtering introduces a significant phase lag. The disturbance estimation almost completely supresses the wave frequency component present in Figure 12, but also has a slight overshoot. This is believed to be caused by the phase lag introduced by the Kalman filter.

When tuning the covariance matrices of the Kalman filter, there is a trade-off between the wave and noise filtering capabilities and the phase lag introduced. In other Kalman based wave filters, such as e.g. [36], there is almost no phase lag. This is because they are filtering the position and heading measurements, and they have a vessel model to predict how this will change ahead of time. In general, there is no model for how the acceleration will change. In the wave filter of (50) the time derivative of the low-frequency acceleration is therefore assumed to be zero-mean Gaussian white noise. This results in greater phase lag.

The severity of the overshoots observed in Figure 14 increases with increasing γ in the disturbance estimator. The presence of a wave filter therefore limits how fast the disturbance estimator can be.

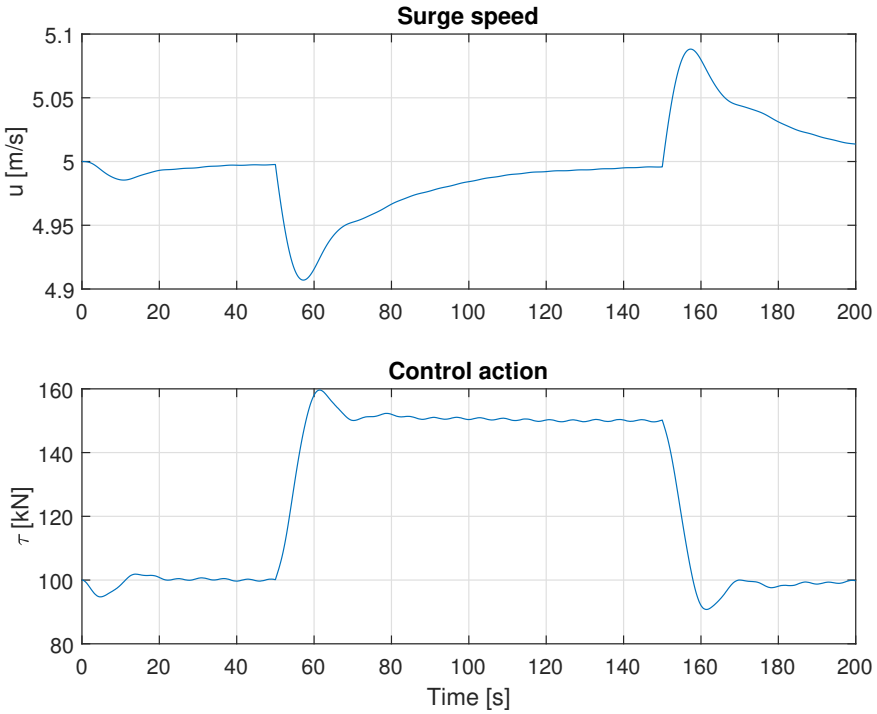

Figure 15: Control performance with acceleration filtering for decoupled surge model attacked by a square pulse disturbance in waves.

Figure 15 shows that the problem with oscillatory control action is handled by the wave filter. The surge speed tracking performance is slightly worse compared to the case with no waves, due to the overshoots of the disturbance estimator. However, it is still superior to the PI controller.

Finally, it is noted that the acceleration based control law used here can not handle biased acceleration measurements. An acceleration bias will lead to a steady-state offset in the disturbance estimation which will give a steady-state offset in the speed control. Proper sensor calibration and alignment is thus paramount for a successful implementation. To gain robustness against biased acceleration measurements, it may be a advantageous to add a very slow integral action to the nominal control law to mitigate the steady-state offset.

5 Control allocation for double ended ferries

In this section, a novel control allocation algorithm is proposed for double ended ferries. It features a fast, nonlinear solving strategy and is inspired by how the captain performs thruster control manually today. Figure 16 illustrates the thruster configuration and definitions used in this section.

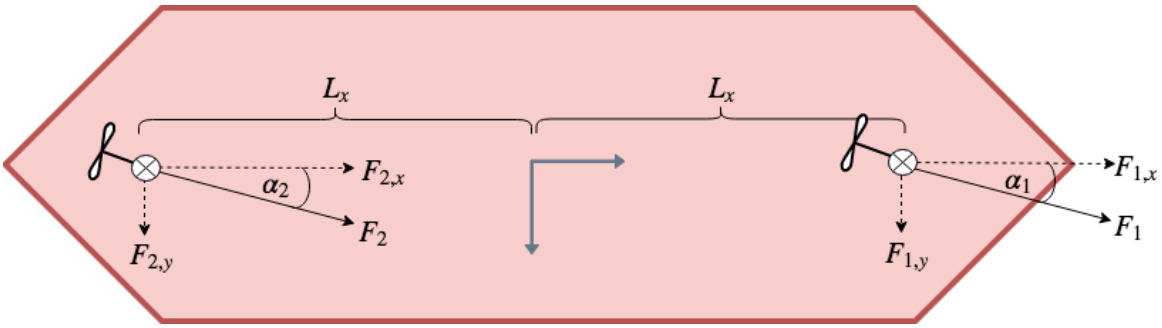

Figure 16: Thruster configuration and definitions for double ended ferries.

5.1 Manual thruster control for double ended ferries

After independent communication with two professional ferry captains, they have described how manual thruster control is performed in car ferries today. This approach has also been experimentally tested on the Autoferry prototype milliAmpere, as described in Section 1.1.

When approaching the dock, one thruster is turned 180 degrees, and both thruster are given a steady, non-zero thrust. To control the surge force, the thrust of one thruster is increased and the other is decreased. To control the sway force, the thrusters are rotated in opposite direction. To control the yaw torque, the thrusters are rotated in the same direction. The advantage of this method is that it yields much faster response from commanded control action to actual control action. This is particularly apparent in surge. With this method, a change of surge force is simply a matter of a small increase or decrease of the RPM or pitch on the thrusters. With both thursters oriented the same direction, the thrusters would need to rotate the azimuths 180 degrees. A typical turn rate for an azimuth for a double ended ferry is 10-20 degrees per second. A reversal of thrust by turning the azimuth would therefore take about 15 seconds. This may be unacceptable in many cases, and would certainly degrade the performance of an automated docking controller. A thrust allocation algorithm for double ended ferries should thus be able to support such a mode of operation.

5.2 Nonlinear scalar allocation algorithm

As mentioned in the Section 2.5.1, the two most commonly used methods for thrust allocation is Pseudo Inverse and Linearized QP, and they both have their limitations. For the case of double ended ferries, as described in Section 7.2, they inhabit both starboard/port symmetry and fore/aft symmetry in hull shape and thruster configuration. By exploiting this symmetry, a novel thrust allocation algorithm is proposed. This can solve the full nonlinear optimization problem fast and robustly.

When setting up the thrust configuration matrix for a double ended ferry, the extended thruster configuration form is used, that is, each thruster is divided into two virtual, fixed thrusters; one pointing in pure surge, and one in pure sway. This removes the dependence of the azimuth angles from the thrust configuration matrix. If the thrust allocation algorithm allocates forces F_x and F_y to the two virtual thrusters constituting a thruster, its thrust, F, can be calculated from

$$F = \sqrt{F_x^2 + F_y^2} \tag{58}$$

The azimuth angle, α, can be calculated from

$$\alpha = arctan(\frac{F_y}{F_x}) \tag{59}$$

Using this, the thrust configuration matrix, $B : \mathbb{R}^4 \mapsto \mathbb{R}^3$, for a double ended ferry becomes

$$B = \begin{pmatrix} 1 & 0 & 1 & 0 \\ 0 & 1 & 0 & 1 \\ -L_{1,y} & L_{1,x} & -L_{2,y} & L_{2,x} \end{pmatrix} \tag{60}$$

where $L_{i,j}$ is the distance from thruster i to the vessel center in the j direction.

By assigning the index 1 to the front thruster and 2 to the aft thruster, and exploiting the symmetry properties of double ended ferries, it is clear that $L_{1,y} = L_{2,y} = 0$ and $L_{1,x} = L_x = -L_{2,x}$. Applying this to (60) yields

$$B = \begin{pmatrix} 1 & 0 & 1 & 0 \\ 0 & 1 & 0 & 1 \\ 0 & L_x & 0 & -L_x \end{pmatrix} \tag{61}$$

A key observation here is that B is a Rank 3 matrix, whereas there are 4 unknown thrusts to be allocated:

$$u = [F_{1,x}, F_{1,y}, F_{2,x}, F_{2,y}]^T$$

Hence, there is in fact only one degree of freedom in the thrust mapping $\tau = Bu$. The main idea for the new thrust allocation algorithm is to reformulate the original optimization problem with 4 variables (7, if slack variables are introduced, as in (32)) into a bounded scalar optimization problem in the one, free variable of the equation $\tau = Bu$.

To do this reformulation, the structure of the solution space of $\tau = Bu$ is studied. First, the augmented matrix for the linear system is set up:

$$\left(\begin{array}{c|c} B & \tau \end{array} \right) = \begin{pmatrix} 1 & 0 & 1 & 0 & X \\ 0 & 1 & 0 & 1 & Y \\ 0 & L_x & 0 & -L_x & N \end{pmatrix} \tag{62}$$

Next, Gaussian elimination is performed on $\left(\begin{array}{c|c} B & \tau \end{array} \right)$ until the matrix is in reduced row echolon form. This yields the equivalent linear system of equations

$$\begin{pmatrix} 1 & 0 & 1 & 0 & X \\ 0 & 1 & 0 & 0 & \frac{N+L_xY}{2L_x} \\ 0 & 0 & 0 & 1 & -\frac{N-L_xY}{2L_x} \end{pmatrix} \tag{63}$$

Written in matrix-vector form, (63) becomes

$$\begin{pmatrix} 1 & 0 & 1 & 0 \\ 0 & 1 & 0 & 0 \\ 0 & 0 & 0 & 1 \end{pmatrix} \begin{pmatrix} F_{1,x} \\ F_{1,y} \\ F_{2,x} \\ F_{2,y} \end{pmatrix} = \begin{pmatrix} X \\ \frac{N+L_xY}{2L_x} \\ -\frac{N-L_xY}{2L_x} \end{pmatrix} \tag{64}$$

Multiplying out (64) and writing out the components yields:

$$F_{1,x} + F_{2,x} = X \tag{65a}$$

$$F_{1,y} = \frac{N + L_xY}{2L_x} \tag{65b}$$

$$F_{2,y} = -\frac{N - L_xY}{2L_x} \tag{65c}$$

This shows that $F_{1,y}$ and $F_{2,y}$ are uniquely determined, whereas in (65a) there is one degree of freedom. A natural choice for the free variable to parametrize the solution space with, is $F_{1,x}$ or $F_{2,x}$. $F_{1,x}$ is chosen here.

The idea is next to search for an optimal solution by trying different choices of $F_{1,x}$. For each step of the optimization, a candidate $F_{1,x}$ is selected. From this, $F_{2,x}$, $F_{1,y}$ and $F_{2,y}$ can be calculated from (65a) - (65c) such that the thrust configuration constraint is satisfied. Now that all the thrust components are known, the thrust and angle for each thruster can be calculated from (58) and (59). Knowing the thrust and angle for each thruster, a cost function can be defined to penalize e.g. large thrusts or a large change of angle. This shows that the value of a cost function for all possible solutions to (65a) - (65c) can be calculated by only varying $F_{1,x}$. Two great advantages are thus achieved:

1. To search for the optimal solution, we only need to solve a **scalar** optimization problem.
2. For every candidate solution, the thrust configuration constraint, $\tau = Bu$, is automatically satisfied. This removes the need for equality constraints in the optimization problem, and the optimization problem can then be reduced to a **bounded** optimization problem, where the only constraints are fixed bounds on $F_{1,x}$.

The reason why this is a great advantage, is that for scalar, bounded optimization problems, there exists fast and robust nonlinear solvers. Two examples are MATLABs *fminbnd* and Python SciPys *fminbound* using Brents Method[41].

With the theoretical foundation in place, the algorithm is stated next.

Algorithm 1: Nonlinear scalar allocation algorithm

1 Input desired control action, previous thrusts and previous angles;
2 Set bounds for the components of the thruster force;
3 Calculate sway force in front thruster from (65b);
4 Calculate sway force in aft thruster from (65c);
5 Formulate a cost function to minimize;
6 Solve a bounded, scalar optimization problem for the surge force in the front thruster;
7 Calculate the surge force in the aft thruster from (65a);
8 Calculate thrust setpoints from (58);
9 Calculate angle setpoints from (59);

One disadvantage over e.g. the QP solver of Section 2.5.3, is that additional equality or inequality contraints can not be added, such as bounds on the change of angle in one time step. However, this does not represent a big problem, because these can be represented as *soft constraints*, i.e. unwanted behaviour is penalized in

the cost function. Since the cost function may be nonlinear, it gives great flexibility in this respect. The cost function can for instance contain logic in the form

$$\text{if} \quad x > x_{max} \quad : \quad cost = cost + cost_{x_{max}} \tag{66}$$

The algorithms described in this section is quite general. It does not specify how to select the bounds in the scalar optimization problem, and neither how to map the allocated thrusts to angles and RPM. These details depend the specific use case. In the remaining sections of this chapter, specific implementations are presented.

5.3 Control allocation for reversible thrusters

Note that Algorithm 1 only specifies the magnitude and direction of the thrust for the thrusters. In the case of propulsors with reversible thrust, a given thrust vector can be achieved in two different ways, by rotating the propulsor 180 degrees and reversing the thrust.

To accommodate this, the optimization problem in Line 6 of Algorithm 1 may be repeated four times:

- Forward thrust on both thrusters
- Forward thrust on front thruster, reversed thrust on aft thruster
- Reversed thrust on front thruster, forward thrust on aft thruster
- Reversed thrust on both thrusters

The solution with lowest cost of the four is then chosen. Also, since most thrusters are significantly less efficient in reverse, a peanalty for running in reverse may be added to the cost function. See Appendix B.1 for an example cost function implementation.

5.4 Control allocation for non-reversible thrusters

In the case of propulsors for which the thrust can not be reversed, the azimuth thruster at the bow should be turned 180 degrees (pointing forwards), such that a braking force may be produced if necessary. As noted in Section 5.1, failure to do so would result in major delays in the delivered thrust.

This may be achieved by restricting the aft thruster to only produce positive surge thrust, and the thruster at the bow to only produce negative surge thrust. This can be implemented in Algorithm 1 by manipulating the bounds used in the scalar bounded optimization problem.

The requirement for the front thruster is that $F_{1,x} < 0$ and $F_{1,x} > -T_{max}$, where T_{max} is the maximum thrust produced by one thruster.

Similarly, the requirement for the aft thruster is that $F_{2,x} > 0$ and $F_{2,x} < T_{max}$. Since the variable of the optimization problem is $F_{1,x}$, these constrains must expressed in terms $F_{1,x}$. This can easily be achieved using (65a). This gives that $F_{1,x} < X$ and $F_{1,x} > X - T_{max}$. The bounds used in the optimization problem is chosen to be the most restrictive of the two. This yields the following bounds:

$$F_{1,x}^{min} = \max(-T_{max}, X - T_{max}) \tag{67}$$

$$F_{1,x}^{max} = \min(0, X) \tag{68}$$

This approach effectively constrains the aft thruster to operate at angles in the rear half plane, and the thruster at the bow to operate at angles in the front half plane.

If small angular displacements are desirable, a *home angle* may be defined for the thrusters, and deviations from this can be penalized in the cost function. See Appendix B.3 for an example cost function implementation.

In the transition mode, as presented in Section 1.1.1, the ferry will decellerate using mostly the drag forces acting on the ship. Since double ended ferries usually don't have rudders, they are dependent of the thrusters producing thrust in order to turn the ship. Using the control allocation of Section 5.4, this problem is overcome, because the thrusters may produce a turning moment without producing a surge force. Surge forces may also be produced simultaneously if corrections in the speed is necessary.

As described in Section 5.1 the standard practice for manual thrust control during docking is to rotate the thruster at the bow 180 degrees, and give both thrusters an equal mean, and controlling the surge speed by balancing the thrust around this. The control allocation algorithm may easily be extended to support this by defining a *mean thrust* in the cost function, and penalize deviations from this. See Appendix B.2 for an example cost function implementation.

5.5 Case study: Control allocation for docking of double ended ferries with symmetric thruster configuration

In this section, a case study is performed to evaluate the performance of the nonlinear scalar allocation algorithm compared to the pseudo inverse method of Section 2.5.2. Also, it serves to illustrate the use of the newly developed algorithm. All parameters used in this case study can be found in Appendix A.2.

In the case study, a simplified thruster model for a nonreversible azimuth thrusters is used. The thrust dynamics are modelled as a saturated first order system:

$$\dot{T} = \frac{1}{\tau}(T_c - T) \tag{69a}$$

$$T = \max(0, \min(T_{max}, T)) \tag{69b}$$

where T is the produced thrust, T_c is the commanded thrust, T_{max} is the maximal thrust and τ is the thrust time constant.

The closed loop azimuth servo is modelled as a proportional controller from angle offset to servo speed with saturation on the maximal servo speed. The dynamics of the servo is neglected, that is, the commanded servo speed is assumed equal to the actual servo speed.

$$\dot{\alpha} = r \tag{70a}$$

$$r = \max(-r_{max}, \min(r_{max}, -K_p(\alpha - \alpha_c))) \tag{70b}$$

where α is the azimuth angle, α_c is the commanded azimuth angle, r is the servo speed, r_{max} is the maximal servo speed and K_p is the proportional gain.

For the nonlinear control allocation, the generic Algorithm 1 is used with the specific implementation for docking. That is, the front thruster is turned 180 degrees and both thrusters are given a steady-state mean thrust of 25% of the maximal thrust. The cost function used here is given in Appendix B.2.

The pseudo inverse solution for the doubled ended ferries with symmetric thruster configuration is calculated from the extended thrust configuration matrix, B, of (61):

$$u = B^{\dagger}\tau_c \tag{71}$$

where $u = [F_{1,x}, F_{1,y}, F_{2,x}, F_{2,y}]^T$ are thrust components and $\tau_c = [X, Y, N]^T$ is the commanded control action. Index 1 is the front thruster, and index 2 is the aft thruster.

Written out, the solution of (71) is

$$F_{1,x} = \frac{X}{2} \tag{72a}$$

$$F_{1,y} = \frac{N + L_x Y}{2L_x} \tag{72b}$$

$$F_{2,x} = \frac{X}{2} \tag{72c}$$

$$F_{2,y} = -\frac{N - L_x Y}{2L_x} \tag{72d}$$

where L_x is the distance from the thrusters to the vessel center.

From (72a)-(72d) the thruster setpoints can be calculated from (58) and (59).

The desired control action in this case study is calculated from a stochastic first order Gauss-Markov model:

$$\dot{\tau}_c + T_{GM}^{-1}\tau_c = w \tag{73}$$

where $T_{GM}^{-1} \in \mathbb{R}^{3\times3}$ is a diagonal matrix of time constants and $w \in \mathbb{R}^{3\times1}$ is zero-mean Gaussian white noise. When comparing the control allocation methods, the same seed is used for w such that τ_c is equal for both methods.

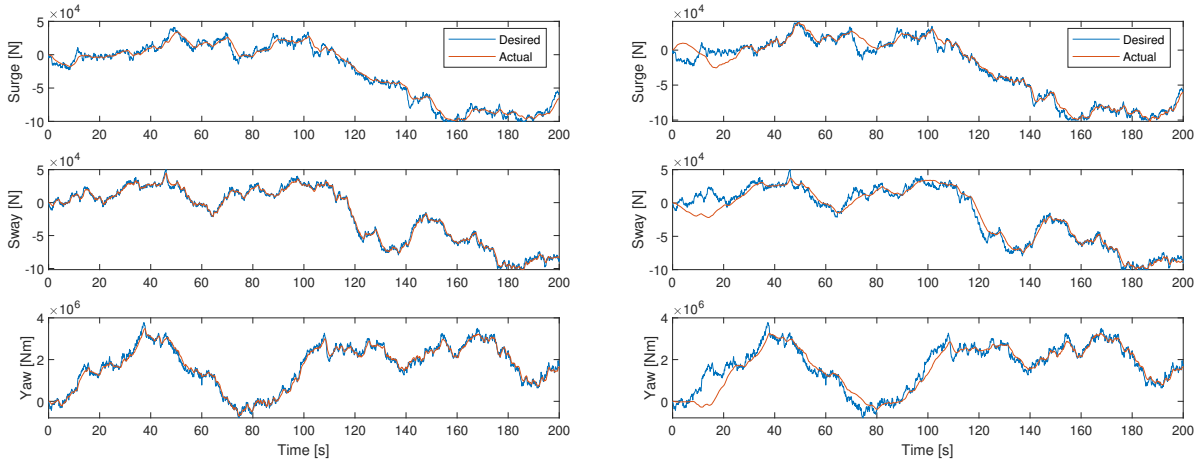

(a) Nonlinear scalar allocation

(b) Pseudo inverse

Figure 17: Commanded and produced forces and moments.

Figure 17 shows the commanded and produced forces and moments from the two control allocation methods. It clearly shows that the nonlinear scalar allocation is better able to produce the desired thrust. Also, the pseudo inverse method sometimes gives large offsets. This is unacceptable when used in motion control loop, as it will give unexpected behaviour and may destabilize the system.

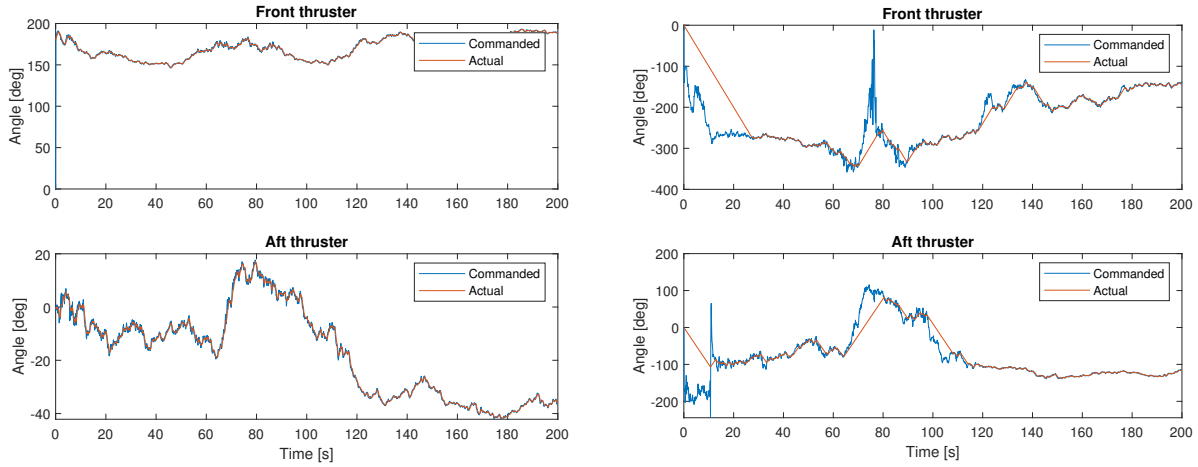

(a) Nonlinear scalar allocation

(b) Pseudo inverse

Figure 18: Commanded and actual azimuth angle.

Figure 18 shows the commanded and actual azimuth angles. It shows that the pseudo inverse method commands an infeasible reference signal for the servos. This leads to the thrusters exerting a force in the wrong direction, and thus explains the erratic behaviour encountered in Figure 17b. From the discussion in Section 5.1, this was expected.

For the nonlinear scalar algorithm, the servos follow their commanded angles very well. It can be observed that the servos work around the home angles of the thrusters (180 degrees for the front thruster, 0 degrees for the aft thruster).

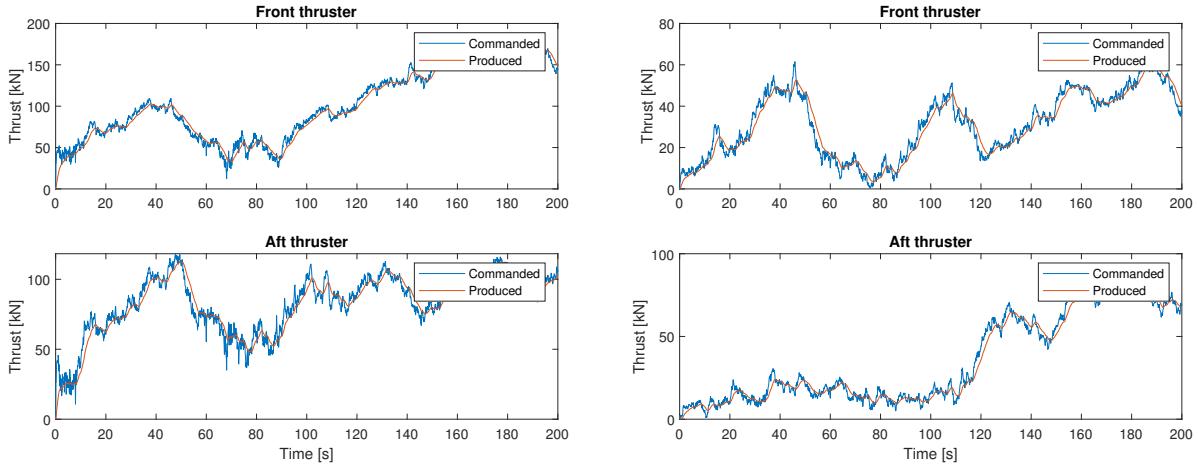

(a) Nonlinear scalar allocation

(b) Pseudo inverse

Figure 19: Commanded and produced thrust.

Figure 19 shows the commanded and produced thrust for the individual thrusters. It shows that in both cases the thruster is able to track is reference quite well. However, the produced thrust is greater in magnitude for the nonlinear scalar allocation. This is as expected since the thrusters have a mean thrust against each other. Also, since the thrusters work in quite small angular offsets away from their home angles, they need to give a larger thrust to produce a given sway force or yaw moment. When tuning the weights in the cost

function for the nonlinear scalar allocation algorithm there is a trade-off between how fast a commanded force is produced and how much thrust is used to produce it. If less weight is enforced on angle change and deviation from home angle and more weight is enforced on thrust usage and thrust change, the algorithm will allow the thruster to have larger angle displacements to use less thrust. However, since the servo speed usually is the limiting factor, this will also yield a larger delay from commanded forces to produced forces.

The findings in this case study indicate that the novel control allocation algorithm is able to solve the allocation problem for ferries very well. Also, it indicates that the simple pseudo inverse solution is unsuited. The quadratic programming method of Section 2.5.3 can probably adress the problems experienced for the pseudo inverse method, however it is still believed to be inferior to the nonlinear scalar algorithm, since it is a linearization of the actual problem and because it is more computationally expensive. Using the MATLAB *quadprog* solver for the quadratic programming method and the MATLAB *fminbnd* solver for the nonlinear scalar method, the latter is, on average, 12.5 times faster for the case considered in this section.

6 A hybrid control system for ferry operations

In this chapter, a hybrid control system for autonomous ferry operations is presented, building on the components developed in Chapters 2, 4 and 5. The modes of operation treated here are **Transit, Transition and Docking**. The components of the control system considered are **Control Allocation, Observer, Motion Control, Guidance and Hybrid Supervisor**, see Figure 4.

To simplify the analysis, control allocation will not be included in the hybrid system. There will a mode switching of the control allocation, this is described in Section 6.1. However, this is decoupled from the rest of the system by assuming that the thrust commanded by motion control is generated instantaneously and exactly. Given that the dynamics of the thrust control is much faster than the motion control, and that the motion control system is robust to modelling errors, this is believed to be a reasonable assumption.

A common observer design for all modes of operation is presented in Section 6.2. Next, in Section 6.3, 6.4 and 6.5 guidance and motion control is presented for Transit, Transition and Docking, respectively. Integrator synchronization for the controllers is treated in Section 6.6. Finally, a switching logic between the modes is proposed and the resulting hybrid dynamical system is established in Section 6.7.

6.1 Switched control allocation

As discussed in Chapter 5, different thrust allocation algorithms are appropriate for the different modes of operation.

For the transit mode, only the aft thruster is used to control the speed and heading. The front thruster will be kept at a constant azimuth angle of 180 degrees, with zero thrust. For the case of a single thruster, the allocation problem is trivial. Motion control commands a surge force, X and a yaw moment, N. Let F_x and F_y be the surge and sway components of the thrust, as in Section 5.2. To generate the desired thrust, it is clear that $F_x = X$ and $F_y = -\frac{N}{L_x}$, where L_x is the distance from the thruster to the vessel center. Using (58) and (59) the thrust setpoint, F, and azimuth angle setpoint, α, is found to be:

$$F = \sqrt{X^2 + \frac{N}{L_x}^2} \tag{74}$$

$$\alpha = \arctan(-\frac{N}{L_x X}) \tag{75}$$

For the transition and docking modes, the designated control allocation algorithms developed in Sections 5.2 and 5.4 will be used.

The control allocation mode will be controlled directly by the switching signal from the hybrid supervisor. Since all the allocation laws are static, that is, they do not depend on time, there is no need for a more involved switching logic. Since the azimuth angle for the front thruster in the transit mode is chosen to be constant equal to 180 degrees, there will not be an unwanted transient in the mode switch from Transit to Transition due to the thruster turning.

6.2 Observer design

As discussed in Section 2.3.2, observers based on inertial navigation are model-free and have excellent transient behaviour. This motivates the choice of using a single INS based observer for all modes of operation.

6.2.1 Observer equations

The chosen observer is the one used by Brodtkorb et al. [34]. That is, the attitude estimation of [27] with the translational motion observer of [25] including the Virtual Vertical Reference. These are presented briefly in Section 2.3.3. Only position measurements are used to aid the translational observer. This is chosen because, as discussed in Section 2.3, GNSS velocity measurements are often inaccurate for low speeds. Furthermore, only heading measurements are used to aid the attitude estimation.

The combined observer equations are stated here for completeness.

$$\dot{\hat{R}} = \hat{R}S(\omega^b_{imu} - \hat{b}^b_{ars}) + \sigma K_P \hat{J} \tag{76a}$$

$$\dot{\hat{b}}^b_{ars} = Proj(\hat{b}^b_{ars}, -k_I vex(\mathbb{P}_a(\hat{R}^T_s K_P \hat{J}))) \tag{76b}$$

$$\dot{\hat{p}}^n_I = \hat{p}^n_{(3,1)} - k_{vvr}\hat{p}^n_I \tag{76c}$$

$$\dot{\hat{p}}^n = \hat{v}^n + C_p \tilde{p}^n \tag{76d}$$

$$\dot{\hat{v}}^n = \hat{f}^n + g^n + C_v \tilde{p}^n \tag{76e}$$

$$\dot{\xi} = -\sigma K_P \hat{J} f_{imu} + C_\xi \tilde{p}^n \tag{76f}$$

$$\hat{f}^n = \hat{R} f_{imu} + \xi \tag{76g}$$

Where $\hat{p}^n_I$ is the virtual vertical reference and $\tilde{p}^n = [-\hat{p}^n_I, N_{gnss} - \hat{p}^n_{(1)}, E_{gnss} - \hat{p}^n_{(2)}]^T \in \mathbb{R}^{3\times 1}$.
The injection gain matrices are

$$C_p = \begin{pmatrix} 0_{2\times 1} & K_p \\ k_{p,vvr} & 0_{1\times 2} \end{pmatrix} \quad C_v = \begin{pmatrix} 0_{2\times 1} & K_v \\ k_{v,vvr} & 0_{1\times 2} \end{pmatrix} \quad C_\xi = \begin{pmatrix} 0_{2\times 1} & K_\xi \\ k_{\xi,vvr} & 0_{1\times 2} \end{pmatrix}$$

where K_p, K_v and $K_\xi \in \mathbb{R}^{2\times 2}$ are injection gains for the horizontal degrees of freedom and $k_{p,vvr}$, $k_{v,vvr}$ and $k_{\xi,vvr}$ are injection gains for the vertical degree of freedom. The other symbols of (76) are described in Section 2.3.3.

6.2.2 A modified attitude estimator for heading measurement injection

In the original attitude estimator of Grip et al. [27], three axis magnetometer measurements was used to aid the attitude observer. However, for marine surface vessels the case is often that only heading measurements are available from an external reference. A different approach is thus necessary. A solution was presented by Bryne et al. [35]. Here, a modification of this approach is proposed for increased accuracy in the attitude estimation.

The measurement injection enters the estimator through the term $\hat{J}$ in (76). $\hat{J}$ is calculated from

$$\hat{J} = \sum_{j=1}^{q} (A^n_j - \hat{R}A^b_j){A^b_j}^T \tag{77}$$

where the matrices A^n_j and A^b_j are related by $A^n_j = RA^b_j$. Grip et al. shows that, under certain assumptions, $\hat{J}$ becomes [27]:

$$\hat{J} = (R - \hat{R})Q^b \tag{78}$$

where Q^b is a matrix satisfying $Q^b \geq \epsilon I$ for some $\epsilon > 0$. From (78) it is clear why $\hat{J}$ is a stabilizing term.

The matrices A_j^b and A_j^n can be constructed in several ways. One approach is the TRIAD algorithm by Shuster and Oh (1981) [3]. Here, vector measurements in the BODY frame, w_j^b, and corresponding vector measurements in the NED frame, w_j^n, are obtained. In the case of two vector measurements, the matrices are calculated from

$$A_1^b = \begin{pmatrix} \frac{w_1^b}{\|w_1^b\|} & \frac{S(w_1^b)w_2^b}{\|S(w_1^b)w_2^b\|} & \frac{S^2(w_1^b)w_2^b}{\|S^2(w_1^b)w_2^b\|} \end{pmatrix}, \quad A_1^n = \begin{pmatrix} \frac{w_1^n}{\|w_1^n\|} & \frac{S(w_1^n)w_2^n}{\|S(w_1^n)w_2^n\|} & \frac{S^2(w_1^n)w_2^n}{\|S^2(w_1^n)w_2^n\|} \end{pmatrix} \tag{79}$$

$$A_2^b = \begin{pmatrix} \frac{w_2^b}{\|w_2^b\|} & \frac{S(w_2^b)w_1^b}{\|S(w_2^b)w_1^b\|} & \frac{S^2(w_2^b)w_1^b}{\|S^2(w_2^b)w_1^b\|} \end{pmatrix}, \quad A_2^n = \begin{pmatrix} \frac{w_2^n}{\|w_2^n\|} & \frac{S(w_2^n)w_1^n}{\|S(w_2^n)w_1^n\|} & \frac{S^2(w_2^n)w_1^n}{\|S^2(w_2^n)w_1^n\|} \end{pmatrix} \tag{80}$$

for S skew-symmetric.

Bryne et al. (2018) [35] and Brodtkorb et al. (2018) [34] use the following measurement vectors:

$$w_1^b = f_{imu}, \quad w_1^n = \hat{f}^n \tag{81a}$$

$$w_2^b = [\cos\psi_m, -\sin\psi_m, 0]^T, \quad w_2^n = [1, 0, 0]^T \tag{81b}$$

where ψ_m is the heading measurement.

(81b) represents a challenge, as it based on the assumption of zero roll and pitch. Experience shows that this has a significant impact on the accuracy of the roll and pitch estimation. As discussed in Section 4.3, accurate roll and pitch estimates are paramount for doing gravity compensation in inertial navigation systems. With this in mind, an alternative approach is proposed next.

From the estimated rotation matrix, $\hat{R}$, estimates of the roll and pitch angle can easily be calculated from

$$\hat{\phi} = \arctan\frac{\hat{R}_{(3,2)}}{\hat{R}_{(3,3)}}, \quad \hat{\theta} = -\arcsin\hat{R}_{(3,1)} \tag{82}$$

Next, an injection attitude, Θ_{inj} is assembled from the estimated roll and pitch and the measured heading

$$\Theta_{inj} = [\hat{\phi}, \hat{\theta}, \psi_m]^T \tag{83}$$

and the corresponding rotation matrix, $R_{inj} = R(\Theta_{inj})$ is calculated.

An alternative measurement vector for w_2^b can then be obtained from

$$w_2^n = [1, 0, 0]^T \quad w_2^b = R_{inj}^T w_2^n \tag{84}$$

The performance of the new attitude estimator is investigated in Section 7.4.

6.3 Transit mode of operation

In the Transit mode of operation, the ferry travels at a high constant service velocity. Because of this, under actuated control is the obvious choice, that is, only surge and yaw are controlled. Since the speed is constant and the curvature of the path is usually low in transit, a simple autopilot design is used.

6.3.1 Guidance

For guidance, the Integral Line-of-sight algorithm presented in Section 2.4.1 is used to generate a heading reference to follow straight-line path segments between waypoints. The switching between waypoints is performed based on the along-track distance to the next waypoint, as apposed to using a radius-of-acceptance. This makes it more robust in the case of large cross-track error when approaching a waypoint. To avoid steps in the heading reference at the instant of waypoint switching, a first order low-pass filter is added on the output from the guidance law. For the speed, a constant forward speed reference is given.

6.3.2 Motion control

For motion control, the heading is controlled using the PID control law of (12). The speed is controlled using the PI control law of (13).

6.4 Transition mode of operation

In the Transition mode, the ferry decelerates from high speed to low speed, and positions itself for docking. This mode presents a challenge from a control perspective. As discussed in Section 4, there will be a rapid change in hydrodynamic forces on the hull, and there may also be rapidly changing current loads. Also, as discussed in Chapter 5.4, energy efficient deceleration will be driven by the drag forces on the hull rather than actively using the thrusters in the transition phase. As double ended ferries normally don't have rudders, they are dependent on the thrusters producing thrust to generate a turning moment. Limited maneuverability is therefore also a challenge.

In the transition mode, the speed will still be too high for overactuated control to be practical. Underactuated control is therefore chosen also here.

6.4.1 Guidance

Adaptive Line-of-sight guidance
In the transition mode, the guidance law is designed to follow a straigh-line path. The heading reference is calculated from the Integral Line-of-signt guidance law, as for the transit mode. However, one big challenge arises here. When using under actuated control, lateral disturbances are counteracted by steering against the disturbance instead of generating a sway force. When the speed becomes low, the ability to withstand lateral disturbances therefore vanishes. Caharija et al. [29] gives conditions for the minimal lookahead distance, Δ, and speed U, required to regulate the cross-track error in path following to zero for a given current speed.

Since the speed is constantly changing in the transition mode, a modification to the Line-of-sight guidance law is proposed by scheduling the lookahead distance based on the vessel speed. This should give adaptive behaviour by increasing the disturbance rejection capabilities at low speed without introducing overshoots at higher speeds.

Consider the kinematic horizontal plane vehicle model for path following of a straight line path

$$\dot{x} = \cos(\psi)u - \sin(\psi)v \tag{85a}$$

$$\dot{y} = \sin(\psi)u + \cos(\psi)v \tag{85b}$$

where x is the along-track position, y is the cross-track error, u is the surge velocity, v is the sway velocity and ψ is the vehicle heading relative to the path.

By assuming $u >> v$, $U = \sqrt{u^2 + v^2} \approx u$. (85b) the becomes

$$\dot{y} = U \sin \psi \tag{86}$$

The control objective is to regulate the cross-track error, y, to zero. The Line-of-sight control law is used:

$$\psi_d = \arctan \frac{-y}{\Delta} \tag{87}$$

Assuming sufficient bandwidth separation between the guidance law and the heading controller, we can approximate $\psi \approx \psi_d$. Inserting the desired heading from (87) for ψ in (86) and using the property $\sin(\arctan(x)) = \frac{x}{\sqrt{1+x^2}}$, the closed loop dynamics for y becomes

$$\dot{y} = \frac{-Uy}{\sqrt{\Delta^2 + y^2}} \tag{88}$$

Linearizing this about $y = 0$, gives finally

$$\dot{y} = -\frac{U}{\Delta} y = -\lambda y, \quad \lambda > 0 \tag{89}$$

which is a stable linear system with convergence rate $\lambda = \frac{U}{\Delta}$.

The proposed adaptive law for Δ is designed to give the same convergence rate for all vehicle speeds:

$$\Delta(t) = \frac{U(t)}{\lambda} \tag{90}$$

where λ is a design parameter.

The performance of the proposed adaptive law is evaluated in Section 7.4.

Cubic speed reference
The speed reference will in this case be time-varying signal. It could for instance be pre-calculated from an optimal speed profile. For simplicity, a cubic interpolation from the high speed, u_0, to the low speed, u_1, is used here. This yields smooth velocity and acceleration references, also at the switching instants. The cubic polynomial used takes the form

$$u_d(t) = c_1 t^3 + c_2 t^2 + c_3 t + c_4 \tag{91}$$

with acceleration reference

$$\dot{u}_d(t) = 3c_1 t^2 + 2c_2 t + c_3 \tag{92}$$

Four conditions are imposed to determine the coefficients c_1, c_2, c_3 and c_4:

1. $u(t) = u_0$
2. $\dot{u}(0) = 0$
3. $u(T) = u_1$
4. $\int_0^T u(t)dt = s_T$

where s_T is the distance between the transition waypoints and T is a specified time to use for the transition.

The two first conditions immediately give $c_3 = 0$ and $c_4 = u_0$. The last two conditions yields a linear system of equations in c_1 and c_2:

$$\begin{pmatrix} T^3 & T^2 \\ \frac{1}{4}T^4 & \frac{1}{3}T^3 \end{pmatrix} \begin{pmatrix} c_1 \\ c_2 \end{pmatrix} = \begin{pmatrix} u_1 - u_0 \\ s_T - u_0 T \end{pmatrix} \tag{93}$$

Solving this, gives the coefficients

$$c_1 = \frac{4(u_1 - u_0)}{T^3} - \frac{12(s_T - u_0 T)}{T^4} \tag{94}$$

$$c_2 = \frac{-3(u_1 - u_0)}{T^2} - \frac{12(s_T - u_0 T)}{T^3} \tag{95}$$

6.4.2 Motion control

For motion control in the transition phase, the concept for disturbance estimation and rejection developed in Chapter 4 is applied.

For the speed control, a model-free approach is used. That is, the model based term, ρ^b in (40) chosen to be zero, and all hydrodynamic forces are thus considered disturbances. This choice is motivated by the difficulty of the hydrodynamic modelling when transitioning from a high-speed regime to a low-speed regime.

It is further assumed that the surge velocity, u, is much greater than the sway velocity, v, such that $U = \sqrt{u^2 + v^2} \approx u$, and that the turn rate, r, is low when following a straight-line path. Then, the coriolis force in surge direction, $m_{RB} r v$, is negligible. The kinetic model then simplifies to

$$m_{RB}\dot{u} = \tau + d \tag{96}$$

A nominal control law is then designed for the nominal control plant model

$$m_{RB}\dot{u} = \tau_{X,nom} \tag{97}$$

The chosen nominal control law is a PI feedback controller with reference feedforward

$$\tau_{X,nom} = m_{RB}\dot{u}_d - K_{p,X}(u - u_d) - K_{i,X}\int (u - u_d)dt \tag{98}$$

The approach of Chapter 4 is followed further to yield the final controller and estimator

$$\tau_X = \tau_{X,nom} - \hat{d}_X \tag{99a}$$

$$\dot{\hat{d}}_X = \gamma(m_{RB}(f_{imu} + R^T g^n)_{(1)} - \tau_{X,nom}) \tag{99b}$$

For the heading control, the approach of Chapter 4 can not be used, since measurements of the yaw acceleration is normally not available. Instead, a different apporach is investigated.

The PID feedback control law of (12) is augmented with a direct feedforward term of the measured sway acceleration:

$$\tau_N = -K_{ff,N}(f_{imu} + R^T g^n)_{(2)} - K_{p,N}(\psi - \psi_d) - K_{d,N}(r - \dot{\psi}_d) - K_{i,N}\int (\psi - \psi_d)dt \tag{100}$$

The rationale of this control law is that in case of an a sway acceleration, caused by e.g. a sudden change in cross current, the ferry should immediately respond by steering in the opposite direction to avoid drifting off the path. However, simulations quickly uncovered that this did not work as intended. This is because when a lateral disturbance attacks the ship, it will turn. When the ship turns, it will inevitably also sideslip. The sideslip motion causes a sway acceleration in the opposite direction of the disturbance, causing the ship to turn the other direction due to the feedforward term. This had a destabilizing effect on the system, and will therefore not be used further. Instead, the simple PID heading controller of (12) is used also for the transition mode. Improved disturbance rejection of lateral disturbances is an important subject for future work, as discussed in Section 8.2.

6.5 Docking mode

In the Docking mode of operation, the ferry maneuvers at low speed until enabling contact with the dock. Here, the speed is low enough for overactuated control to be appropriate and necessary.

6.5.1 Guidance

For guidance, the third-order reference filter of Section 2.4.2 will be used. As opposed to Figure 7, only saturation elements for acceleration will be used, because saturation of velocity may yield a discontinuous velocity reference if the ferry enters docking mode with a greater velocity than the saturation.
The guidance law provides three degree of freedom reference signals for positions, velocities and accelerations. The filter will be initialized with the position and velocity at the instant of switching from Transition. The desired acceleration will be initialized to the desired surge acceleration from the transition mode at the instant of switching, rotated to the NED frame. The setpoint is kept constant equal to the desired position and heading at the dock.

For a complete autodocking system, a more involved guidance system is needed to ensure a collision-free path towards the dock. However, since path planning and collision avoidance is not the focus of this thesis, a reference filter is used for simplicity.

6.5.2 Motion control

For motion control, the nonlinear PID control law of (11) with reference feedforward of velocity and acceleration will be used.

6.6 Integrator synchronization

When switching from one mode to another, it is important to synchronize the states properly. Since the ferry does not have time to stop and build a model of the disturbances, the controller must utilize the states from the previous mode to initialize the new mode.

The integrator states are shared between all three modes of operation, in a vector $\xi \in \mathbb{R}^{3\times 1}$.

6.6.1 Transit to transition

When switching from transit mode to transition mode, there are three states that must be initialized:

- The integrator for the heading PID controller, ξ_N, governed by $\dot{\xi}_N = K_{i,N}(\psi - \psi_d)$
- The integrator for the PI speed controller, ξ_X, governed by $\dot{\xi}_X = K_{i,X}(u - u_d)$
- The disturbance estimate, $\hat{d}_X$, from (99b)

These integral states are related to the shared integrator vector by $\xi = [\xi_X, 0, \xi_N]$ in the transition mode. Note that ξ in this case represents BODY frame forces.

Since the heading controllers are the same for the transition and transit mode, the heading integral state is transferred directly:

$$\xi_N^+ = \xi_N \tag{101}$$

For the speed controller it is assumed steady-state conditions at the instant of switching. Then, the control action in surge will be equal and opposite to the disturbances in surge. Also, in steady state, the control

action will be equal to the integral state. The disturbance estimate is therefore initialized to negative the integral state at the instant of switching.

$$\hat{d}_X^+ = -\xi_X \tag{102}$$

The slow integrator for the speed controller in the transition mode is there only to correct for any steady-state biases or misalignment errors in the accelerometer. Since no knowledge of this exists, the best guess is to initialize it to zero:

$$\xi_X^+ = 0 \tag{103}$$

6.6.2 Transition to docking

When switching from transition to docking, the three degree of freedom integral state for the docking controller must be initialized. In this case, a switch from under actuated to fully actuated control occurs. Also, the integral states for a DP controller is normally calculated in the NED frame, since environmental loads are most likely be close to constant in the NED frame, not the BODY frame.

In the transition mode, the controller was model free. All hydrodynamic forces were considered as disturbances. In the docking mode, the controller is based on the low speed model of Section 2.1.3. The drag and added mass forces should therefore not be included in the integral states for the docking controller.

Since Integral Line-of-sight guidance is used in the transition mode, the vessel will control its heading such that the sway force on the vessel is zero (weathervaning). Assuming steady-state conditions at the instant of switching, the translational body frame disturbance vector will thus be only have a surge element, represented by the disturbance estimate and the surge integral state from the transition mode.

The following jump is proposed:

$$\xi^+ = R(\psi)([-\hat{d}_X + \xi_{(1)}, 0, \xi_{(3)}]^T + D\nu) \tag{104}$$

where $\hat{d}_X$ is the surge disturbance estimate, $R(\psi)$ is the three degree of freedom rotation matrix, $D \in \mathbb{R}^{3\times3}$ is the low speed damping matrix and $\nu \in \mathbb{R}^{3\times1}$ is the three degree of freedom body frame velocity.

The added mass forces are not removed from the integral states since it is assumed that the prevailing acceleration will be in the surge direction, and added mass is typically small in surge [21].

6.7 Resulting hybrid control system

In this section, the combined hybrid system is formulated using the framework presented in Section 3.4.

When formulating the hybrid system, only the plant dynamics and the controllers are considered. The interactions between the plant and the guidance system is not considered. It is assumed that the guidance system only provides the hybrid system with time-varying reference signals, and that the path following control objective is satisfied if the vessel folows its heading reference. The observer error dynamics are not considered, since there is no switching in the observer, and the observer is shown to be UGES in [34]. In the hybrid system, state feedback is thus used, assuming that a nonlinear separation principle holds. The thrust allocation and thruster dynamics are also not included in the hybrid system formulation. It is assumed that the commanded control action from the controller is produced exactly. These assumptions require attention in future work.

For the plant dynamics, a three degree of freedom maneuvering model with coriolis forces and nonlinear damping is used. The model should represent the maneuvering dynamics of the vessel well for both high

speed and low speed by an appropriate choise of the nonlinear damping matrix. The disturbances due to environmental loads are modelled as a slowly varying bias. Wave frequency motion is not included.

The switching between modes is performed when the ferry enters a ball set around prescribed points on the route.

The state vector for the hybrid system is defined as $x = [\eta^T, \nu^T, b^T, \hat{d}_X, \xi, \sigma]^T \in \mathbb{R}^{13} \times \{1, 2, 3\}$ where $\eta = [N, E, \psi]^T$ is the vessel position and heading in the NED frame, $\nu = [u, v, r]^T$ is BODY frame velocity vector, $b \in \mathbb{R}^3$ is the bias vector, $\hat{d}_X$ is the surge disturbance estimate, $\xi \in \mathbb{R}^3$ are the integral states for the controllers and σ is a discrete variable describing the current mode of operation. $\sigma = 1$ for Transit, $\sigma = 2$ for Transition and $\sigma = 3$ for Docking.

The continuous dynamics for the hybrid system can then be written:

$$\dot{\eta} = R(\psi)\nu \tag{105a}$$
$$\dot{\nu} = M^{-1}(-C(\nu)\nu - D_{NL}(\nu)\nu + \tau + b) \tag{105b}$$
$$\dot{b} = -T_b^{-1} b \tag{105c}$$
$$\dot{\hat{d}}_X = \gamma(m_{RB} a^b_{(1)} - (m_{RB}\dot{u}_d - K^{(2)}_{p,X}(u - u_d) - \xi_{(1)})) \tag{105d}$$
$$\dot{\xi} = \begin{cases} [K^{(1)}_{i,X}(u - u_d), 0, K^{(1)}_{i,N}(\psi - \psi_d)]^T & \text{if } \sigma = 1 \\ [K^{(2)}_{i,X}(u - u_d), 0, K^{(2)}_{i,N}(\psi - \psi_d)]^T & \text{if } \sigma = 2 \\ K^3_i(\eta - \eta_d) & \text{if } \sigma = 3 \end{cases} \tag{105e}$$
$$\dot{\sigma} = 0 \tag{105f}$$

where

$$\tau = \begin{cases} [-K^{(1)}_{p,X}(u - u_d) - \xi_{(1,1)}, 0, -K^{(1)}_{p,N}(\psi - \psi_d) - K^{(1)}_{d,N}(r - \dot{\psi}_d) - \xi_{(3)}]^T & \text{if } \sigma = 1 \\ [m_{RB}\dot{u}_d - K^{(2)}_{p,X}(u - u_d) - \xi_{(1)}, 0, -K^{(2)}_{p,N}(\psi - \psi_d) - K^{(2)}_{d,N}(r - \dot{\psi}_d) - \xi_{(3)}]^T & \text{if } \sigma = 2 \\ Ma_d + D\nu_d - R(\psi)^T K^{(3)}_p(\eta - \eta_d) - K^{(3)}_d(\nu - \nu_d) - R(\psi)^T \xi & \text{if } \sigma = 3 \end{cases} \tag{106}$$

The matrices M, $C(\nu)$ and $D_{NL}(\nu)$ are defined in [21] Section 7.1. $T_b \in \mathbb{R}^{3\times3}$ is a diagonal matrix of time constants for the bias model. m_{RB} is the rigid body mass. K_p, K_d and K_i are controller gains. The subscript denotes the degree of freedom and the superscript denotes the mode of operation. $D \in \mathbb{R}^{3\times3}$ is a linear damping matrix. $a_b \in \mathbb{R}^3$ is an input signal representing the acceleration of the ship relative to an inertial frame, minus the body frame gravity vector.

The discrete dynamics can be written as:

$$\eta^+ = \eta \tag{107a}$$
$$\nu^+ = \nu \tag{107b}$$
$$b^+ = b \tag{107c}$$
$$\hat{d}^+_X = -\xi_{(1)} \tag{107d}$$
$$\xi^+ = \begin{cases} [0, 0, \xi_{(3)}]^T & \text{if } \sigma = 1 \\ R(\psi)([-\hat{d}_X + \xi_{(1)}, 0, \xi_{(3)}]^T + D\nu) & \text{if } \sigma = 2 \end{cases} \tag{107e}$$
$$\sigma^+ = \sigma + 1 \tag{107f}$$

Note that the jump map does not include a jump in the case $\sigma = 3$. This is because the solutions to the hybrid system are *eventually continuous*. That is, after the jump from transition to docking, the system will

never jump again.

The solutions can jump from transit to transition if (N, E) is within an open ball set $\delta\mathbb{B}(p_1)$ and $\sigma = 1$. They can jump from transition to docking if (N, E) is within an open ball set $\delta\mathbb{B}(p_2)$ and $\sigma = 2$. δ is a prescribed radius of acceptance, and $p_1, p_2 \in \mathbb{R}^2$ are the selected (N,E) points for switching. The jump set thus becomes

$$D = (\delta\mathbb{B}(p_1) \times \mathbb{R}^{11} \times \{1\}) \cup (\delta\mathbb{B}(p_2) \times \mathbb{R}^{11} \times \{2\}) \tag{108}$$

The solutions can flow in the entire domain of the system. According to Definition 3.3, both solutions that continue to flow and solutions that jump are valid when the jump set and flow set overlap. To avoid this ambiguity, the jump set is removed from the domain to obtain the flow set. The flow set therefore becomes

$$C = (\mathbb{R}^{13} \times \{1, 2, 3\}) \setminus D \tag{109}$$

Denoting the flow map of (105) $f(x)$ and the jump map of (107) $g(x)$, the hybrid system can finally be written as

$$x \in C \quad \dot{x} = f(x) \tag{110a}$$

$$x \in D \quad x^+ = g(x) \tag{110b}$$

7 Case study: Double ended car ferry MF Gloppefjord

With the high research activity related to autonomous ferries, establishing a high-fidelity simulator for testing of control algorithms for ferry operations is called for. In this chapter the development of a simulation platform for the Anda-Lote site and the vessel MF Gloppefjord is the topic. This simulator is currently in use by several master students at NTNU. Then, the entire control system developed in this thesis is tested in the simulator. This includes the guidance system, motion control, observer and control allocation.

7.1 The Anda-Lote crossing

The case used in the simulator is the stretch across Nordfjorden between Anda and Lote at the west coast of Norway. The duration of the crossing is 11 minutes, with departures every 20 minutes from each side. The site is operated by Fjord1 AS.

Figure 20: The ferry strech between Anda and Lote. Source: www.1881.no

The Anda-Lote site features several innovations. One is the fully automated charging and docking tower delivered by Stemmann and Cavotec. The tower includes a robotic arm which grabs the ferry and pulls it to the dock using a vacuum pad, and connects to a charger. See Figure 21.

Figure 21: The charging tower "FerryCharger" and automated docking solution at the Anda-Lote site. Source: Teknisk Ukeblad

The environmental conditions at Anda-Lote are harsh. The site is located deep within the narrow Norwegian fjords, and is therefore sheltered from waves. However, it is exposed to strong cross-currents and winds [33].

7.2 MF Gloppefjord and MF Eidsfjord

The ferries that operate the Anda-Lote site are the sister ships MF Gloppefjord and MF Eidsfjord. The main characteristics of the ferries are given in Table 1.

Table 1: Main characteristics of MF Gloppefjord. Source: [33]

Characteristic	**Value**
Delivered year	2017
Carrying capacity	120 cars + 349 passangers
Length between perpendiculars	102.6m
Length overall	106.0m
Breadth	17.2m
Draft	3.8m
Thrusters	2 x 900kW Azipull
Battery capacity	2 x 540kWh

The ferries have a standard design for double ended car ferries, with fore-aft symmetry in both the hull and the thruster configuration. The ferries also have an automated crossing system delivered by Rolls-Royce.

7.3 Development of a high fidelity simulation environment

The simulator is based on a *SINTEF Ocean VeSim* vessel model for a generic double ended car ferry, kindly provided by Rolls-Royce Marine. The vessel model uses numerical hydrodynamic calculations from well known software, such as Veres and HullVisc. The vessel simulator features:

- A unified maneuvering and seakeeping model
- User provided thruster models
- Environmental loads including current forces, dynamic wind loads from several wind spectra, and first and second order wave loads from several wave spectra.

The vessel model showed erratic behaviour of the thrusters in some cases. Therefore, a simplified thruster model based on (69) and (70) is used in the case study. Also, the vessel model had very low surge damping for low velocities, giving unrealistically long decay times. A modified resistance curve was therefore created, with similar characteristics for high speed but more linear damping at low speed.

For rapid development and testing of control systems *MathWorks Simulink*, is well suited. With this in mind, an interface from VeSim to Simulink was created. Two different approaches was investigated.
First, the VeSim model was imported to Simulink as a Functional Mock-up Unit (FMU). This is a standardized way of packaging models for co-simulation or model exchange. This standard is called Functional Mock-up Interface (FMI) [38]. With support of SINTEF Ocean developers, an FMU export of the VeSim model was created. This model was successfully imported to Simulink using the FMU import tool. However, attempting to run a simulation with the FMU resulted in a terminating crash of Simulink. After lengthy inquiries with SINTEF Ocean and MathWorks, it was discovered to be caused by a bug in the Simulink FMI Master. As of 26.09.2018, Mathworks reports that the bug has been fixed and will be available in the next release of MATLAB 2018b. This approach is attractive since it is built on a standardized interface. However, to ensure progress in the thesis work, a different solution was pursued until the FMI solution is available.

The other solution was based on SINTEF Oceans *Common Simulation Interface* (CSI). This is a simulation bus used for communication between different models. CSI runs as a server, to which models may connect through a network socket. There exists a Java API for CSI. Since MATLAB seamlessly supports Java

scripting, creating a Simulink interface to CSI is feasible. CSI uses publish/subscribe communication. In Simulink, an interface was developed to handle this communication, by interfacing the relevant signals.

In Simulink, sensor models was also developed, as shown in Figure 22. They include:

- A GNSS model, implemented by adding Gaussian white noise to the true North, East and Down positions from the vessel simulator.
- A compass model, implemented by adding Gaussian white noise to the true heading angle from the vessel simulator.
- An IMU model based on the Simulink "Three-Axis Inertial Measurement Unit" block [40]. This model includes sensor noise for the accelerometers and rate gyros, sensor bias for the rate gyros and second order sensor dynamics for the acceleromers and rate gyros. Linking this sensor model to the VeSim model required some preprossesing of signals. BODY frame acceleration from VeSim was obtained, and added to a coriolis term calculated by the true angular and linear velocities of the vessel. The resulting acceleration was input to the IMU sensor model. The true vessel attitude was also obtained, and the NED frame gravitational acceleration was transformed to the BODY frame using this attitude. The resulting BODY frame gravitational acceleration was also input to the IMU sensor model. This is in accordance with (16)-(18).

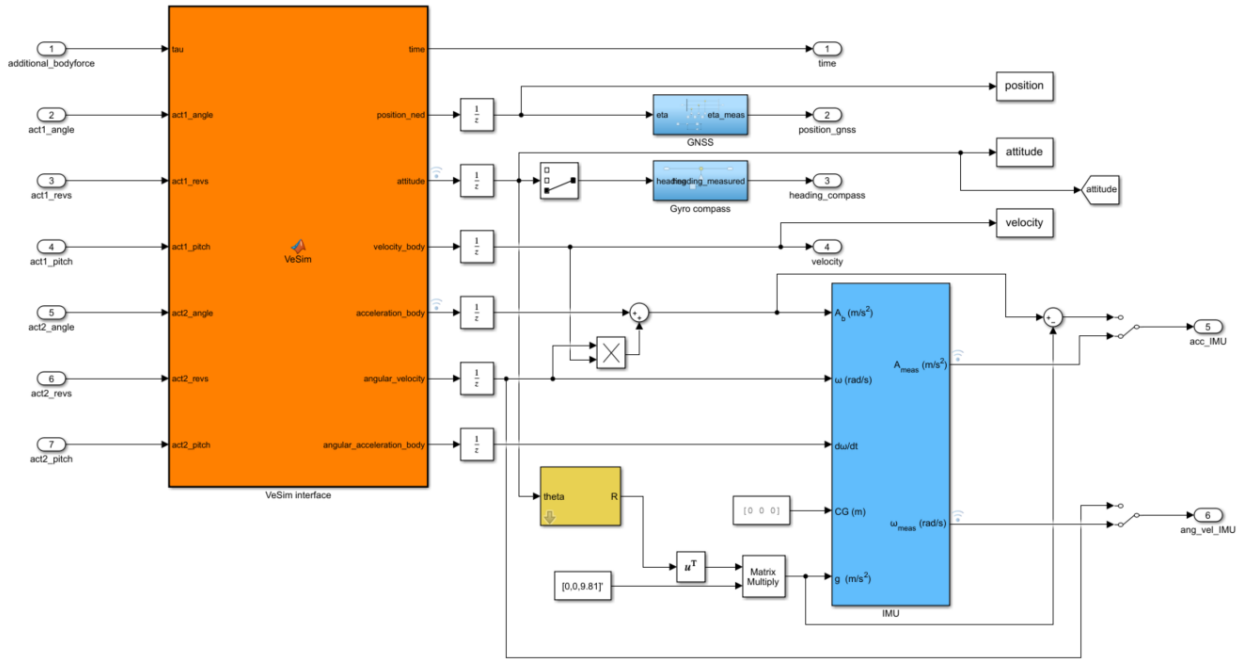

Figure 22: Implementation of Simulink interface with sensor models

The implementation shown in Figure 22 was wrapped by a final block, only interfacing the inputs and outputs that are realistic to include for a vessel. The inputs are the thruster setpoints, that is, speed, pitch and angle for each of the azimuth thrusters. The outputs are the measurements from the sensor models. An input of an additional BODY force and an output of the velocity was also added for debugging purposes. The final block is shown in Figure 23. An initialization script was also added, where environmental conditions and initial conditions are set.

Figure 23: Simulink block for the VeSim interface

7.4 Simulation results and discussion

In this section the developed control system is tested and evaluated through five different scenarios. These scenarios are chosen to highlight important aspect of the methods developed in this thesis. Results for each scenario is presented and discussed along the way. All parameter values used in the simulations are given in Appendix A.3.

7.4.1 Full system test

In this scenario, the full system is tested in calm sea, with no wind or current. The simulation starts at the service speed of $5m/s$, right after switching from the take-off mode of operation to the transit mode of operation. The ferry continues the operation until completing docking at $(N, E) = (0, 0)$. The route resembles the actual trajectory used by MF Gloppefjord from Lote to Anda.

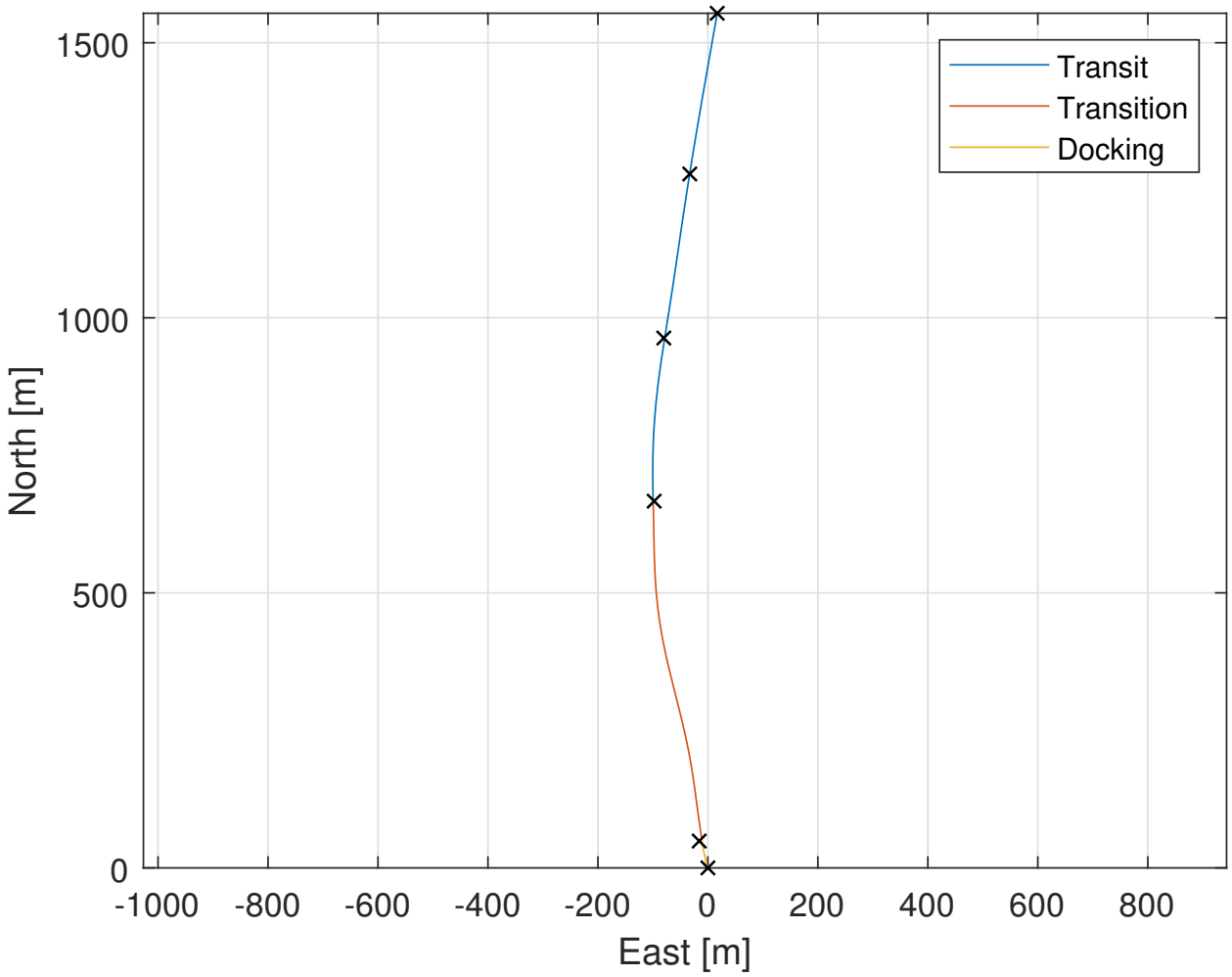

Figure 24: Trajectory for full system test

Figure 24 shows the trajectory of the ferry in the North-East plane. The plot indicates that the ferry is able to track its waypoints well is, except for a slight overshoot in the transition mode due to the heading change at the waypoint 4.

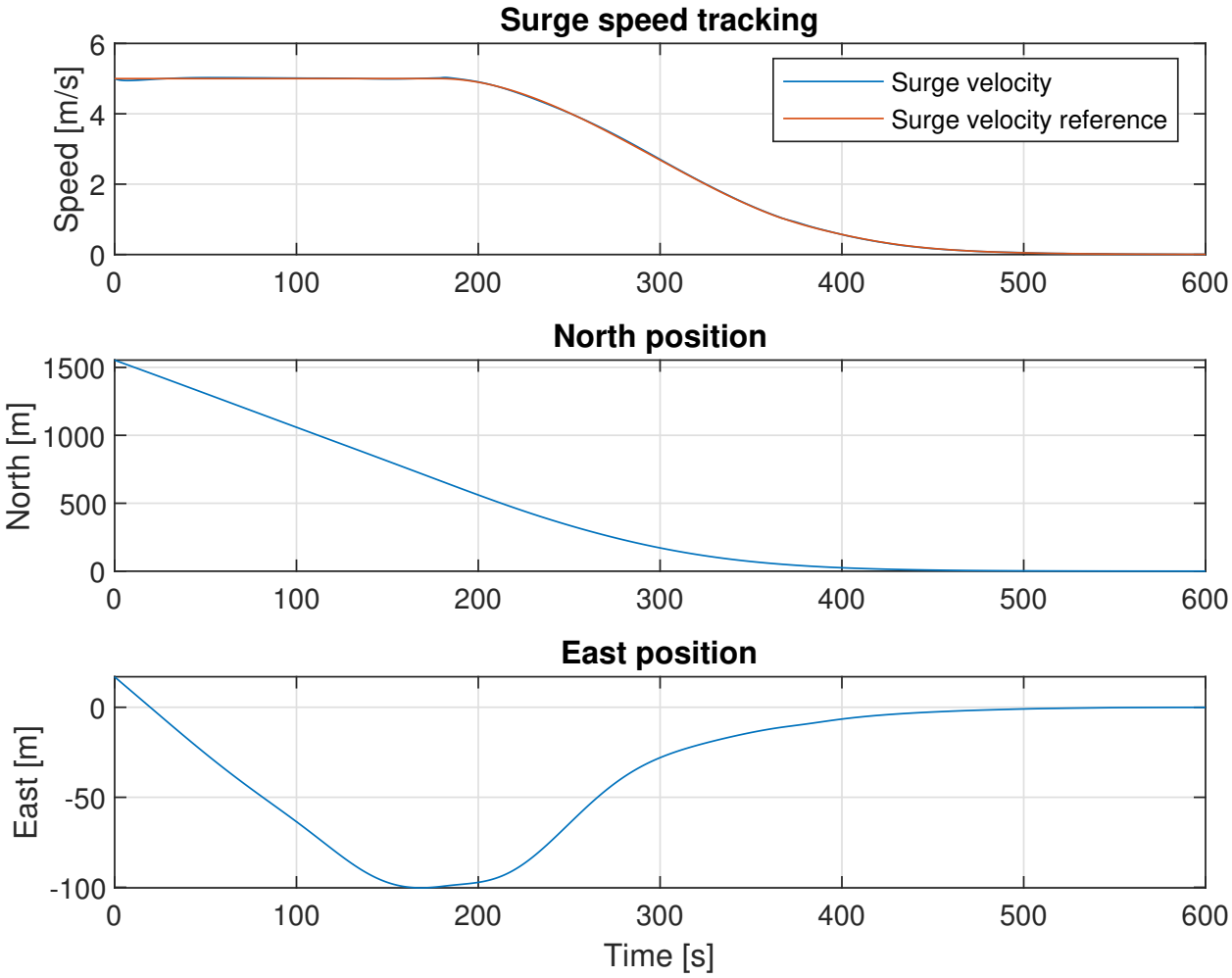

Figure 25: Speed profile and position for full system test

Figure 25 show the speed tracking and the north and east position of the ferry. The speed plot shows that the ferry follows its speed reference very well. There is no visible discontinuities or kinks at the switching instants. Both the north and east position converge monotonically to zero during docking.

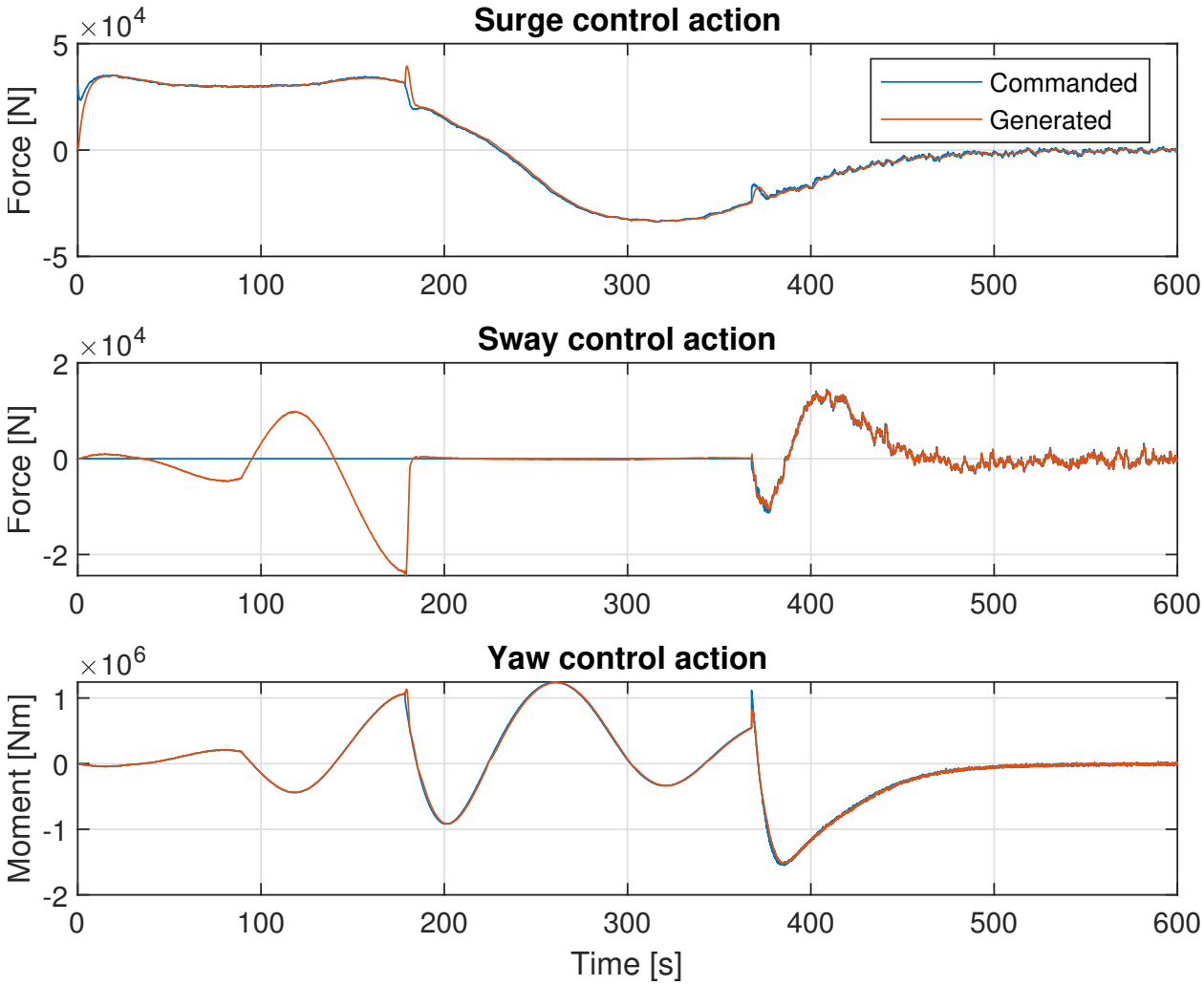

Figure 26: Commanded and generated control action for full system test

Figure 26 shows the control action commanded by the controller, and the actual generated thrust from the thrusters. The generated thrust coincides well with the commanded thrust, indicating succsessful control allocation. However, at the switch from transit to transition, there is a short transient where the produced surge force deviates. This is believed to be caused by a jump in the angle reference to the azimuth servos due to the switch from using only the aft thruster to using both. The thrusters will then produce a force in the wrong direction while the azimuth servos are turning. Methods for a smoother transition should be investigated further.

Note also that the sway force is uncontrolled in the transit mode of operation, while it immediately drops to zero when switching to transition mode and using both thrusters.

7.4.2 Adaptive Line-of-sight performance in current

In this section, the ferry is exposed to a cross-current of $0.5m/s$. The adaptive lookahead scheduling proposed in Section 6.4.1 is compared with two static lookahead values. The convergence rate, λ, is chosen to be 0.025. This give a lookahead value $\Delta = 200m$ for the transit mode, when the speed is constant equal to $5m/s$.

When the speed decreases, the lookahead distance decreases down to $\Delta = 40m$ when the speed reaches $1m/s$.

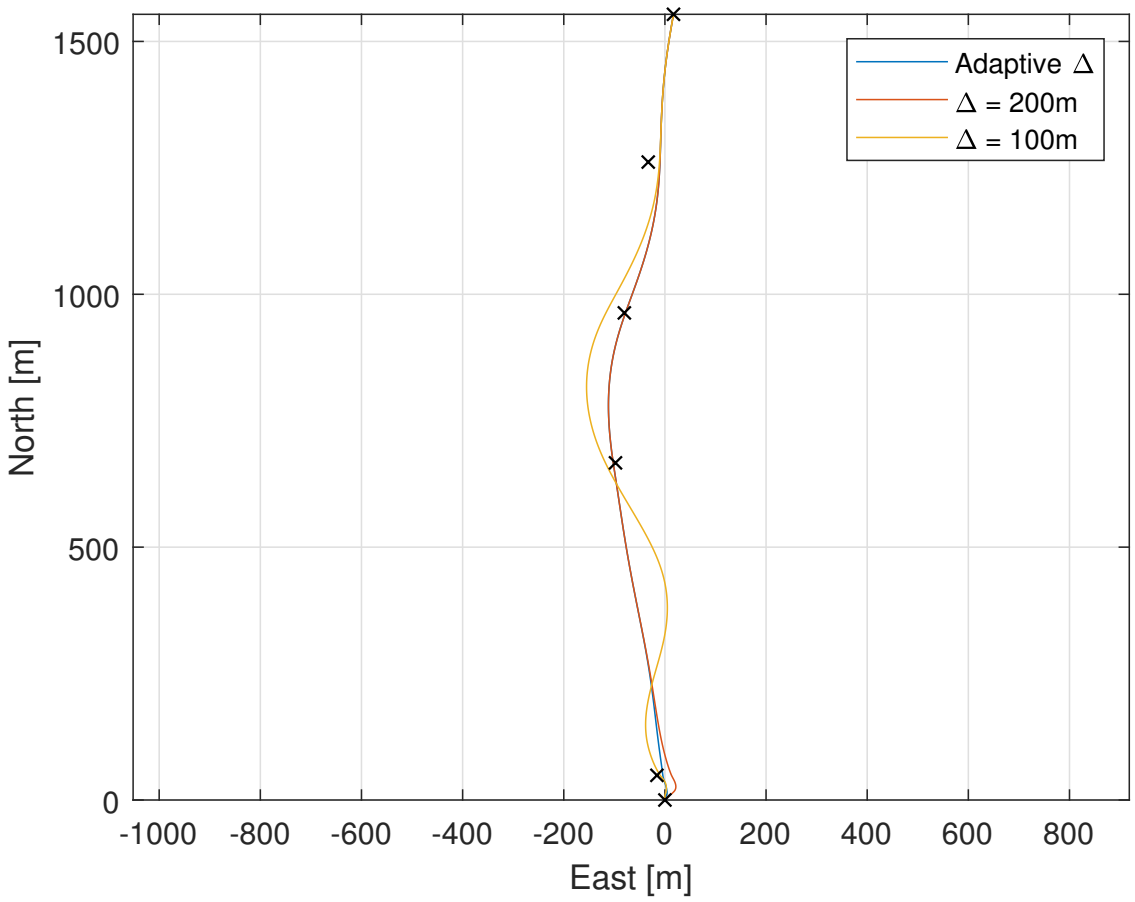

Figure 27: Trajectories comparing adaptive and static Line-of-sight guidance

Figure 27 shows the effect of lookahead on the trajectories. The shortest static lookahead distance, $\Delta = 100m$ yields large overshoots, and unacceptable behaviour. The adaptive guidance law performs identically to the static choice of $\Delta = 200m$ at high speeds. However, towards the end of the transition phase, the latter start drifting off the path when the velocity is decreased. The trajectory for the adaptive guidance law rejects the cross-current better at low speeds. These results indicate that no single choice of Δ is able to perform well in both high and low speeds. The proposed adaptive guidance law seems like a promising solution to this problem.

7.4.3 Square pulse disturbance rejection

In this section, the disturbance rejection capabilities of the acceleration based methodology developed in Section 4 is evaluated in the simulator. Surge speed tracking performance is compared with a slow and a fast integrator, when attacked by a square pulse disturbance in surge during the transition mode at $t = 250s$.

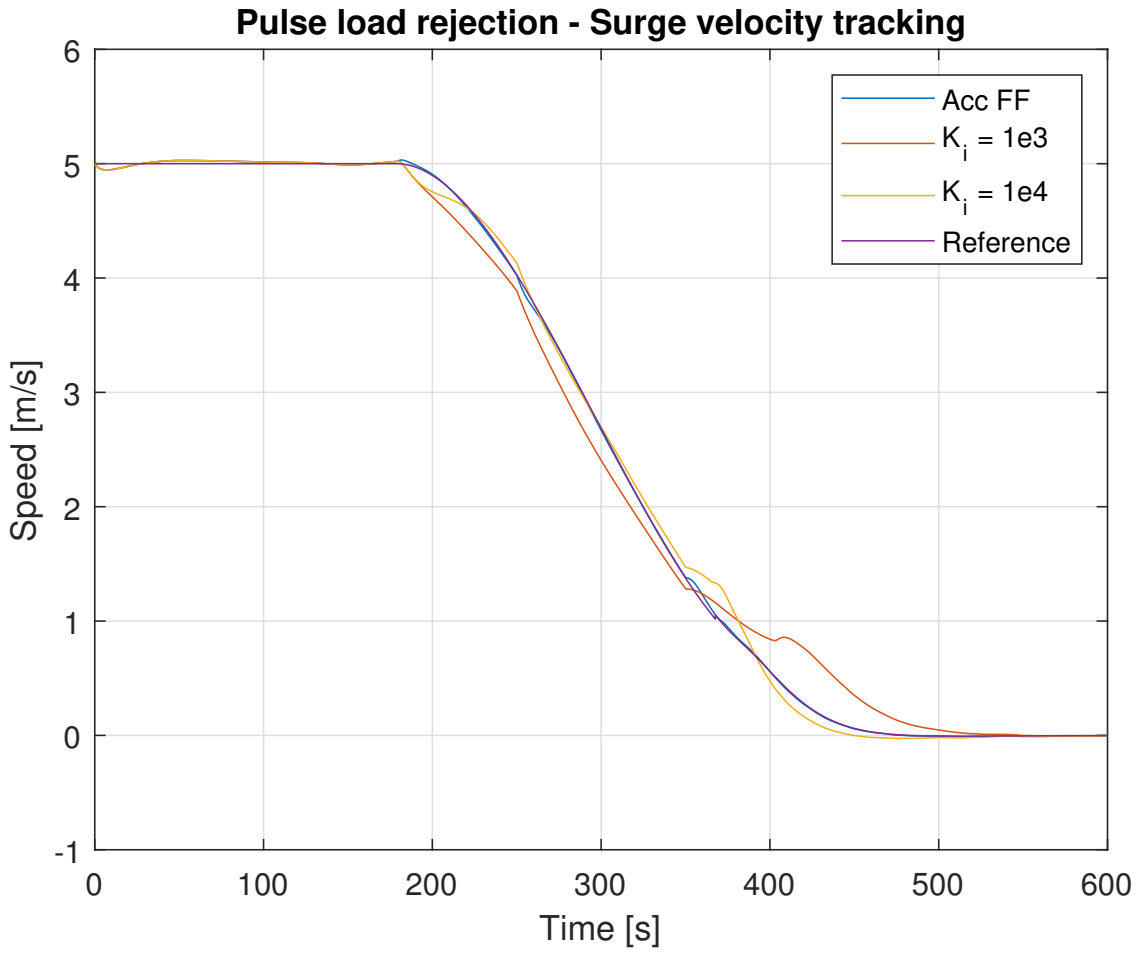

Figure 28: Surge velocity tracking performance under square pulse disturbance.

Figure 28 shows the surge speed for the different controllers, together with the speed reference signal. The figure clearly shows that the slow integrator has very bad performance. It is not able to follow the speed reference at the time of the switch from transit mode to transition mode. The tracking error increases when the pulse attacks. The integrator slowly builds up and compensates for the disturbance, but when the disturbance ceases, the built up integral leads to a large overshoot.

The fast integrator has similar problems, but on a smaller scale. Also, it introduces some oscillatory behaviour. The acceleration based controller follows its reference very well, and is not effected much by the disturbance.

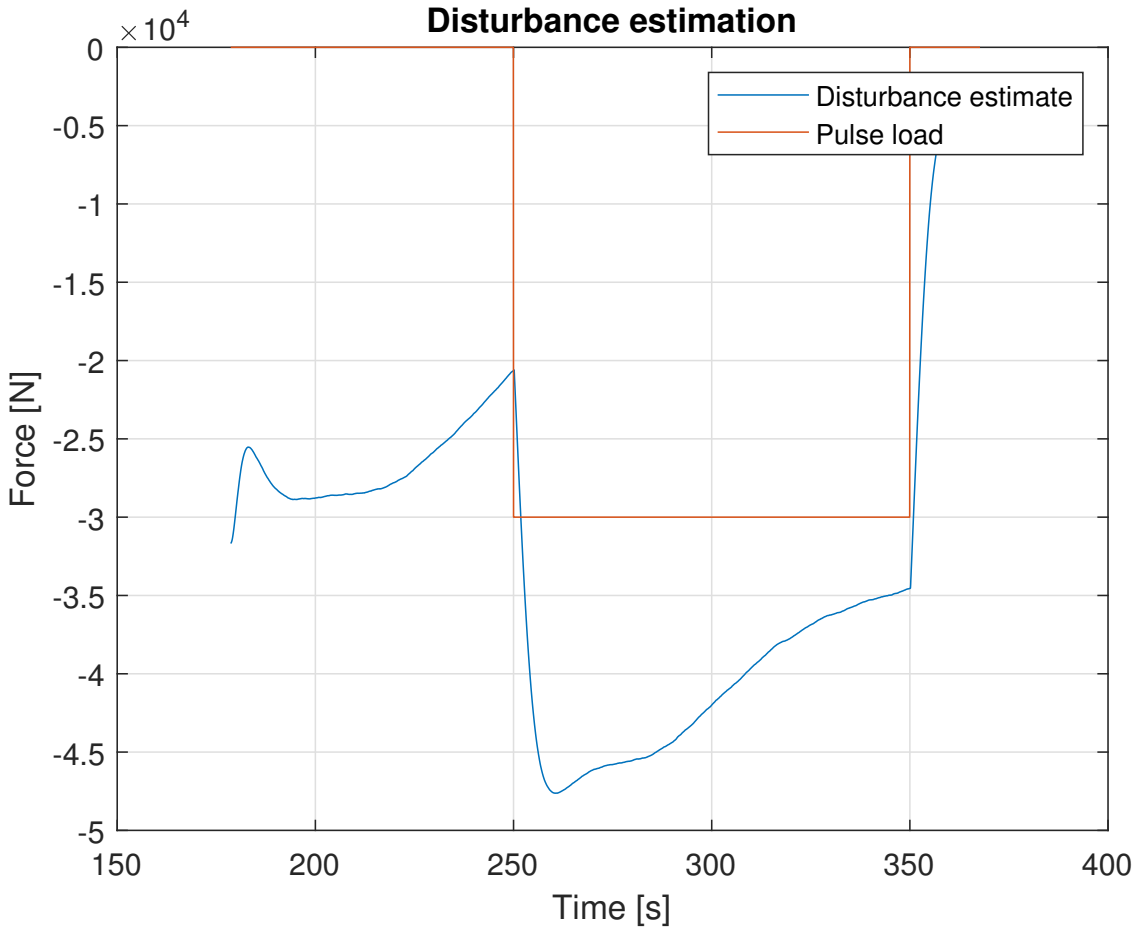

Figure 29: Disturbance estimate for square pulse disturbance

Figure 29 shows the disturbance estimate together with the square pulse. Note that the controller in the transition mode is model free, and all hydrodynamic forces are considered as disturbances. The disturbance estimate in Figure 29 therefore includes the surge drag force and surge added mass force in addition to the square pulse.

The plot shows that the disturbance estimator quickly updates to compensate for the disturbance, with no overshoot. The magnitude of the disturbance estimate decreases in time because the speed decreases and therefore the drag force decreases.

7.4.4 Effect of waves and wave filtering

In this section, the effect of waves is investigated. The sea state is generated by Pierson-Moskowitz spectrum with significant wave height $1.0m$ and peak period 4.0 seconds. This is believed to be representative for a moderate sea state in a narrow fjord.

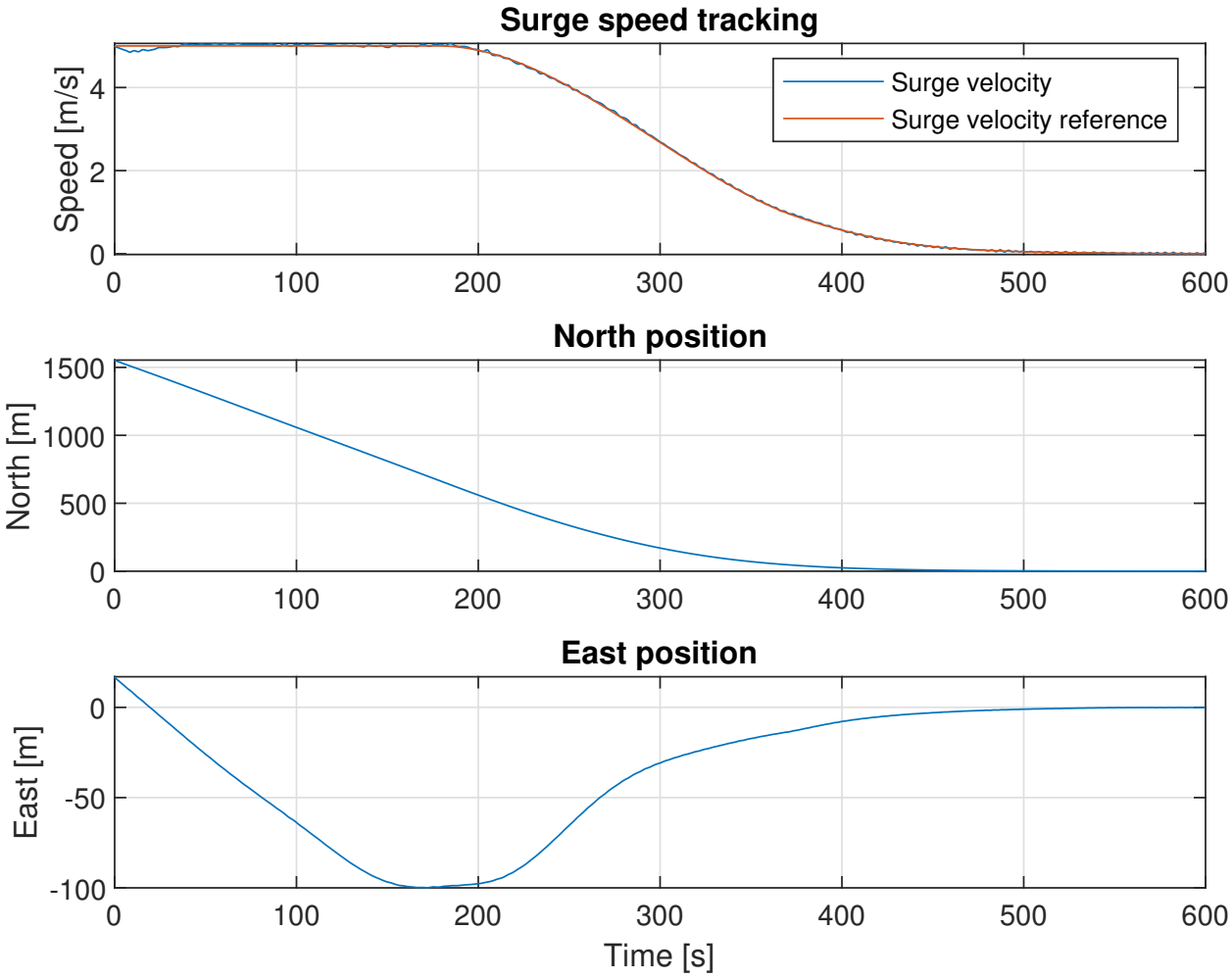

Figure 30: Speed profile and positions in waves

Figure 30 shows that the ferry is still able to complete the control objective well, although there are some minor oscillations in the surge velocity.

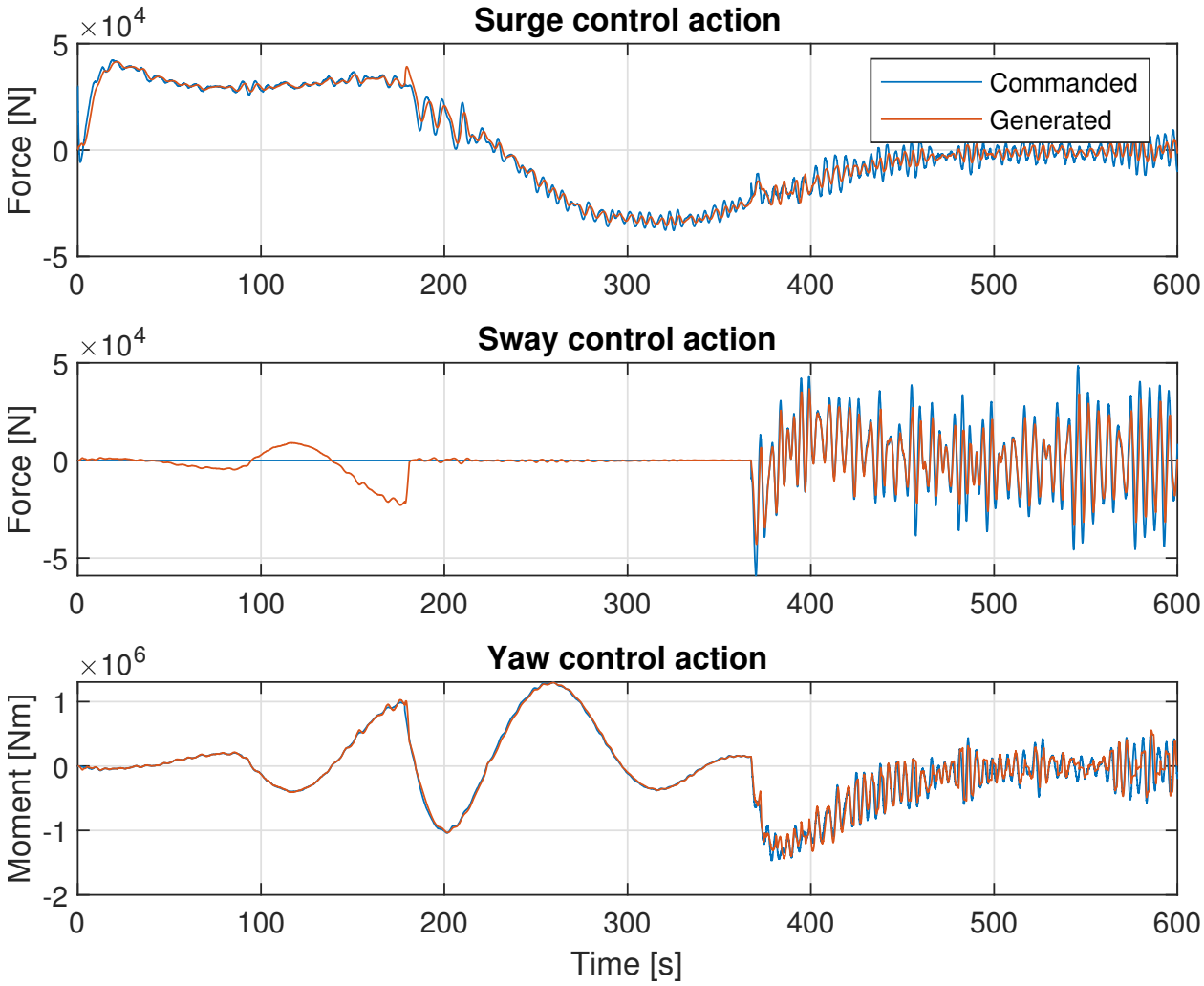

Figure 31: Commanded and generated control action in waves

Figure 31 shows the corresponding control action. It shows that the wave frequency motion induces an unacceptable level off oscillations in the control action.

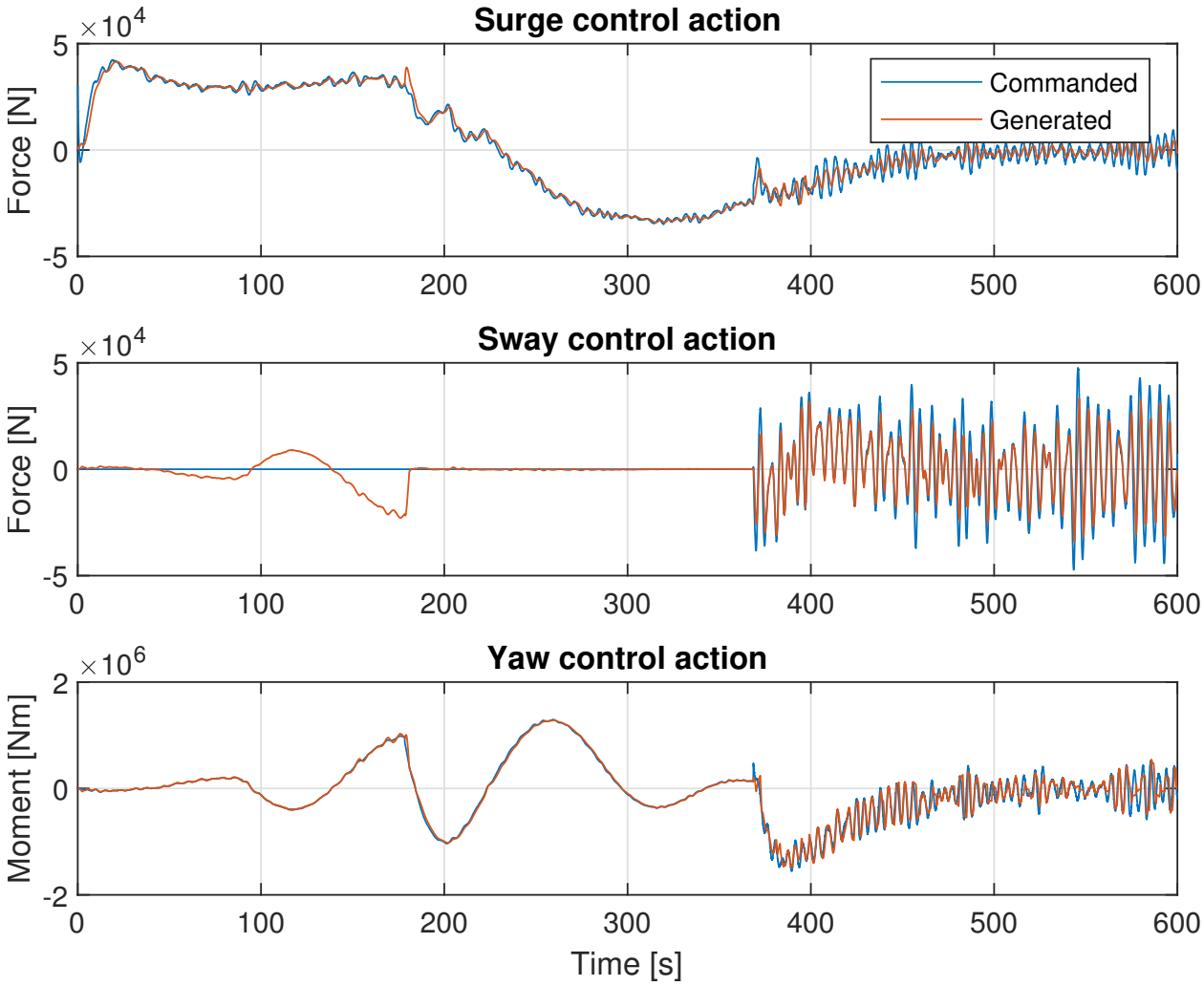

Figure 32: Commanded and generated control action in waves with wave filtering

Figure 32 shows the control action in the same case, but using the wave filter developed in Section 4.3 to filter the acceleration measurements. The input to the wave filter includes both the accelerometer measurement term and the gravity compensation term from (49), since both these terms are heavily influenced by the wave frequency motion. The plot shows that the wave filter effectively reduces the control action oscillations in the transition mode.

The oscillation are most severe for the docking mode, and reducing this is a topic for future work. One alternative is to use a hybrid observer with wave filtering in docking mode, such as that of Brodtkorb et al. [34]. Also, Bryne et al. has extended the observer used in this control system to include wave filtering by adding notch filters at the outputs [24][35].

7.4.5 Attitude estimation

In this section, the performance of the proposed attitude estimator in Section 6.2.2 is compared to the original estimator used in [34] and [25].

The ferry is uncontrolled and at rest with north heading. It is pertubated by waves from a Pierson-Moskowitz

spectrum with significant wave height $1.0m$ and peak period 5.0 seconds. The dominant wave direction is 45 degrees. The angular rate gyros are given a sensor bias $10^{-5}\frac{rad}{s}$, corresponding to a drift rate of approximately $2\frac{deg}{h}$.

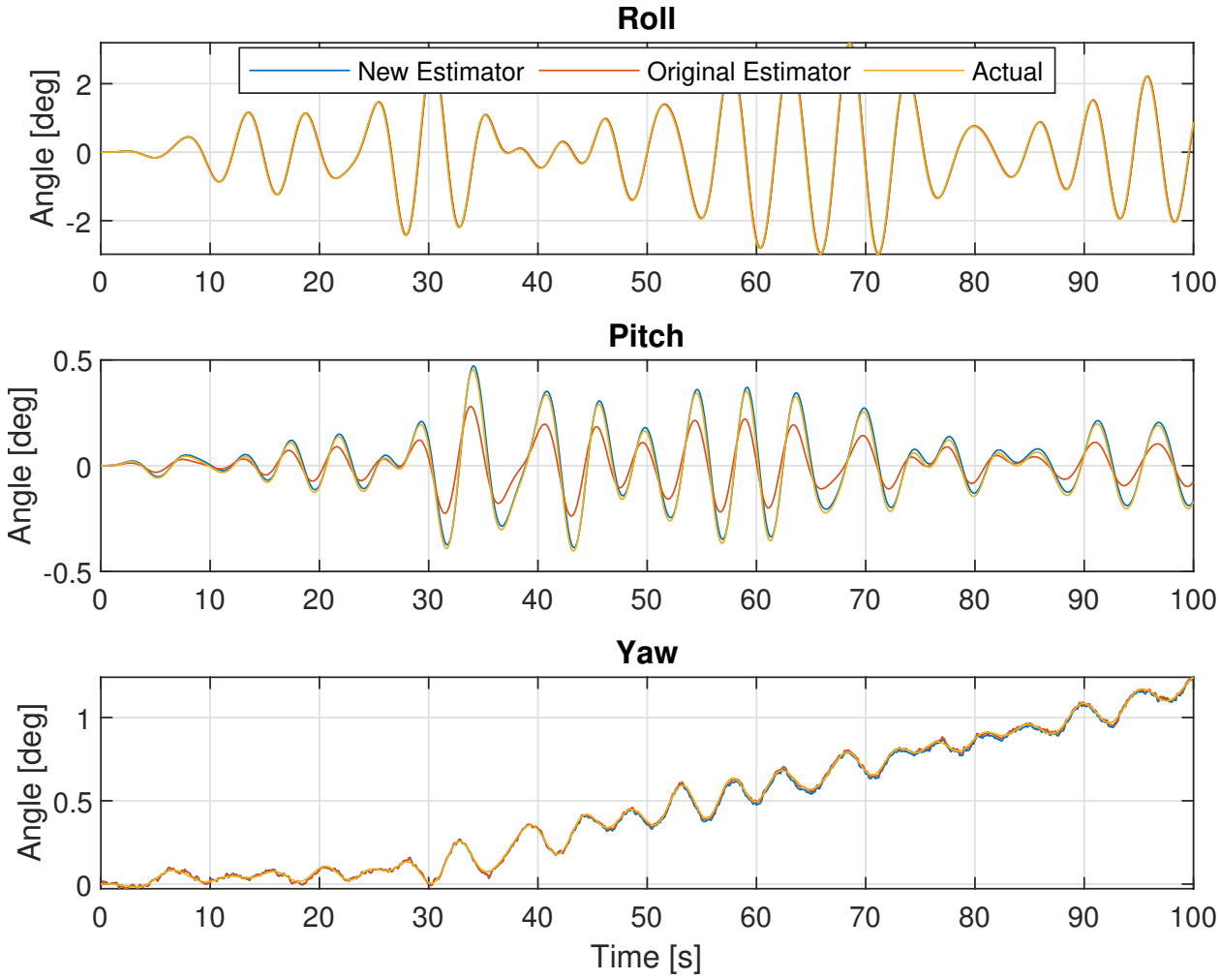

Figure 33: Attitude estimates for proposed attitude estimator compared with the original estimator

Figure 33 shows the estimated attitude from the new and the original estimator together with the true attitude. It shows that both observers produce very good estimates of the roll and yaw angles. However, the original estimator has significantly more inaccurate estimation of the pitch angles compared to the new estimator.

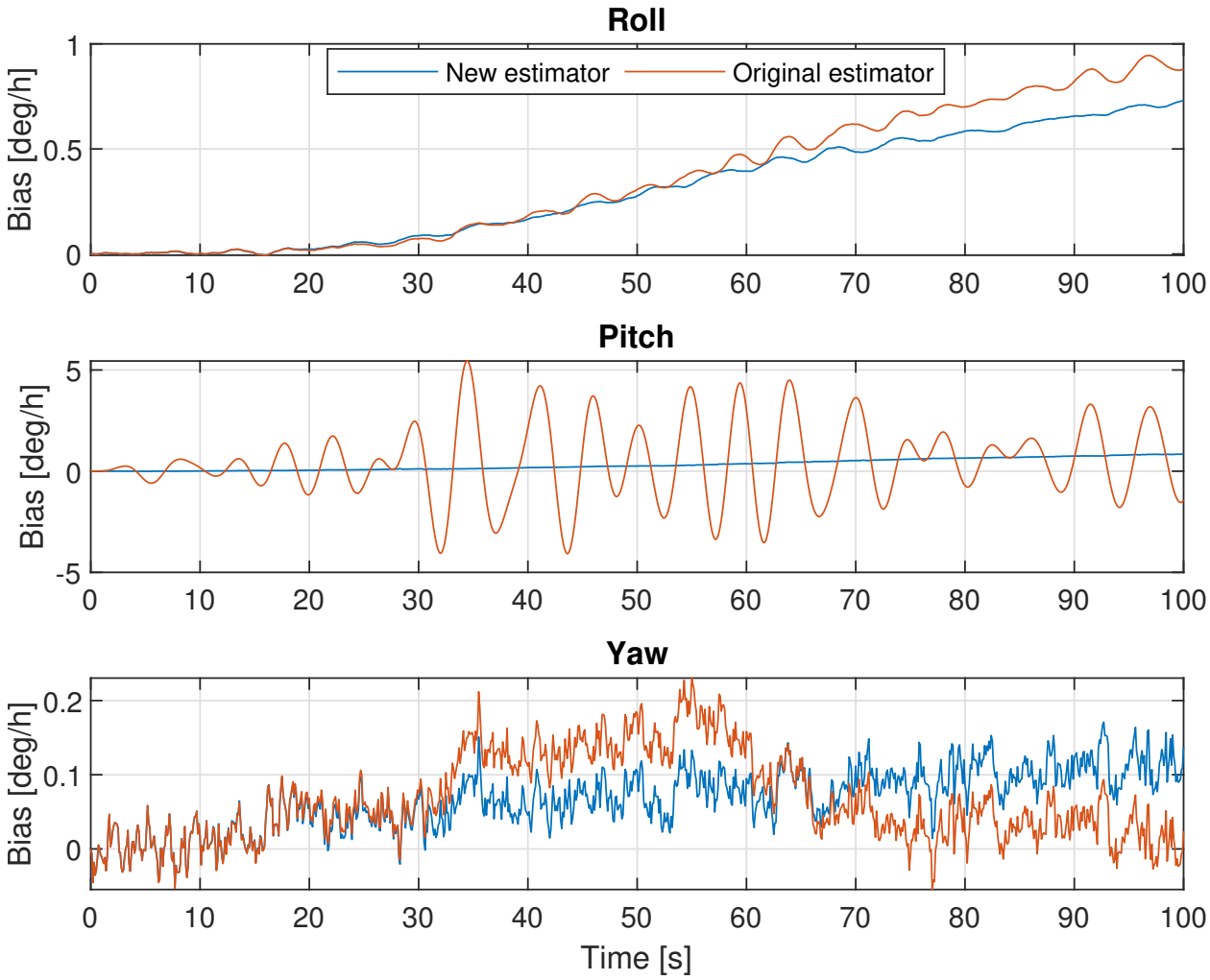

Figure 34: Gyro bias estimate for proposed attitude estimator compared with the original estimator

Figure 34 shows bias estimates for the angular rate gyros. It shows that the original bias estimator has large oscillations in pitch. This is as expected, since the bias estimator is driven by the attitude estimation error term, $\hat{J}$, from (77). As discussed in Section 6.2.2, the measurement vector used in the original estimator assumes zero roll and pitch, and this untrue assumption propagates to the bias estimate through $\hat{J}$.

The results of this section suggest that the proposed estimator gives improved attitude estimation. However, formal analysis should follow to investigate if this modification has implications on the exponential stability results for this estimator.

8 Conclusions and further work

8.1 Conclusions

The topic of this thesis has been hybrid control of autonomous ferries. Methods to address the some of the challenges associated with automation of ferry operations has been proposed. The focus has been on transit, transition and docking modes of operation.

Chapter 2 gave a brief introduction to mathematical modelling and control of marine vessels.

In Chapter 3, a review of the literature and history of hybrid system was presented. It showed a relatively young and active field of research. Furthermore, it showed that the literature may coarsely be divided into two groups: The systems approach, popularly used by the control engineering community and the automata approach, commonly used by the computer science community. Applications to marine control was presented. Finally, a general mathematical framework was introduced which is particularly applicable for stability analysis of nonlinear hybrid control systems.

In Chapter 4, a methodology for using Inertial Measurement Units (IMUs) to improve transient response and disturbance rejection was introduced. A discussion of the challenges associated with using IMUs in an operational setting was given, explaining their limited use in marine control system today. It was noted that is likely going to change with the advent of robust, high-precision and low cost MEMS sensors.
In Section 4.1, a model for integrating accelerometer measurements for control of rigid bodies was proposed. It showed how an open-loop estimate of disturbances could be obtained by combining model based terms with accelerometer measurements.
In Section 4.2, a combined disturbance estimator and controller was introduced, by splitting the control law into a nominal part and a disturbance feedforward part. A closed-loop disturbance estimator can be obtained in this setting.
In Section 4.3 noise and wave filtering of acceleration measurements was considered. Wave filtering is of paramount importance, since the first order wave frequency acceleration often dominates the low-frequency acceleration. A Kalman filter for wave filtering was proposed. The development showed that it is difficult to do filtering without introducing a phase lag because there normally is no model for how the low-frequency acceleration changes.
In Section 4.4 a case study was performed. The topic was disturbance estimation and rejection in speed control of a decoupled surge model under a square pulse disturbance. The results showed that the disturbance estimator was quickly able to estimate and compensate for the disturbance at calm seas. Comparisons was made to traditional integral action disturbance rejection. This showed that the disturbance rejection capabilities using acceleration measurements could not be obtained using integral action without introducing large oscillations. Next, the effect of waves was investigated. The results showed that wave motion introduced a large wave frequency component to the control action when using acceleration measurements. Introducing the Kalman based wave filter, the first order wave frequency components was effectively reduced. However, the phase lag introduced by the wave filter lead to oscillatory behaviour of the disturbance estimator. This effectively places a bound on the feedback gain used in the disturbance estimator. It was shown that good performance without large oscillations could still be obtained by proper tuning of the wave filter and the disturbance estimator.

In Chapter 5, control allocation for double ended ferried with symmetrical thruster configuration was the topic. First, it was described how manual thruster control are normally is performed by ferry captains today.
In Section 5.2 a novel control allocation algorithm for ferries was proposed. The allocation problem was formulated as a scalar optimization problem, for which fast nonlinear solver exist. Next, specific implementational issues to apply this algorithm to ferries with reversible thrusters and non-reversible thrusters was given. The chapter finished off with a case study using a simplified model of azimuth thrusters. The per-

formance of the novel algorithm was compared to the commonly used Pseudo Inverse method. The results showed superior performance of the proposed algorithm. Finally, it was noted that many of the challenges faced by the pseudo inverse method could be addressed by the Quadratic Programming method. However, it is more computationally expensive than the novel algorithm.

In Chapter 6 a hybrid control system for ferry operations was developed. This included a guidance system, observer, motion controller and control allocation.
First, a switched control allocation system was proposed. For the observer, the GNSS aided inertial navigation system of Section 2.3.3 was used for all modes of operation. A modified attitude estimator for this observer was proposed, presumably giving improved roll and pitch estimates.
Next, guidance laws and motion controllers were presented for all modes of operation. Most notably, a novel adaptive Line-of-sight guidance law was proposed for the transition mode, to ensure smooth path following at high speed while still rejecting the effects of current at low speed.
A switching logic for integrator synchronization was proposed. It was discussed why this is important for smooth switching and transfer of the disturbance estimates between the modes.
Finally, the hybrid control system was formulated using the mathematical framework introduced in Section 3.4.

In Chapter 7, a case study was performed for the double ended car ferry MF Gloppefjord at the Anda-Lote site.
An introduction to the ferry and the site was given first. Then, the development of a high-fidelity simulator for ferry operations was presented. This included a SINTEF VeSim vessel simulator, thruster models, environmental loads and sensor models.
In Section 7.4, the hybrid control system of Chapter 6 was implemented in Simulink, and tested using the developed simulator.
First, the full system was tested for a ferry operation consisting of the transit phase, transition phase and docking. The results showed good path following capabilities, with mostly smooth transition between the modes of operation. The control allocation introduced a small transient when switching from transit to transition. Next, a cross-current was introduced, and the performance of the adaptive Line-of-sight guidance law was evaluated. The results showed promising performance in both high speed and low speed compared to a static guidance law.
A scenario to test the disturbance rejection capabilities and the speed tracking during the transition mode was tested next. The results confirmed the results of the simplified case study of Section 4.4. The effect of waves was also studied. The Kalman based wave filter effectively reduced the first order wave frequency oscillations during the transition mode. However, there were very large oscillation during docking. This was expected due to the absence of a wave filter in the observer.
Finally the modified attitude estimator of Section 6.2.2 was tested by inducing roll and pitch motion from waves. The results showed that both the original and the modified estimator gave good estimates of the roll and yaw motion. However, the modified estimator gave far better pitch estimates.

All in all, this thesis has given several contributions for control of autonomous ferries. Simulations indicate promising performance. The work has demonstrated that the method of hybrid control provides a flexible platform for integrating heterogeneous components in a control system, and for formalizing the switching between them. A disadvantage is a quite complex system, with many tuning parameters.
The thesis also shows that utilizing acceleration measurements in the controller can give increased performance, but the work has also highlighted several complications with using IMUs in an operational setting. This boils down to a question of performance versus cost and complexity.
Finally, the work indicates that the nonlinear scalar allocation algorithm is a good candidate for control allocation for double ended ferries with symmetrical thruster configuration, both in terms of performance and computational complexity.

8.2 Further work

This thesis has introduced several new methods for control and estimation. Due to the time constraints of the project thesis, there has been limited formal analysis of these. Also, there are other important problems to be addressed in the control of autonomous ferries. The most important suggestions for further work are given below.

- The thesis has proposed a method for fast disturbance rejection in surge. However, rejection of lateral disturbances are equally important to handle. An example is the rapid change in cross current when the ferry comes in shelter from the dock. An unsuccessful approach to this was investigated in Section 6.4.2 utilizing the sway acceleration. An interesting approach to pursue is using the 4 IMU sensor setup proposed in [30] to obtain the angular acceleration in yaw, and follow the same disturbance estimation and rejection method as used for surge in this thesis.

- Wave filtering in the observer has not been considered in this thesis, yielding unacceptable oscillations in the docking control action. Solutions to this should be investigated. One solution is using a switched observer which includes wave filtering in the docking mode. Also, an extention to the observer used in this thesis has been made in [25], to include wave filtering.

- Formal analysis of the disturbance estimation and rejection method developed in Chapter 4 should be performed. Some results are given in [30]. It is also interesting to investigate the effect of misalignment errors or sensor bias, and the effect on stability by adding integral action in the nominal control law to compensate for this.

- Stability conditions should be investigated for the Adaptive Line-of-sight guidance law in terms of the required convergence rate, λ, for a given current velocity.

- It should be investigated if the modification of the attitude estimator proposed in Section 6.4.1 has implications for the exponential stability results of the original attitude estimator.

- A hybrid system formulation including the guidance system should be developed. Since Line-of-sight guidance is a closed-loop guidance law, using feedback from the ships sensors, it is problematic to separate the guidance system from the rest of the system, as is done in the hybrid system formulation of Section 6.7. Also, convergence to the path can not be analyzed using the existing formulation, since it does not include the cross-track error dynamics in the guidance system.

- Stability for the hybrid system should be analyzed. This can for instance include a *stability-of-set* analysis of the docking position from any initial condition. An alternative analysis which may be simpler, is to investigate stability for the switching between two consecutive modes.

- Extensions of this work should be made to include the takeoff and dockside modes of operation. The takeoff mode of operation can probably use a similar approach as the transition mode. However, the dockside mode requires new methodology to handle the contact forces with the quay, and to prevent slip-off while loading and unloading.

References

[1] H. S. Witsenhausen, "A Class of Hybrid-State Continuous-Time Dynamic Systems," *IEEE Transactions on Automatic Control*, 1966, ISSN: 15582523. DOI: 10.1109/TAC.1966.1098336.

[2] J. G. Balchen, N. A. Jenssen, E. Mathisen, and S. Sælid, *A dynamic positioning system based on Kalman filtering and optimal control*, 1980.

[3] M. D. SHUSTER and S. D. OH, "Three-axis attitude determination from vector observations," *Journal of Guidance, Control, and Dynamics*, vol. 4, no. 1, pp. 70–77, 1981, ISSN: 0731-5090. DOI: 10.2514/3.19717. [Online]. Available: http://arc.aiaa.org/doi/10.2514/3.19717.

[4] L. Tavernini, "Differential automata and their discrete simulators," *Nonlinear Analysis*, 1987, ISSN: 0362546X. DOI: 10.1016/0362-546X(87)90034-4.

[5] S. Salcudean, "A Globally Covergent Angular Velocity Observer for Rigid Body Motion," 1991.

[6] P. Antsaklis, J. Stiver, and M. Lemmon, "Hybrid system modeling and autonomous control systems," *Hybrid Systems*, pp. 366–392, 1993. [Online]. Available: http://www.springerlink.com/index/p62226341550744t.pdf.

[7] A. Back, J. Guckenheimer, and M. Myers, "A dynamical simulation facility for hybrid systems," pp. 255–267, 1993. DOI: 10.1007/3-540-57318-6{_}32. [Online]. Available: http://link.springer.com/10.1007/3-540-57318-6_32.

[8] A. Nerode and W. Kohn, "Models for hybrid systems : automata, topologies, controllability, observability," *Hybrid Systems, Lecture Notes in Computer Science*, pp. 317–356, 1993. DOI: 10.1007/3-540-57318-6{_}35.

[9] M. S. Branicky, "Studies in Hybrid Systems: Modeling, Analysis, and Control," *Electrical Engineering*, 1995.

[10] O. Faltinsen, *Sea loads on ships and offshore structures*. 1998, ISBN: 0-521-45870-6. DOI: 9780521458702.

[11] J. P. FOSSEN T. I. & STRAND, "Passive nonlinear observer design for ships using Lyapunov methods.pdf," *Automatica*, vol. 35, pp. 3–16, 1999.

[12] J. Hespanha, "Tutorial on supervisory control," *Lecture Notes for the workshop Control using Logic and Switching for the 40th Conf. on Decision and Contr.*, pp. 1–46, 2001.

[13] B. Vik, "A nonlinear observer for GPS and INS integration," *Decision and Control, 2001. Proceedings of*, no. December, 2001, ISSN: 01912216. DOI: 10.1109/.2001.980726. [Online]. Available: http://ieeexplore.ieee.org/xpls/abs_all.jsp?arnumber=980726.

[14] J. P. Hespanha and A. S. Morse, "Switching between stabilizing controllers," *Automatica*, vol. 38, no. 11, pp. 1905–1917, 2002, ISSN: 00051098. DOI: 10.1016/S0005-1098(02)00139-5.

[15] H. K. Khalil, "Nonlinear Systems," *Prentice-Hall, New Jersey*, 2002, ISSN: 0949-1775. DOI: 10.1007/978-1-4757-3108-8.

[16] J. P. Hespanha, "Hysteresis-based switching algorithms for supervisory control of uncertain systems Hysteresis-based switching algorithms for supervisory control of uncertain systems," *University of California Postprints*, vol. 39, pp. 263–272, 2003.

[17] T. D. Nguyen, A. J. Sørensen, and S. Tong Quek, "Design of hybrid controller for dynamic positioning from calm to extreme sea conditions," *Automatica*, vol. 43, no. 5, pp. 768–785, 2007, ISSN: 00051098. DOI: 10.1016/j.automatica.2006.11.017.

[18] T. I. Fossen, T. Johansen, and T. Perez, "A Survey of Control Allocation Methods for Ships and Underwater Vehicles," *2006 14th Mediterranean Conference on Control and Automation*, no. December, p. 20, 2008. DOI: 10.1109/MED.2006.235844.

[19] R. Mahony, T. Hamel, and J.-M. Pfimlin, "Nonlinear Complementary Filters on the Special Orthogonal Group," vol. 23, no. 5, pp. 9–28, 2008, ISSN: 00207179. DOI: 10.1080/00207179.2012.693951.

[20] T. D. Nguyen, A. J. Sørensen, and S. T. Quek, "Multi-operational controller structure for station keeping and transit operations of marine vessels," *IEEE Transactions on Control Systems Technology*, vol. 16, no. 3, pp. 491–498, 2008, ISSN: 10636536. DOI: 10.1109/TCST.2007.906309.

[21] T. I. Fossen, *Handbook of Marine Craft Hydrodynamics and Motion Control*. 2011, ISBN: 9781119991496. DOI: 10.1002/9781119994138.

[22] R. Goebel, R. G. Sanfelice, and A. R. Teel, *Hybrid Dynamical Systems : Modeling, Stability, and Robustness*. Princeton University Press, 2012, p. 227, ISBN: 1400842638. [Online]. Available: https://books.google.no/books?hl=en&lr=&id=JwrOY03fuGQC&oi=fnd&pg=PP1&dq=info:Tl8gDI0O3QEJ:scholar.google.com&ots=TpU8ELWhbC&sig=r7zQ6kma2MhE_uw-qkAhnS2oQNI&redir_esc=y#v=onepage&q&f=false.

[23] H. F. Grip, T. I. Fossen, T. A. Johansen, and A. Saberi, "Nonlinear observer for GNSS-aided inertial navigation with quaternion-based attitude estimation," *2013 American Control Conference*, pp. 272–279, 2013, ISSN: 07431619. DOI: 10.1109/ACC.2013.6579849. [Online]. Available: http://ieeexplore.ieee.org/document/6579849/.

[24] T. H. Bryne, T. I. Fossen, and T. A. Johansen, "Design of Inertial Navigation Systems for Marine Craft with Adaptive Wave Filtering aided by Triple-Redundant Sensor Packages," no. 7491, pp. 1–23, 2015. DOI: 10.1002/10.1002/acs.

[25] T. Bryne, T. I. Fossen, and T. A. Johansen, "A Virtual Vertical Reference Concept for for Applications Sea Surface Applications at the GNSS / INS Applications at the Sea Surface," *IFAC-PapersOnLine*, vol. 48, no. 16, pp. 127–133, 2015, ISSN: 2405-8963. DOI: 10.1016/j.ifacol.2015.10.269. [Online]. Available: http://dx.doi.org/10.1016/j.ifacol.2015.10.269.

[26] D. De Almeida Fernandez, *An output feedback motion control system for ROVs: Guidance, navigation and control*, June. 2015, ISBN: 9788232609000.

[27] H. F. Grip, T. I. Fossen, T. A. Johansen, and A. Saberi, "Globally exponentially stable attitude and gyro bias estimation with application to GNSS/INS integration," *Automatica*, vol. 51, pp. 158–166, 2015, ISSN: 00051098. DOI: 10.1016/j.automatica.2014.10.076. [Online]. Available: http://dx.doi.org/10.1016/j.automatica.2014.10.076.

[28] T. H. Bryne and T. I. Fossen, "Introductory Lecture Notes on Aided Inertial Navigation Systems," no. August, 2016.

[29] W. Caharija, K. Y. Pettersen, M. Bibuli, P. Calado, E. Zereik, J. Braga, J. T. Gravdahl, A. J. Sørensen, M. Milovanović, and G. Bruzzone, "Integral line-of-sight guidance and control of underactuated marine vehicles: Theory, simulations and experiments," *IEEE Transactions on Control Systems Technology*, vol. 24, no. 5, pp. 1623–1642, 2016.

[30] O. K. Kjerstad and R. Skjetne, "Disturbance Rejection by Acceleration Feedforward for Marine Surface Vessels," *IEEE Access*, vol. 4, pp. 2656–2669, 2016, ISSN: 21693536. DOI: 10.1109/ACCESS.2016.2553719.

[31] G. I. Bitar, "Towards the Development of Autonomous Ferries," no. September, 2017.

[32] S. Skjong and E. Pedersen, "Nonangular MPC-Based Thrust Allocation Algorithm for Marine Vessels - A Study of Optimal Thruster Commands," *IEEE Transactions on Transportation Electrification*, vol. 3, no. 3, pp. 792–807, 2017, ISSN: 23327782. DOI: 10.1109/TTE.2017.2688183.

[33] Tore Stensvold, *Dette er verdens første helelektriske fergesamband - Tu.no*, 2017. [Online]. Available: https://www.tu.no/artikler/dette-er-verdens-forste-helelektriske-fergesamband/438991?key=IfQmbvmi.

[34] A. H. Brodtkorb, S. A. Værnø, A. R. Teel, A. J. Sørensen, and R. Skjetne, "Hybrid controller concept for dynamic positioning of marine vessels with experimental results," *Automatica*, vol. 93, pp. 489–497, 2018, ISSN: 00051098. DOI: 10.1016/j.automatica.2018.03.047. [Online]. Available: https://doi.org/10.1016/j.automatica.2018.03.047.

[35] T. H. Bryne, R. H. Rogne, T. I. Fossen, and T. A. Johansen, "A virtual vertical reference concept for aided inertial navigation at the sea surface," *Control Engineering Practice*, vol. 70, no. March 2017, pp. 1–14, 2018, ISSN: 09670661. DOI: 10.1016/j.conengprac.2017.09.009. [Online]. Available: http://dx.doi.org/10.1016/j.conengprac.2017.09.009.

[36] A. J. Sørensen, "Marine Cybernetics," pp. 1–35, 2018.

[37] Bastø Fosen, *Samarbeider om teknologi til fremtidens ferger - Bastø Fosen*. [Online]. Available: http://basto-fosen.no/nyheter/samarbeider-om-teknologi-til-fremtidens-ferger-article3399-132.html.

[38] *Functional Mock-up Interface*. [Online]. Available: https://fmi-standard.org/.

[39] *History of Computers and Computing, Birth of the modern computer, The bases of digital computers, relay*. [Online]. Available: http://history-computer.com/ModernComputer/Basis/relay.html.

[40] *Implement three-axis inertial measurement unit (IMU) - Simulink*. [Online]. Available: https://www.mathworks.com/help/aeroblks/threeaxisinertialmeasurementunit.html.

[41] *scipy.optimize.fminbound — SciPy v1.1.0 Reference Guide*. [Online]. Available: https://docs.scipy.org/doc/scipy/reference/generated/scipy.optimize.fminbound.html.

[42] T. Stensvold, – *ASIA KOMMER FOR FULLT. VI HAVNER BAKPÅ OM VI IKKE GIR GASS - TU.NO*. [Online]. Available: https://www.tu.no/artikler/ntnu-autonomi-er-en-stor-satsing-for-oss-vi-har-100-som-tar-doktorgraden/440081?key=EWNVcNHQ.

[43] ——, *Nå er MF Folgefonn verdens første fartøy med automatisk dokking - Tu.no*. [Online]. Available: https://www.tu.no/artikler/na-er-mf-folgefonn-verdens-forste-fartoy-med-automatisk-dokking/435810?key=cDVcEUuO.

Appendix A Parameters

In this appendix the numerical values used in the simulations are given.

A.1 Disturbance estimation and rejection using acceleration measurements case study

Table A1: Parameters for disturbance estimation and rejection using acceleration measurements case study

Description	**Symbol**	**Value**
Ship rigid body mass	m_{RB}	$2 \times 10^6 kg$
Surge added mass	$X_{\dot{u}}$	$-1 \times 10^5 kg$
Linear drag coefficient	X_u	$0 \frac{Ns}{m}$
Quadratic drag coefficient	$X_{\|u\|u}$	$-4 \times 10^3 \frac{Ns^2}{m^2}$
Desired surge speed	u_d	$5 \frac{m}{s}$
Proportional gain	K_p	$1 \times 10^5 \frac{Ns}{m}$
Slow integral gain	$K_{i,low}$	$5 \times 10^3 \frac{N}{m}$
Fast integral gain	$K_{i,high}$	$5 \times 10^4 \frac{N}{m}$
Disturbance tracking gain	γ	$0.2 \frac{1}{s}$
Wave filter natural frequancy	ω_0	$1.05 \frac{rad}{s}$
Wave filter damping ratio	ζ	$0.1[-]$
Process noise covariance matrix	Q	$\begin{pmatrix} 5 \times 10^{-3} & 0 \\ 0 & 2 \times 10^{-4} \end{pmatrix}$
Measurement noise covariance	R	10^{-7}
Acceleration measurements wave amplitude	A_w	$0.01 \frac{m}{s^2}$
Acceleration measurements wave period	T_w	$6.0s$

A.2 Control allocation case study

Table A2: Parameters for control allocation case study

Description	**Symbol**	**Value**
Thrust time constant	τ	$2.0s$
Max thrust	T_{max}	$200kN$
Max servo speed	r_{max}	$10\frac{deg}{s}$
Servo proportional gain	K_p	$3.0\frac{m}{s}$
Distance from thruster to vessel center	L_x	$50m$
Gauss-Markov noise power	p_{GM}	$3 \times 10^{-3} \frac{N^2}{s^2}$
Gauss-Markov time constants	$T_{GM,(1,1)}, T_{GM,(2,2)}, T_{GM,(3,3)}$	$2000s$
Gauss-Markov gain	K_{GM}	$\begin{pmatrix} 2000 & 0 & 0 \\ 0 & 2000 & 0 \\ 0 & 0 & 80000 \end{pmatrix}$
Mean thrust	T_{mean}	$50kN$
Weight on angle change	$w_{\Delta\alpha}$	10
Weight on thrust usage	w_T	0.1
Weight on thrust change	$w_{\Delta T}$	0.1
Weight on deviation from home angle	w_α	3
Weight on deviation from mean thrust	$w_{\delta T}$	0.1

A.3 MF Gloppefjord case study

In this appendix, the parameter values used in the MF Gloppefjord case study are given.

Table A3: Parameters for MF Gloppefjord case study. Part 1

Description	**Symbol**	**Value**
Guidance paramters		
Radius of acceptance	δ	$150m$
Adaptive LOS convergence rate	λ	0.025
LOS Integral gain	σ	1.5
Heading reference low-pass time constant	T_ψ	$10s$
Transition start speed	U_0	$5\frac{m}{s}$
Transition end speed	U_1	$1\frac{m}{s}$
Transition time	T	$190s$
Reference filter natural frequency	ω_0	0.05
Reference filter damping ratio	ζ	1.3
Reference filter max acceleration	a_{max}	$[0.025, 0.0167, 0.005]\frac{m}{s^2}$
Observer paramters		
Attitude integral gain	k_I	0.01
Attitude proportional gain	K_p	$\begin{pmatrix} 1 & 0 & 0 \\ 0 & 1 & 0 \\ 0 & 0 & 1 \end{pmatrix}$
Attitude injection gain	σ	1.5
TMO position injection gain on position estimate	C_p	$\begin{pmatrix} 0 & 2.0 & 0 \\ 0 & 0 & 2.0 \\ 2.24 & 0 & 0 \end{pmatrix}$
TMO position injection gain on velocity estimate	C_v	$\begin{pmatrix} 0 & 4.0 & 0 \\ 0 & 0 & 4.0 \\ 0.45 & 0 & 0 \end{pmatrix}$
TMO position injection gain on integral state	C_ξ	$\begin{pmatrix} 0 & 0.01 & 0 \\ 0 & 0 & 0.01 \\ 0.035 & 0 & 0 \end{pmatrix}$
VVR Gain	k_{vvr}	5.43

Table A4: Parameters for MF Gloppefjord case study. Part 2

Description	**Symbol**	**Value**
Controller parameters		
Transit heading controller proportional gain	$K_{p,N}^{(1)}$	10^7
Transit heading controller derivative gain	$K_{d,N}^{(1)}$	5×10^6
Transit heading controller integral gain	$K_{i,N}^{(1)}$	10^5
Transit speed controller proportional gain	$K_{p,X}^{(1)}$	10^5
Transit speed controller integral gain	$K_{i,X}^{(1)}$	5×10^3
Transition speed controller proportional gain	$K_{p,X}^{(2)}$	10^5
Transition speed controller integral gain	$K_{i,X}^{(2)}$	10^3
Docking controller pole placement natural period	T_n	$50s$
Docking controller pole placement damping ratio	ζ	1.0
Docking controller integral gain	K_i	$K_p \frac{2\pi}{10T_n}$
Control plant model linear damping matrix	D	$\begin{pmatrix} 3.2 \times 10^3 & 0 & 0 \\ 0 & 1.5 \times 10^5 & 0 \\ 0 & 0 & 1.5 \times 10^8 \end{pmatrix}$
Control plant model mass matrix	M	$\begin{pmatrix} 1.5 \times 10^6 & 0 & 0 \\ 0 & 2.4 \times 10^6 & 0 \\ 0 & 0 & 1.5 \times 10^9 \end{pmatrix}$
Disturbance estimator gain	γ	0.2
Kalman wave filter natural frequency	ω_n	1.57
Kalman wave filter damping ratio	ζ	0.1
Kalman wave filter measurement noise covariance	R	10^{-6}
Kalman wave filter process noise covariance	Q	$\begin{pmatrix} 0.005 & 0 \\ 0 & 0.00002 \end{pmatrix}$

Table A5: Parameters for MF Gloppefjord case study. Part 3

Description	**Symbol**	**Value**
Thruster model parameters		
Max thrust	T_{max}	$200kN$
Thrust time constant	τ	$1.5s$
Max turn rate servo	r_{max}	$12\frac{deg}{s}$
Distance from thruster to vessel center	L_x	$45m$
Sensor model parameters		
Noise power GNSS	p_{GNSS}	0.02
Noise gain GNSS	k_{GNSS}	0.05
Noise power heading compass	p_ψ	0.02
Noise gain heading compass	k_ψ	0.001
Noise power accelerometers	p_{acc}	2×10^{-9}
Noise power rate gyros	p_{ars}	10^{-10}
Gyro bias	b_{ars}	10^{-5}
Accelerometer natural frequency for second order dynamics	$\omega_{0,acc}$	190
Accelerometer damping ratio for second order dynamics	ζ_{acc}	0.707
Rate gyro natural frequency for second order dynamics	$\omega_{0,ars}$	190
Rate gyro damping ratio for second order dynamics	ζ_{ars}	0.707

Appendix B Example cost functions

In this appendix, some example cost functions for the different variations of the nonlinear scalar allocation algorithm are given.

B.1 Docking mode allocation for reversible thrusters

```
%% Cost function for docking mode with reversible thrusters
function cost = cost_fcn_docking_rev(Fx1, Fy1, Fy2, tau_x, F1_last, ...
                            F2_last, a1_last, a2_last, reverse1, reverse2)

    %Weights. Angles in deg, thrust in kN
    a = [10  10];%Cost of change of angle
    b = [0.1  0.1];%Cost of thrust usage
    c = [0.1  0.1];%Cost of thrust change
    d = [3  3];%Cost of deviation from home angle
    e = [0.1  0.1];%Cost of deviation from mean thrust
    f = [1  1];%Cost of running in reverse

    home_angle = [180  0];%deg
    mean_thrust = [50  50];%kN

    %Calculate thrust and chage of angle, convert to degs and kN;
    Fx1 = min(-eps, Fx1);
    Fx2 = tau_x - Fx1;
    a1 = atan2(Fy1,Fx1);
    a2 = atan2(Fy2,Fx2);
    F1 = sqrt(Fx1^2 + Fy1^2)*1e-3;
    F2 = sqrt(Fx2^2 + Fy2^2)*1e-3;

    if reverse1
       a1 = a1 + pi;
       F1 = -F1;
    end

    if reverse2
        a2 = a2 + pi;
        F2 = -F2;
    end

    move1 = shortest_angle_path(a1_last,a1)*180/pi;
    move2 = shortest_angle_path(a2_last,a2)*180/pi;
    a1_last = a1_last*180/pi;
    a2_last = a2_last*180/pi;
    F1_last = F1_last*1e-3;
    F2_last = F2_last*1e-3;

    %Calculate cost terms
    cost_angle_change = a(1)*move1^2 + a(2)*move2^2;
    cost_thrust = b(1)*F1^2 + b(2)*F2^2;
```

```
44      cost_thrust_change = c(1)*(F1-F1_last)^2 + c(2)*(F2-F2_last)^2;
45      cost_angle_dev = d(1)*(home_angle(1) - (a1_last + move1))^2 + d(2)*(
            home_angle(2) - (a2_last + move2))^2;
46      cost_thrust_dev = e(1)*(mean_thrust(1)-F1)^2 + e(2)*(mean_thrust(2)-F2)^2;
47      cost_reverse = f(1)*double(reverse1)*F1^2 + f(2)*double(reverse2)*F2^2;
48
49      cost = cost_angle_change + cost_thrust + cost_thrust_change + ...
50          cost_angle_dev + cost_thrust_dev + cost_reverse;
51  end
```

B.2 Docking mode allocation for nonreversible thrusters

```
%% Cost function for docking mode with nonreversible thrusters
function cost = cost_fcn_docking_nonrev(Fx1, Fy1, Fy2, tau_x, F1_last, F2_last, a1_last, a2_last)

    %Weights. Angles in deg, thrust in kN
    a = [10 10];%Cost of change of angle
    b = [0.1 0.1];%Cost of thrust usage
    c = [0.1 0.1];%Cost of thrust change
    d = [3 3];%Cost of deviation from home angle
    e = [0.1 0.1];%Cost of deviation from mean thrust

    home_angle = [180 0];%deg
    mean_thrust = [50 50];%kN

    %Calculate thrust and chage of angle, convert to degs and kN;
    Fx1 = min(-eps, Fx1);
    Fx2 = tau_x - Fx1;
    a1 = atan2(Fy1,Fx1);
    a2 = atan2(Fy2,Fx2);
    F1 = sqrt(Fx1^2 + Fy1^2)*1e-3;
    F2 = sqrt(Fx2^2 + Fy2^2)*1e-3;
    move1 = shortest_angle_path(a1_last,a1)*180/pi;
    move2 = shortest_angle_path(a2_last,a2)*180/pi;
    a1_last = a1_last*180/pi;
    a2_last = a2_last*180/pi;
    F1_last = F1_last*1e-3;
    F2_last = F2_last*1e-3;

    %Calculate cost terms
    cost_angle_change = a(1)*move1^2 + a(2)*move2^2;
    cost_thrust = b(1)*F1^2 + b(2)*F2^2;
    cost_thrust_change = c(1)*(F1-F1_last)^2 + c(2)*(F2-F2_last)^2;
    cost_angle_dev = d(1)*(home_angle(1) - (a1_last + move1))^2 + d(2)*(home_angle(2) - (a2_last + move2))^2;
    cost_thrust_dev = e(1)*(mean_thrust(1)-F1)^2 + e(2)*(mean_thrust(2)-F2)^2;

    cost = cost_angle_change + cost_thrust + cost_thrust_change + cost_angle_dev + cost_thrust_dev;
end
```

B.3 Transition mode allocation for nonreversible thrusters

```
%% Cost function
function cost = cost_fcn_transition(Fx1, Fy1, Fy2, tau_x, F1_last, F2_last,
    a1_last, a2_last)
    %Weights. Angles i deg, thrust i kN
    a = [10 10];%Cost of change of angle
    b = [0.1 0.1];%Cost of thrust usage
    c = [0.1 0.1];%Cost of thrust change
    d = [3 3];%Cost of deviation from home angle

    home_angle = [180 0];

    %Calculate thrust and chage of angle, convert to degs and kN;
    Fx1 = min(-eps, Fx1);
    Fx2 = tau_x - Fx1;
    a1 = atan2(Fy1,Fx1);
    a2 = atan2(Fy2,Fx2);
    F1 = sqrt(Fx1^2 + Fy1^2)*1e-3;
    F2 = sqrt(Fx2^2 + Fy2^2)*1e-3;
    move1 = shortest_angle_path(a1_last,a1)*180/pi;
    move2 = shortest_angle_path(a2_last,a2)*180/pi;
    a1_last = a1_last*180/pi;
    a2_last = a2_last*180/pi;
    F1_last = F1_last*1e-3;
    F2_last = F2_last*1e-3;
    angle_dev1 = shortest_angle_path(deg2rad(home_angle(1)),a1)*180/pi;
    angle_dev2 = shortest_angle_path(deg2rad(home_angle(2)),a2)*180/pi;

    cost_angle_change = a(1)*move1^2 + a(2)*move2^2;
    cost_thrust = b(1)*F1^2 + b(2)*F2^2;
    cost_thrust_change = c(1)*(F1-F1_last)^2 + c(2)*(F2-F2_last)^2;
    cost_angle_dev = d(1)*(angle_dev1)^2 + d(2)*(angle_dev2)^2;

    cost = cost_angle_change + cost_thrust + cost_thrust_change +
        cost_angle_dev;
end
```